The Effect of a Confining Cover Layer on Backward Erosion Piping Process

Investigation of the initial heave progression

by

A.C Willemstein

in partial fulfilment of the requirements for the degree of
Master of Science
in Applied Earth Science

at the Delft University of Technology,
to be defended publicly on 21 December at 11:00 am

Student Number: 5617499
Project duration: December 2022 - December 2023
Faculty: Civil Engineering and Geosciences, Delft

Thesis Committee:	Prof. Dr. M.A. Hicks	TU Delft, Chairman
	Dr. Ir. R.B.J. Brinkgreve	TU Delft, Supervisor
	Prof. Dr. Ir. M. Kok	TU Delft, Supervisor
	M. Sanders	Daily Supervisor Royal HaskoningDHV
	A. Wiggers	Supervisor Royal HaskoningDHV

TUDelft

Preface

This thesis finalises my MSc in Applied Earth Science at the Delft University of Technology within the specialisation in Geo-Engineering. The research has been conducted with the contribution and support of both Delft University of Technology and Royal Haskoning DHV. The process of conducting and writing this thesis was a long and bumpy road, one which I could have taken on my own. Therefore, there are a few thank yous to all who have helped me in the process. Starting off with my thesis committee members; Prof, Dr. M.A Hicks, Dr. Ir. R.B.J. Brinkgreve and Prof. Dr. Ir. M. Kok who have guided me in what they expected this thesis required.

Besides my committee, I would like to thank everyone at Royal HaskoningDHV, M. Sanders and A. Wiggers. Monique for helping in the day-to-day running and planning of this thesis, making sure, especially in the beginning what the next required step should be. To Albert for the mountain of knowledge and patience you provided. Together we had many fruitful and interesting discussions on the subject that triggered and motivated me to keep searching.

For all the people around me, my friends, parents and boyfriend, Nick I would also like to give my appreciation for all the support during this time. Many memories have been made during my time at the Delft University of Technology that will be treasured dearly throughout the rest of my life.

A.C Willemstein
Delft, December 2023

Abstract

The Netherlands is prone to flooding as more than a quarter of the country lies under sea level. To combat flooding and ensure that the country remains dry structures such are levees and dikes have been installed. However, older water retaining structures are more than ever failing the stringent safety standard assessments. These older conventional reinforcement measures, including berm constructions, are not only costly but require an expanse of ground to ensure performability.

Backward erosion piping is an internal erosion mechanism during which shallow pipes are formed in the direction opposite to the flow underneath water-retain structures as a result of the gradual removal of low cohesive material by the action of water. This mechanism is an important failure mechanism in both levees and dams where a cohesive layer covers a sand layer. Although failure resulting from backward erosion piping is not common, several levee failures in the United States, China and the Netherlands have been attributed to this mechanism.

There are mitigation measures known to stop the backward erosion mechanism. One such measure is the placement of a seepage wall, to create a physical barrier directly in the flow path trying to reach the lowest region of the hydraulic head.

A review of the literature showed that current design rules only consider groundwater flow calculations when determining the likelihood of hydraulic heave, one of the failure modes within the backward erosion process. Hydraulic heave in the backward erosion piping context is closely linked to the quicksand condition, essentially stating that once the effective stress is zero, the sand particles become suspended, liquifying a solid layer. The absence of an assessment of the effective stresses during the design process in conjunction with hydraulic heave has contributed to the main research question addressed by this thesis; *How does a restricted exit for groundwater flow affect hydraulic heave compared to Terzaghi's free exit situation?*.

The definition of hydraulic heave and corresponding particle suspense equilibrium founded by Terzaghi and Peck (1948) is still used today. Over the years the method has had limited alterations and is still based on those original experiments conducted on excavation pits. However, levee geometry in the Netherlands consists most of the time of an impermeable cover layer, which was not taken in the original experiments.

To determine the effects of a confined cover layer, a study was formulated to compare Terzaghi's free-flow formulas to scenarios with and without the presence of a confined cover layer. From these simulations, a constricted exit dominated the flow path, increasing the hydraulic gradient at the entrance to the well. Terzaghi's formulas were verified at the bottom of the inserted seepage wall but did not take into consideration the high concentrations of flow at the well entrance.

Next, an analysis was completed on simplified geometry about stability, effective stresses

and hydraulic heave progression. The numerical software PLAXIS was used to compute the models. The calculations indicated that the hydraulic heave at the entrance to the well was initiated at a relatively low hydraulic head, however, progression ceased to grow once the fluidization or heave zone grew to a certain size.

The calculations where only groundwater flow was modelled observed the current design rules predicting hydraulic heave. It was possible to relate the observed difference in critical gradient caused by the applied hydraulic head, flow concentration, hydraulic conductivity and configuration of well opening to the high local hydraulic gradients.

In the effective stress analysis, it was observed that a confined cover layer significantly impacts the direction of principal stresses within the sand layer. The weight of the layer bears down on the sand layer, causing vertical spreading of stresses as a result of shear stresses. The rotation of the vertical stresses resulted in a pressure bulb occurring under the well, with isobars of pressure forming a bulb shape. It is observed that the fluidization progression was impacted by the pressure bulb, determining its shape and rate of progression.

The results of this thesis show that Terzaghi and Peck (1948) and Sellmeijer (1988) can determine the upper bound with regards to hydraulic heave under a well entrance through a confined cover layer. This method is a quick solution to calculating hydraulic heave and will generate a very conservative answer. However, to fully understand the impact of a confined cover layer on a system, an effective stress analysis is required and highly beneficial.

Contents

Nomenclature

Symbols

Symbol	Definition	Unit
σ	Total Stress	$[kN/m^2]$
σ'	Effective Stress	$[kN/m^2]$
u	Pore Pressure at a point in the ground	$[kN/m^2]$
u_{stat}	Groundwater pressure in the absence of flow	$[kN/m^2]$
γ	Weight density of soil	$[kN/m^3]$
γ_w	Weight density of groundwater	$[kN/m^3]$
γ_{sat}	Saturated soil unit weight	$[kN/m^3]$
γ_{unsat}	Unsaturated soil unit weight	$[kN/m^3]$
γ'	Buoyant weight density (effective density) of the ground	$[kN/m^3]$
z	Vertical distance or depth of the point in the ground below the ground surface	$[m]$
ϕ	Hydraulic Head	$[m]$
ϕ_z	Elevation Head	$[m]$
ϕ_p	Pressure Head	$[m]$
ϕ_v	Velocity Head	$[m]$
ϕ_{limit}	Limit potential head	$[m]$
ϕ_c	the critical hydraulic head	$[m]$
h_p	Hinterland phreatic level	$[m]$
i	Hydraulic head gradient	$[-]$
i_c	Critical hydraulic gradient	$[-]$
p	Pressure	$[kN/m^2]$
p'	Vertical overburden or surcharge pressure at the ground surface	$[kN/m^2]$
g	Acceleration due to Gravity	$[m/s^2]$
v	Velocity	$[m/s]$
d	Thickness of confining cover layer	$[m]$
n	Porosity	$[-]$
e	Void ratio	$[-]$
k	Coefficient of hydraulic permeability	$[m/day]$
q_i	Flow velocity in i direction	$[m/s]$
s	Direction of flow (x, y, z)	$[-]$
Q	Discharge	$[m^3/day]$
L	Minimum seepage length	$[m]$
C_{creep}	Creep factor	$[-]$
G_s	Specific gravity	$[kg/m^3]$
E'_{ref}	Young's modulus	$[kN/m^2]$
ν	Poisson's ratio	$[-]$
c	Cohesion	$[kN/m^2]$

Symbol	Definition	Unit
φ'	Friction angle	[°]
ψ	Dilatancy angle	[°]
F_r	the resistance term, being the strength of the sand	[−]
F_g	the geometry term, which depends on the ratio of the sand layer thickness sand the seepage length	[−]
F_s	the scale term, relating the particle size and the seepage length	[−]
θ	the bedding angle	[°]
η	the coefficient of White	[−]
κ	the intrinsic permeability of the piping sensitive sand layer	$[m^2]$
d_{70}	the particle diameter for which 70% passes through a sieve	[−]
d_{70m}	mean d_{70} in the small scale tests	[−]
RD	the relative density	[−]
RD_m	the average density in small-scale tests (0.725)	[−]

<div align="right">

1

</div>

<div align="right">

Introduction

</div>

1.1. Levee failure in the Netherlands

The Netherlands and water have always had a strained relationship. Water is vital for the country's economic growth and providing a way of life for its people, but has also caused great destruction to land and people. Located in a delta, twenty-five percent of the Netherlands lies under sea level. If levees were not present in the country's infrastructure, half of the population would experience flooding regularly and with climate change, sea level rising and ground settlement, the threat of flooding is growing. An extensive network of water barriers exists, nearly 17,000km long (Unie van Waterschappen (2019)) consisting of levees, dams, dunes and locks.

In the past, the usual response was to strengthen the levees by taking the highest observed water level as the reference point. All of this changed with the Storm Surge of 1953. Record high water levels were recorded, resulting in more than 150 levee breaches in the regions of Zeeland, South Holland and North Brabant. After the destruction in 1953, the government appointed a committee of experts, known as the Delta Commission, to advise on a response. Not only did they advise plans to rebuild and protect the areas affected, but stricter requirements were also introduced for the entire country, weighing the cost of reinforcements against the reduction of flood risk. Although extensive study and reinforcements have been carried out, reducing the flood risk dramatically, flooding and levee failure still occur today.

A suburb in Wilnis, experienced flooding in the summer of 2003, not due to a high water event, but extreme high temperatures. The heat wave caused the polder of Groot Mijdrecht to become so dry, that the peak shrunk and cracked, causing the levee to slide (Middendorp (2015)).

1.2. Levee failure by backward erosion piping

Most of the levees are river levees constructed from low permeable materials such as clay and are often located on sandy aquifers. When water levels vary with time, the hydraulic gradient over levees increases, resulting in the movement of groundwater underneath a levee, often also referred to as seepage. This movement potentially could cause erosion through sediment transportation, leading to the phenomenon of backward erosion piping (BEP), also known as piping (van Beek (2015)). Shallow pipes form at the sand or silt layer interface and a cohesive top layer, progressing in the opposite direction of water flow. When the entire pipe is formed

it further deepens and widens, undermining the structure, and potentially resulting in levee failure. Mitigation methods exist to try to reduce flow concentration to certain areas within the levee system, reducing the possibility of backward erosion piping, such as a berm or cut-off wall but these require sufficient space and material.

1.2.1. Hydraulic Heave

Within the backward erosion piping phenomenon, a certain sequence of events is required to achieve alternative leave failure. One of these events within the failure path is the process of hydraulic heave. When the pressure of flow becomes greater than the weight of the particles within a low cohesive layer, the particles become suspended or fluidized, initiating hydraulic heave.

1.3. Progressive fluidization

Terzaghi and Peck (1948) introduced fundamental reasoning concerning hydraulic heave, during excavation pit experiments, creating the fluidisation prism concept. The fluidization process was observed during these experiments, where no confining cover layer was present, to occur in a rather rectangular or prism-like manner. This concept is still in many ways the main design concept when determining the extent of hydraulic heave within a levee problem, where such a fluidization prism is established off the extreme project limits, producing an uppermost limit for hydraulic heave.

Progressive fluidisation is a new concept for determining hydraulic heave, where the effect of a confined cover layer is taken into account. Instead of a static predefined zone, this concept aims to look at flow nets, exit and critical hydraulic gradients effective stress, over time and hydraulic head differences.

Although this concept is still being drafted, from theoretical literature and previous experiments focusing on hydraulic failure the following assumptions have been made;

- Horizontal growth will dominate rather than vertical growth
- Quicksand is highly permeable resulting in a damping effect on pipe growth.

1.4. PLAXIS

Within this research, the computer application PLAXIS will be used to perform finite element analyses (FEA). The PLAXIS 2D software will perform a 2D analysis of deformation, stability, and water flow in the geotechnical engineering problem presented in this report.

1.5. Problem Statement

Recent research work has led to the improvement of the Dutch assessment rules (van Beek (2015)), and in combination with more stringent safety standards has led to an increase of required seepage lengths to ensure enough safety against failure. Fulfilling the new assessment rules has a large impact on the cost of the strengthening of dikes, in particular densely populated areas and of historic value. Conventional measures such as a berm or cutoff walls are becoming costly due to the large amount of land area required, and long stretches needing to be reinforced. Alternative potentially cost-effective innovative mitigation measures are becoming attractive, such as the placement of a seepage wall.

Currently, piping research with seepage walls and safety assessments are often based on experimental or numerical modelling using arbitrary model widths or even two-dimensional(2D) assumptions (Vandenboer, van Beek, and Bezuijen (2018)). These models such as Sellmeijer (1988) and Terzaghi, Peck, and Gholamreza (1996), do not resemble the common Dutch levee system. Even today safety calculations are being based on models where an impermeable cover layer between the sandy porous layer and the ground level is not taken into consideration. This leads to too many assumptions being formed, a conservative design and high costs. Limited research has been conducted into the effects of such a cover layer on the initiation and progression of backward erosion piping (Sellmeijer (1988); Robbins, Stephens, et al. (2020)), gaps of knowledge can still be noted concerning the behaviour of the pipe(s) when reaching a mitigation measure.

1.6. Objective

Currently, the Dutch guidelines for hydraulic heave use the 2020 Eurocode 7 design rule. This rule is based on the upward seepage forces acting against the weight of the soil, reducing the vertical effective stress to zero. Over the years, little alteration to the rule has occurred, providing a very realistic 2-dimensional representation when a confining cover layer is not present. However, the geology in the Netherlands often sees a confining clay layer being present over a porous sand layer, restricting exit flow. The current design rule does not consider the implementation of such a confining cover layer, therefore, the goal of this thesis is to *assess the effect of a confining cover layer on the hydraulic gradient near a concentrated exit, compared to the current design rules.*

1.6.1. Research Question

The following questions will support this research:

How does a restricted exit for groundwater flow affect hydraulic heave compared to Terzaghi's free exit situation?

The above question will be answered in relation to the following statement:

The cover layer properties, such as thickness and weight, are leading design-determining properties of seepage walls.

Sub-questions
1. How does a seepage wall affect the failure paths and physical processes of a backward erosion pipe's progression?
2. In the case of a constant water level difference what are the factors causing heave to stop expanding?
3. How do the exit well dimensions affect the rate of initial pipe erosion?
4. To what extent does a confining cover layer affect the occurrence and progression of quicksand and heave?

1.7. Relevance

Since the renewal of the Dutch assessment rules many levees do not meet the requirements regarding backward erosion piping, requiring reinforcement. Indicative studies show that approximately half of the levees that Dutch Water Authority Rivierenland operates will not pass

the current safety assessment criteria for piping (Rosenbrand, Wiersma, and Förster (2019)). The Netherlands are increasingly incorporating new backward erosion piping mitigation measures instead of the traditional berm solution into the levees, greatly due to limited space. Land needed for levee reinforcement construction is not only limited by houses but also other properties, services for electricity and gas, culture issues and ecological limitations, such as Natura 2000 restrictions. Claiming this land from landowners is no easy feat, and time-consuming due to the legal processes involved. Therefore, these new backward erosion piping mitigation measures are becoming more attractive.

1.8. Research approach

This section describes the methods used for the different components of the research project and the associated chapters, and how these are related, see also figure 1.1. In order to answer the research questions and to fulfil the provided objectives, the study is divided into two key parts; theoretical background and research.

Backward erosion has already been extensively investigated by other researchers. This thesis therefore begins in part 1 (chapters 2, 3 and 4) with a description of the relevant literature and theoretical ideas. Important definitions will be clarified and explained in context with the backward erosion piping phenomena. A description of the backward erosion piping process, including the failure path, is provided in chapter 3. Furthermore, relevant past experiments, prediction models and design rules were presented.

Part 2 reports the PLAXIS calculations used to address the research questions. Chapter 5 explores Terzaghi's formulas and relationships between flow and hydraulic head. Section 6.5 assesses Terzaghi's hydraulic heave equations against PLAXIS calculations of a free exit situation. Although current design rules are based solely on groundwater flow calculations, hydraulic heave requires sand particle movement, where the effective stress is $0kN/m^2$. This can not be analysed with groundwater flow calculations, requiring stability calculations to be performed. Three different models will be presented in chapter 6 to determine the relationship between the hydraulic head, hydraulic heave and progressive fluidization.

The report ends with chapters containing discussion, conclusions and recommendations. Any additional information related to the research can be found in the appendix.

Chp 1: *Introduction*

Part 1: *Theoretical Background*

Chp 2: *Definitions*

Chp 3: *The Physics of Backward Erosion Piping*

Chp 4: *Prediction Models and Design Rules*

Sub-question 1 & 2

Part 2*: Research*

Chp 5: *Groundwater Calculations*

Without confining cover layer

With confining cover layer

Model validation

Chp 6: *Effective Stress Analysis*

Without confining cover layer

With confining cover layer

Model validation and verification

Sub-question 3 & 4

Chp 7: *Discussion*

Chp 8: *Conclusions and Recommendations*

Appendix

Figure 1.1: Thesis outline

Part I

Theoretical Background

2

Definitions

Geotechnical definitions vary among researchers and is therefore important to clarify the different terms used within this research, to eliminate confusion among the readers.

2.1. Definition of Levee failure and Initial failure

This study will use the definition of levee failure as Rijkswaterstaat (2023) defines it. A levee fails when there is a loss of primary function, which is retaining water and preventing flooding of the hinterlands or polders. A full breach is not required to cause flooding of the hinterlands, for example overtopping, but the majority of a breach is present.

2.2. Darcy's Law

Darcy's law governs the flow of oil, water, and gas in porous media. The law states that the discharge rate is proportional to the gradient in the hydraulic head and the hydraulic conductivity. Bernoulli's equation allows one to estimate the direction and rate of flow according to Darcy's law

$$q_x = -k_x \frac{\partial \phi}{\partial x}, \qquad q_y = -k_y \frac{\partial \phi}{\partial y}, \qquad q_z = -k_z \frac{\partial \phi}{\partial z} \qquad (2.1)$$

Darcy's law can be simplified if the direction of flow (s-direction) is known. Simple flow problems are often used to solve with following

$$q = -ki \qquad \text{with} \qquad i = \frac{\Delta \phi}{\Delta s} \qquad (2.2)$$

q	$[m/day]$	Discharge rate
k	$[m/day]$	Hydraulic conductivity
$\frac{\Delta \phi}{\Delta s} = i$	$[-]$	Hydraulic Gradient

The quantity of $\Delta \phi / \Delta s$ is the increase of the groundwater head per unit length, in the direction of flow, also known as the hydraulic gradient i. Once there is seepage and an open exit, the vertical hydraulic gradient, near the exit determines whether or not erosion will commence.
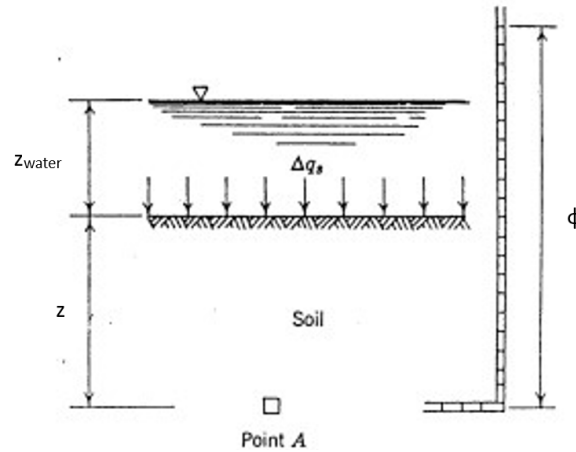
Figure 2.1: Upward flow in soil (Lambe and Whitman (1969))

2.3. Definition of the Quick Conditions and Quicksand

The shear strength of cohesionless soil is directly proportional to the effective stress. When cohesionless soil is subjected to a water condition that results in zero effective stress, the strength of the soil becomes zero; a quick condition then exists. A quicksand condition, in other words, is when the shear strength of the soil is zero due to the absence of effective stress. Because cohesion soils can have strength even at zero effective stress, they do not necessarily become quick at zero effective stress.

The effective stress is zero when the pore pressure equals the total stress the effective stress is zero. Two common situations in soil mechanics where this equality is presented below (Lambe and Whitman (1969));

1. An upward fluid flow of such magnitude that the total upward water force equals the total soil weight (for an unloaded soil element), and the seepage force equals the submerged soil weight, commonly known as quicksand.
2. A shock on certain loose soils causes a volume decrease in the soil skeleton with the result that the effective stress is transferred to pore pressure. This situation is known as liquefaction.

This research will focus on the first situation, quicksand.

2.3.1. Quicksand

The hydraulic gradient necessary to make the effective stress of a soil sample equal to zero follows from the definition equation of effective stress $\sigma' = \sigma - u$, concerning figure 2.1. No horizontal stresses are taken into account.

$$\sigma' = \sigma - u = z * \gamma_{sat} - \phi * \gamma_w \qquad (2.3)$$

Following Darcy's law equation 2.1, the hydraulic gradient is defined as

$$i = \frac{\phi - z}{z} \qquad \text{or} \qquad \phi = z(i+1) \qquad (2.4)$$

For quick condition, $\sigma'_v = 0$ and $i = i_c$, so that

$$\gamma_{sat} = \gamma_w + i_c * \gamma_w \qquad (2.5)$$

and

$$i_c = \frac{\gamma_{sat} - \gamma_w}{\gamma_w} = \frac{\gamma'}{\gamma_w} \tag{2.6}$$

Since the ratio $\frac{\gamma'}{\gamma_w}$ is usually close to unity, the critical gradient i_c required to cause a quick condition, is approximately equal to 1. Note that the flow must be vertically upwards, in the opposite direction to the soil unit weight, for the equations 2.3 to hold. Also, equation 2.3 requires that the soil element be unloaded, and the vertical effective stress in the element with no flow must depend only on the buoyant unit weight. Equation 2.6 is the so-called heave criterion, determining whether or not heave will occur within the system.

3

The Physics of Backward Erosion Piping

Backward erosion piping (BEP) is an internal erosion mechanism by which hollow spaces, pipe-like structures, are formed in or underneath water-retaining structures as a result of the removal of soil by water action (van Beek, Bezuijen, and Sellmeijer (2013)). Other terms found in the literature referring to the same process include seepage and piping. This research is restricted to the type of BEP that occurs in the foundation of water-retaining structures, where a cohesive confined cover layer overlies a sandy aquifer.

3.1. Sequence of Processes

The backward erosion piping process requires a certain sequence of sub-mechanisms and conditions to initiate initial failure (van Beek, Bezuijen, and Sellmeijer (2019)). The three conditions required to begin the BEP process are as follows; sufficient hydraulic head, impermeable cohesive roof to prevent pipe collapse and an open unfiltered exit. The different sub-mechanisms leading to a potential levee failure as a result of backward erosion are displayed in figure 3.1, where it can be noted that backward erosion is only one phase (phase 2) of the complete process. The processes of internal erosion may be broadly broken into four phases:

- Phase 1: initiation of erosion through seepage
- Phase 2: continuation of backward erosion
- Phase 3: progression to form a pipe and widening of the pipe
- Phase 4: initiation of breach
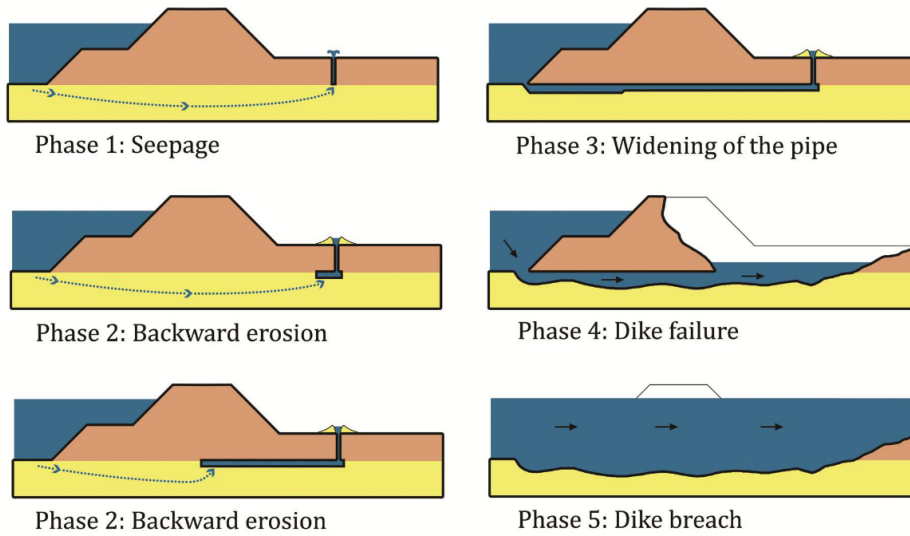
Figure 3.1: Phases leading to the breach of a levee due to backward erosion piping van Beek, Bezuijen, and Sellmeijer (2013)

Not only are certain sub-mechanisms and conditions required to initiate the backward erosion piping process, but a sequence of events within the sub-mechanisms must be held throughout the process. The figure below (figure 3.2) shows a generic failure path for a soil levee (Deltares (2020)) containing the sub-mechanism and the order of events leading to failure. The steps leading to the levee will be referred to as failure nodes. The physics of the failure paths are introduced in section 3.3.
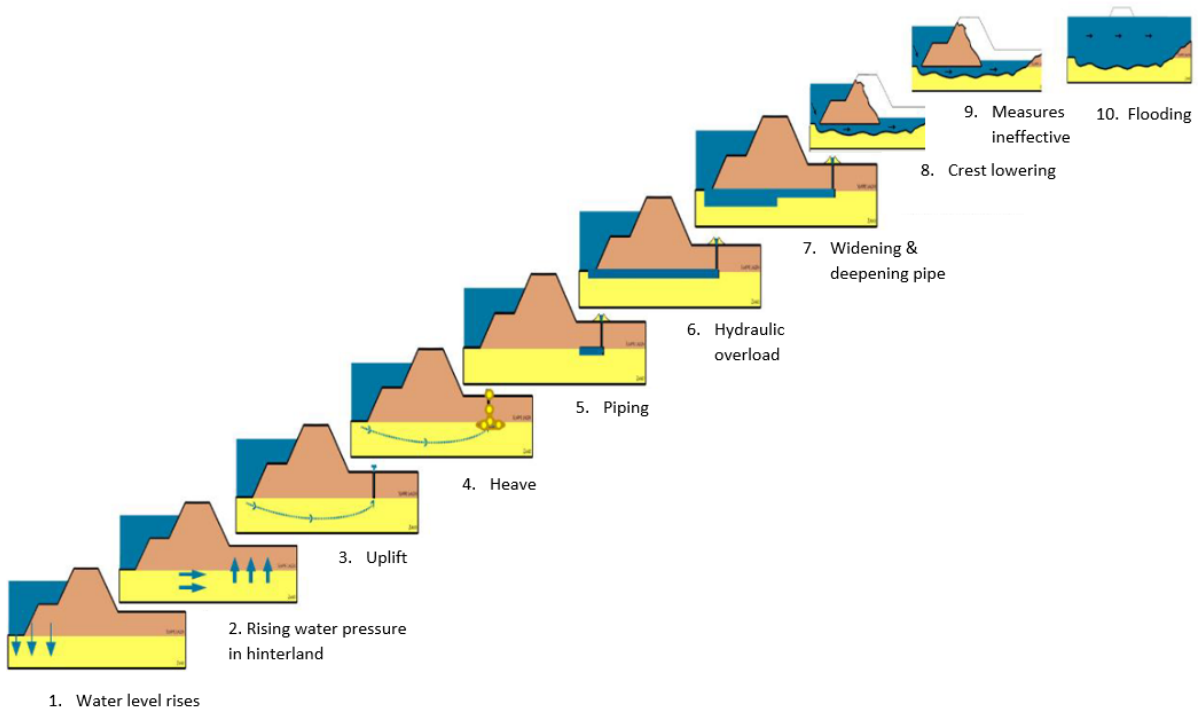
Figure 3.2: Illustration of a generic failure path with an explanation of how the piping mechanism develops for a dike (Deltares (2020))

3.2. Mitigation Measures

To combat levee instabilities caused by backward erosion piping the process of continuation of backward erosion under the flood deference to the riverside must be stopped. Many traditional measures, such as berms, relief wells and seepage walls are still in use within the Dutch water infrastructure. However, in densely populated areas, especially areas of historic interest in combination with the high scenic value of the landscape, little space is available for traditional strengthening measures against backward erosion piping. Thus, alternative cost-efficient piping mitigating techniques are becoming more attractive (Förster, Koelewijn, et al. (2019)). Although innovative measures are increasingly being tested, this thesis focuses on seepage walls. Seepage walls are the main method to combat BEP in the Netherlands. Other mitigation measurements are described in appendix A.2

3.2.1. Seepage Walls (Heaveschermen)

In situ vertical barriers, seepage walls (in American literature also known as seepage cutoff walls) have been used for over 40 years to control the horizontal flow of groundwater in the subsurface (Evans, Ruffing, and Elton (2015)) and continue to be the chosen reinforcement measure against the occurrence of piping, a failure node within the backward erosion piping process. By placing a continuous, impermeable heave screen at the bottom of the inner slope (or verge) of the existing dike, the seepage current is altered at the location of the screen, reducing flow concentration at certain points. Flow is forced either downwards under the screen or sideways along it (figure 3.3).
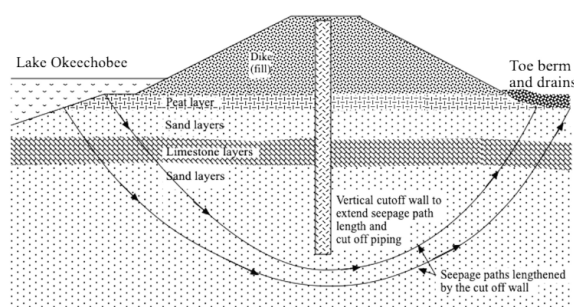
Figure 3.3: Herbert Hoovers Levee cutoff wall

With strong updrafts behind the screen, quicksand can form when the vertical gradient of the seepage current is so large that the grain stress reduces to zero. The formation of quicksand by updrafts is called 'heave'. As the name implies, the operation of the heave screen is based on counteracting a heave condition behind the screen. However, the heave screen will not prevent other initial processes from taking place, such as the occurrence of sand-carrying wells; the beginning of pipe growth between the well and the screen; or local fluidization directly under the overburden. The screen functions as an anti-piping measure as long as these initial processes do not progress to erosion pipes passing the screen. These processes will be explained further in section 3.3

Seepage walls were originally designed to dewater excavation pits, improve slope stability, reduce water flow into excavations, and prevent contaminant transportation in the 1980s. Seepage walls were adapted for widespread use to improve the properties of underlying materials and improve the properties of the dam or levee. Countless materials could be used to construct a seepage wall and numerous ways to build them. It is desired

that the wall is homogeneous and has low permeability (hydraulic conductivity).

3.3. Backward erosion piping failure path

Failure due to backward erosion piping requires a specific sequence of processes to occur as mentioned in section 3.1. Researchers such as van Beek, Bezuijen, and Sellmeijer (2013), Forster et al. (2012) and de Bruijn (2013) have extensively researched this sequence of processes determining that within each sequence individual events must occur to cause levee failure, creating a failure path. Figure 3.4 is an extension of figure 3.2 dictation the failure path, where a seepage wall is present.

Several initiating events, such as well formation and pipe formation must take place before the process of heave and vertical erosion can occur at the location of the screen. If there is no or virtually no confining cover layer, the free outflow is experienced and the description of the failure path becomes somewhat simpler, with the removal of the failure nodes 2 to 5, displayed in figure 3.2.

The following sections will further explain the physical processes when a seepage wall is present, concerning relevant studies and calculation models.
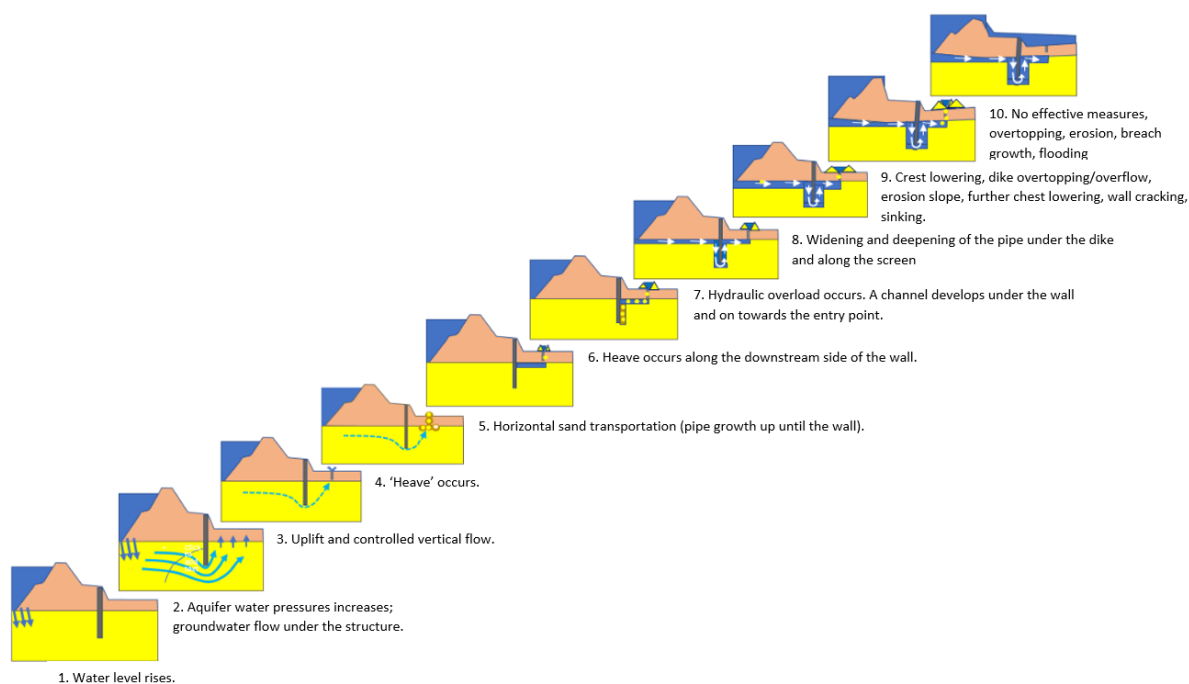
Figure 3.4: Illustrations of events in the failure path, which describe the failure path of piping with a seepage wall. There is no flow through the wall and isotropic behaviour in the sand is assumed (Kraaijenbrink (2022)).

3.3.1. Water level and pressure rising (failure node 1 & 2)

Hydraulic head (groundwater head or head) differences over the levee, caused by a high water event, ensure that groundwater wants to flow from high hydraulic head positions (river, lake or sea) to positions of lower head (polder side). The hydraulic head represents the mechanical

energy per unit weight of fluid in the system, Bernoulli defined this as

$$\phi = \phi_z + \phi_p + \phi_v$$
$$\phi = z + \frac{p}{\gamma_w} + \frac{v^2}{2g}$$

(3.1)

Where:

ϕ	$[m]$	Hydraulic head
ϕ_p	$[m]$	Pressure head
ϕ_z	$[m]$	Elevation head
ϕ_v	$[m]$	Velocity head
v	$[m^2]$	Velocity
g	$[m/s^2]$	Acceleration due to gravity

For most flow processes in soil, the velocity is generally small and therefore neglected.

3.3.2. Uplift (failure node 3)

The rise in water level, causes an increase in the hydraulic head will be experienced. With the elevation head, due to the weight of the water, remaining constant, will following equation 3.1 see a porewater pressure build-up in the sandy porous layer. The flow will begin to Seepage in the lower hydraulic head positions. If no confining impermeable layer is present, seepage can flow freely out of the porous layer to the surface. If a confining layer is present, the flow is restricted restricting flow, with porewater pressures building up at the sand-confining layer interface.

When, with increasing water levels, the hydraulic head on the polder side is high enough the pressure build-up could lift and tear the confining cover layer, commonly known as *uplift*. This uplift will occur when the pore pressure in the sand layer exceeds the weight of the cover layer. The head potential in the sand layer at which the equilibrium is present is called the limit potential ϕ (Forster et al. (2012)).

The limit potential is calculated as follows

$$\phi_{limit} = h_p + d\frac{\gamma_{sat} - \gamma_w}{\gamma_w}$$

(3.2)

Where:

ϕ_{limit}	$[m]$	Head in the aquifer (sand layer) at the interface with the cover layer
h_p	$[m]$	Hinterland phreatic level
d	$[m]$	Thickness of confining cover layer

3.3.3. Heave (failure node 4)

When the confining cover layer is ruptured by uplift or when there is no blanket, the water in the aquifer can seep upwards through the exit point. Fluidisation, 'Heave', or 'quicksand', are some of the many terms used for a situation in which the vertical grain tensions in a sand layer disappear under the influence of a vertical groundwater flow. Sand loses its cohesion of the grain skeleton as a result of the increase in water pressure (in the pores) and becomes liquidised. The initiation of a pipe involves the onset of movement or suspension of a group of particles in an intact sand layer.

γ' $[kN/m^3]$ Buoyant unit weight
n $[-]$ Porosity
e $[-]$ Void ratio
Gs $[-]$ Specific Gravity

Critical Heave Gradient

Fluidization of the sand bed will occur when the seepage pressures counterbalance the submerged weight of the grains, such that the effective stresses are reduced to zero (Robbins and Van Beek (2015), van Beek, Bezuijen, and Sellmeijer (2013)). Terzaghi first introduced the critical heave gradient (i_c) in 1922 based on the vertical equilibrium of a soil particle.

$$i_c = \frac{\gamma_{sat} - \gamma_w}{\gamma_w} = \frac{\gamma'}{\gamma_w} = \frac{(1-n)(\gamma_p - \gamma_w)}{\gamma_w} = \frac{Gs - 1}{1 + e} \tag{3.3}$$

where n is the porosity, γ_p, γ_w, γ' are the unit weight of the particles, water and buoyant unit weight of soil respectively.

At expansion or grain flotation equilibrium, the sand turns from a solid soil matrix into a fluid sand-water mixture. It is to be noted that even though the pressure gradients might be high enough to cause fluidization, it does not always cause sand transportation required for pipe formation. This thick sand-water mixture is stagnant, with hardly any velocity.

When the flow is sufficient enough to move sand grains, a phenomenon called water boiling occurs. The sand "dances" in the well on the rising water, but the upward pressure is not yet high enough to throw the sand over the edge of the well. The fluid flow is in equilibrium with the weight of the fluidised soil mass, producing this 'boiling' effect.

3.3.4. Piping (failure node 5): Horizontal sand transportation and Pipe formation until seepage wall

The equilibrium situation described above can be disturbed when the fluid flow is sufficient to carry soil particles outside of the fluidized zone, beginning backward erosion. With each surge of fluidisation, particles are deposited in a ring outside the sand boil centre, in an increasing 'sand volcano', also referred to as 'sand boils'. The sand deposited on the surface is transported from the aquifer. In the aquifer, hollow spaces between the two layers are formed with the cover layer forming the roof. Two aspects are involved in the formation; sand must become detached from the grain package or skeleton in which it was contained and begin to roll (indicated in figure 3.5). First in the small channels in all directions and eventually developing in one main direction. From the moment the canal starts to grow back to the outer water (where the water from the river flows into the sand package) *"piping"* occurs.
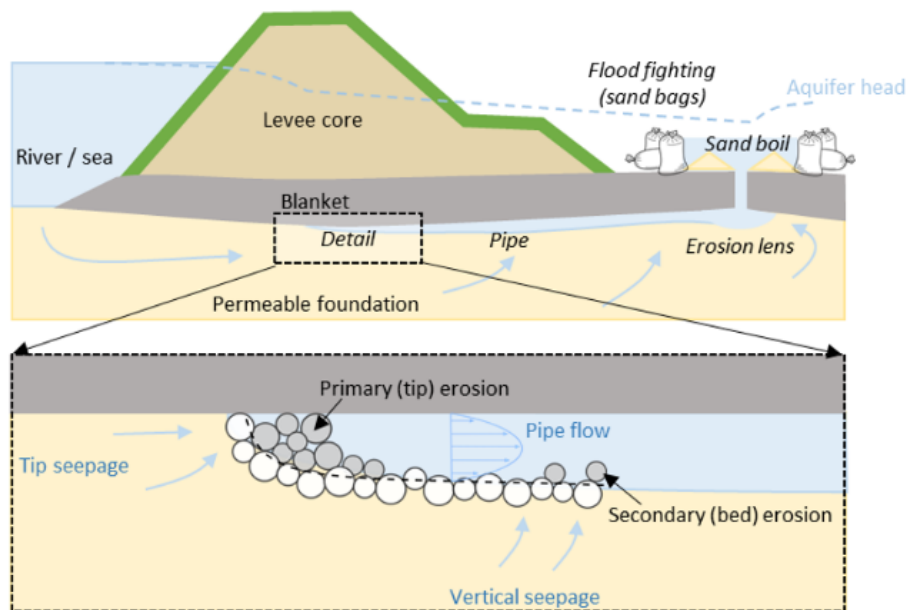
Figure 3.5: Sand particle transportation in a pipe Pol (2022)

Erosion of the front of the pipe and erosion of the walls causes the progression of the pipe. At the tip of the pipe the hydraulic gradient increases as the pipe acts as a drain, which in turn fuels the groundwater flow leading to further erosion. Once a specific critical hydraulic head gradient is reached the pipe can no longer stop growing, eventually connecting the upstream and downstream sides.

3.3.5. Heave occurrence along downstream of seepage wall (failure node 6)

Once the pipe has reached the mitigation wall, flow is greatest in the vertical direction. When the vertical equilibrium of a soil particle is tripped, as explained in failure node 4 (section 3.3.3), a vertical pipe is formed along the seepage wall, transporting sand back and out of the well to the surface.

3.3.6. Hydraulic overload (failure node 7)

When the pipe develops fully and reaches the upstream water level, a direct hydraulic connection is established between upstream and downstream. The flux through the pipe increases dramatically, causing the deepening and widening of the pipe.

3.3.7. Widening and deepening of pipe (failure node 8)

The flow through the pipe causes shear stress on the grains at the pipe walls and bottom, causing the pipe to deepen and widen until the particles are in limit-state equilibrium with the water passing the particles.

3.3.8. Crest lowering (failure node 9)

Chest lowering can occur when the pipe becomes too big, leading to overtopping/overflowing, causing further erosion of the chest. The seepage has the potential to sink and /or tilt the crest towards the polder. Two situations could occur if the continuous pipe reaches a certain width;

the levee can settle by closing the pipe with or without crest lowering, or there could be slope instabilities with or without eventual levee failure van Beek, Bezuijen, and Sellmeijer (2019).

3.3.9. Ineffective measures and flooding (failure node 10)

Complete levee failure will occur when preventive measures, such as a seepage wall, can not be effectively applied. The breach will grow and the polder will flood.

3.4. Summary

Backward erosion piping is an internal erosion mechanism as a result of the gradual removal of sandy material by the action of water. Shallow pipes are formed in the opposite direction to the flow underneath water retaining structures as a result of the gradual removal of sandy material by the action of water. It is an important failure mechanism in both levees and dams where sandy layers are covered by a cohesive layer. Certain required sub-mechanisms and conditions are required to begin the initial failure of a levee; initial erosion through seepage, continuation of backward erosion, progression in the opposite direction to form pipes and widening of such pipes and the initiation of a levee breach.

4

Prediction models and Design Rules

The prediction of the backward erosion piping phenomenon has received much attention in the past, with certain failure nodes, such as piping, receiving more attention than others. and is still being investigated to this day. Starting with simple empirical rules at the beginning of the previous century, with ongoing research the prediction models have become more physics-based, and are often founded or calibrated using experimental data.

4.1. Early Prediction models (1900-1970)

When designing levees and dams prediction models can be used to determine the extent of piping, which dates back to the early last century. Since the turn of the last century, the process of piping has been studied in the context of weir and dam design. At the time, no distinction was made between backward erosion and suffusion as a piping mechanism.

4.1.1. Bligh (1910)

Bligh (1910) produced one of the first and foremost design rules concerning piping, establishing that piping is dependent on the head difference, seepage length and both the horizontal and vertical lines of creep (seepage length) underwater retaining structures for specific soil types.

$$\Delta\phi \leq \Delta\phi_c = \frac{L}{C_{creep}} \tag{4.1}$$

$\Delta\phi_c$	$[m]$	critical hydraulic head difference
L	$[m]$	minimum seepage length
C_{creep}	$[-]$	creep factor

Adaptation of Bligh for Dutch levee design
Bligh's rule does not consider a confining cover layer, therefore a correction is required when applied to Dutch levee design. Vertical particle transportation through a crack, such as a well, causes resistance created by the fluidized sand grains. A critical hydraulic head gradient reduction of 0.3 across the cover layer was introduced to determine the resistance Rosenbrand and Van Beek (2017), Forster et al. (2012).

$$\Delta\phi \leq \Delta\phi_c = \Delta\phi - 0.3 * d \tag{4.2}$$

d $[m]$ cover layer thickness

4.1.2. Lane (1935)

Lane (1934) continued with Bligh's rule, adding the importance of the distinction between horizontal and vertical flow. According to Lane, the vertical resistance to seepage is significantly larger than the horizontal resistance to seepage. As a result, the horizontal seepage length is reduced by a factor of three (equation 4.3). The creep factor used is also more conservative than that used in Bligh, scaled to the extent to which the subsoil is resistant to washing out (Deltares (2017)).

$$\Delta\phi \leq \Delta\phi_c = \frac{\frac{1}{3}L_h + L_v}{C_{creep}} \tag{4.3}$$

Where:

L_h $[m]$ horizontal seepage length
L_v $[m]$ vertical seepage length

4.1.3. Harza (1935)

Piping cannot occur if sand heave is impossible, so Harza (1935) calculated the uplift head near the seepage wall toe for different situations using the electric analogy method (Tanaka and Verruijtii (1999)). It was noted that, as the exit gradient approaches infinity near the toe for horizontal sand layers without cutoffs, the foundation of the soil should never be at the same level as the dam body. The approach was more scientific than empirical modelling, focusing on the exit hydraulic gradient i_{exit}. Harza (1935) hypothesised that the critical condition is reached when the maximum value of the exit hydraulic gradient $i_e max$ becomes just equal to the critical hydraulic gradient of soil i_c.

4.1.4. Terzaghi and Peck (1967)

Terzaghi and Peck (1964) described the mechanics of piping due to heave by assuming the fluidization of a prism of sand (figure 4.1a) downstream of a structure. For piping to occur, the excess hydrostatic pressure at the base of the structure must equal the weight of the overlaying sand. Terzaghi, Peck, and Gholamreza (1996) introduced the use of flow nets to compute the hydraulic pressure around the structure (figure 4.1a). Experimental results were extracted from two-dimensional tests in homogeneous cohesionless soils (Terzaghi, (1922)), where a rectangular-shaped failure zone was lifted by the pore pressure to indicate that the height and width of the failure prism are the depth of wall D and its half $D/2$ respectively.

(a) Groundwater flow net (Terzaghi, Peck, and Gholamreza (1996))

(b) The possible failure zones for heave (1) and for the initiation of piping (2) are shown (Garai (2016))
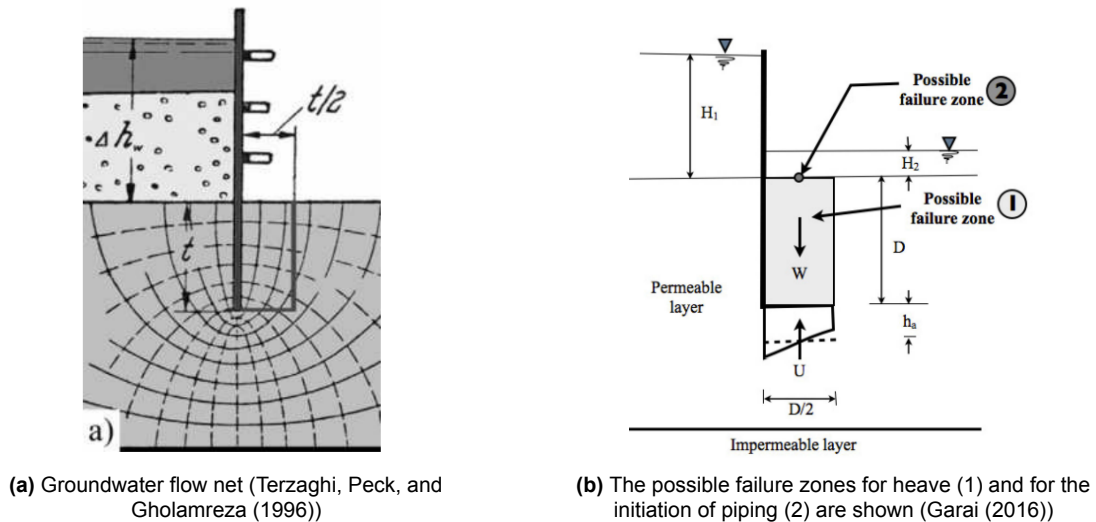
Figure 4.1: Terzaghi's hydraulic heave model for a single row sheet pile structure

The rise of the prism is resisted by the weight and the vertical side shearing such as friction and cohesion. It is assumed that at the instant of failure, the effective horizontal stress on the sides of the prism and the corresponding frictional resistance is practically zero. And, for sand, the cohesion is also practically zero Tanaka and Verruijtii (1999). Therefore the prism rises as soon as the resultant force of the excess pore water pressure (u) becomes equal to the submerged weight of the prism.

4.1.5. Sellmeijer

One of the key design rules used in the Netherlands is the 2011 version of Sellmeijer (1988). Through the years this design rule has undergone many adaptations but is still based on the so-called idealised geometry, figure (4.2). The idealised levee geometry consists of a clay levee with a ditch on top of a homogeneous isotropic sand layer with constant and finite thickness. With this geometry, no uplift is required in the piping process, due to the ditch already providing a way through the cohesive layer. Sellmeijer's formulation is just one of many that do not take into consideration a cohesive cover layer above the homogeneous sand layer, which requires uplift before heave can occur.
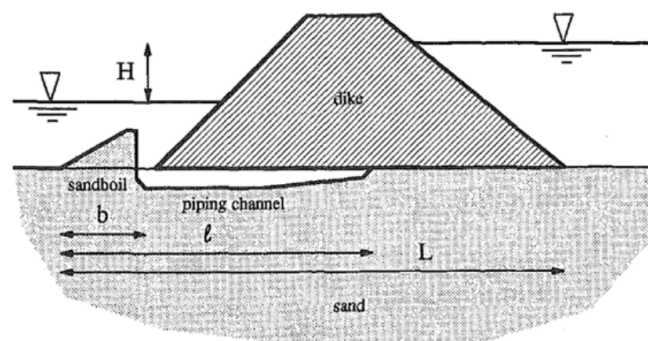
Figure 4.2: Sellmeijer's idealised geometry

The design rule is used to determine a critical hydraulic gradient for which the progression

of a pipe to the upstream side can occur. Sellmeijer (1988) simulated the progression of a pipe with a mathematical model based on experiments conducted during a large research program for the Centrum Onderzoek Waterkeringen or the Water Defences Research Center (C.O.W.), in collaboration with the Soil Mechanics department at the TUDelft. This project had the intention of investigating the mechanisms of piping to produce recommendations for levee design.

Assuming pipe equilibrium at some point in time, at which the grains at the bottom of the pipe reach a limit-state equilibrium, a model for predicting the head difference across the levee was developed. Four distinct forces are considered in the particle force balance; vertical forces include the weight of a particle vertical flow force with drag force due to the channel flow and horizontal flow force consists of the horizontal forces (Kramer (2014)). Sellmeijer determined a relation between the hydraulic head difference over the levee ΔH and the pipe length at which the grains are in equilibrium and do not move out of position. When the pipe reaches a critical pipe length the critical hydraulic head difference over the levee ΔH_{crit} is also reached. Regardless of the ΔH an equilibrium situation can not occur anymore and the pipe will progressively erode and grow to the river side of the levee. The three differential equations are formulated in appendix A.1.

The original version of the Sellmeijer rule (4-forces rule) described above was used in Dutch engineering practice and dates back to 1994 Forster et al. (2012). Many alterations and revisions to Sellmiejer's original model were made due to the fact that vertical and horizontal gradients were questioned for experiments on coarse sands, leading to the 2-force rule Sellmeijer, de la Cruz, et al. (2011). The latest version of the Sellmeijer rule which is used in Dutch engineering practices dates back to 2009 Forster et al. (2012). The physics behind the revised rule has not changed; only the relation between the parameters and the ΔH_{crit} has been altered resulting in a more conservative piping rule where a smaller ΔH_{crit} is obtained. The 2-force rule formula reads:

$$\Delta \phi_c = F_r F_s F_g L \tag{4.4}$$

where

$$F_r = \eta \frac{\gamma_{p'}}{\gamma_w} tan\theta \left(\frac{RD}{RD_m} \right)^{0.35} \left(\frac{U}{U_m} \right) \tag{4.5}$$

$$F_s = \frac{d_{70}}{\sqrt[3]{\kappa L}} \left(\frac{d_{70,m}}{d_{70}} \right)^{0.6} \tag{4.6}$$

$$F_g = 0.91 \left(\frac{D}{L} \right)^{\frac{0.28}{\left(\frac{d}{L} \right)^{2.8} - 1} + 0.04} \tag{4.7}$$

Where:

$\Delta\phi_c$	$[m]$	the hydraulic head difference over the levee
F_r	$[-]$	the resistance term,being the strength of the sand
F_g	$[-]$	the geometry term, which depends on the ratio of the sand layer thickness sand the seepage length
F_s	$[-]$	the scale term, relating the particle size and the seepage length
L	$[m]$	horizontal seepage length
γ	$[kN/m^3]$	the volumetric weight of the sand
γ_w	$[kN/m^3]$	the volumetric weight of the water
θ	$[°]$	the bedding angle
η	$[-]$	the coefficient of White
κ	$[m^2]$	the intrinsic permeability of the piping sensitive sand layer
d_{70}	$[-]$	the particle diameter for which 70% passes through a sieve
d_{70m}	$[-]$	mean d_{70} in the small scale tests
d	$[m]$	the aquifer thickness
ϕ_c	$[m]$	the critical hydraulic head
RD	$[-]$	the relative density
RD_m	$[-]$	the average density in small-scale tests (0.725)

The design rule of Sellmeijer mentioned above in equations 4.4, 4.5, 4.6, 4.7, requires quite a number of different input parameters. To obtain the parameters a good understanding of the surrounding sub-soil conditions is required.

4.1.6. Sellmeijer (2011): Head reduction factor (0,3d rule)

Sellmeijer proposed an adaption of his previous rule where a confining cove layer is taken into consideration. In situations with a covering layer (e.g. clay and/or peat) on a piping-sensitive layer, where a vertical crack or well through the thickness, d, of the cover layer is present, the resistance created by the fluidized sand in grain uplift should be taken into consideration. Sellmeijer adapted the method to account for the reduction in the hydraulic head by 0.3 times the thickness of the cover layer.

$$(\Delta\phi - 0.3d) \leq \frac{\Delta\phi_c}{\gamma} \tag{4.8}$$

d	$[m]$	thickness of the cover layer
γ	$[-]$	safety factor, 1.2

Sellmeijer's rule only assesses the horizontal backward erosion in the piping-sensitive layer. Therefore a head reduction rule across the levee has been introduced to account for the resistance due to the fluidized sand particles in the vertical well channel Couwenberg (2021). This reduction is also known as the '0.3d rule' Forster et al. (2012).

4.1.7. Baldock, Cylinder Tests

Baldock et al. (2004) investigated the behaviour of a sand-water suspension when the flow is vertical. At a certain flow velocity and flow pressure in the sand, the sand undergoes a quicksand condition according to Terzaghi's critical heave criterion (sec:3.3.3). Starting with sand in a fixed packing on the bottom of the cylinder, the flow rate was increased, allowing the suspended sand to expand and the mixture's density to decrease. Baldock found a relationship between flow rate and the height of the sand-water suspension in the cylinder, figure 4.3. The

higher the flow rate (w_s), the higher the suspension in the column (ϕ_s) and the lower the density of the suspension.
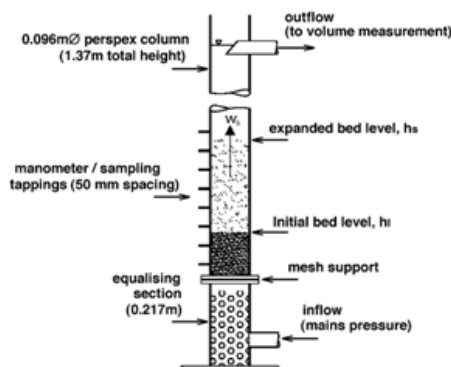

Figure 4.3: Fluidization and sediment cylinder test Baldock et al. (2004)

4.1.8. Robbins

In Robbins and Griffiths (2019) this principle of expanding suspension with increasing approach velocity has been applied to the process in a sand-carrying well. The pressure head loss in the burst channel was determined based on equations from fluid mechanics. This calculated pressure head was compared with the measured pressure head losses at two sand-carrying wells in practice: a well near IJzendoorn, along the Waal in the Lower Betuwe, with relatively coarse sand and one with fine sand along the Mississippi near Mayersville. For both situations, the pressure head loss appeared to be well explained by theory, see Figure 2 4 4. The pressure head loss at IJzendoorn was approximately 0.6 times the thickness of the top layer and at Mayersville this was almost 0. It should be noted that the thickness of the top layer was limited in both cases (approx. 1.5m). The researchers concluded that the magnitude of the pressure head loss depends on the grain diameter, the dimensions of the well (the diameter of the hole in the overburden in this case) and the flow rate in the well. The pressure head loss decreases with a decrease in grain diameter, a decrease in hole diameter and an increase in flow rate.

This study mainly provides a picture of important influencing factors that can determine pressure development. The absolute value of the measured pressures themselves cannot be applied one-to-one to other situations. Currently, there are still insufficient practical observations such as Robbins and Griffiths (2019) available to derive generic rules of thumb in which parameters such as the flow rate in the well and a grain distribution parameter of the sand under the well can be used as input. The pressure drop in the well can change during the different stages of piping due to the changing water and sand supply to the well.

4.2. Current design rules; hydraulic failure

The European Committee for Standardization (2022) commonly known as Eurocode 7 has defined multiple failure types that could occur once a pipe reaches a seepage wall, in this instance, induced by porewater pressure or porewater seepage. Figure 4.4 displays the possible failure paths from the instance that the pipe reaches the seepage wall up until levee failure, as suggested in Eurocode 7.
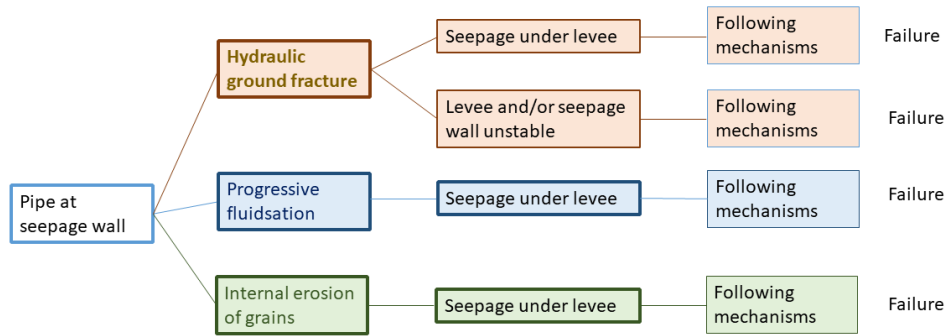
Figure 4.4: Failure path and failure node at seepage wall

4.2.1. Hydraulic ground failure

Within the concept of Eurocode 7 the safety factor for the avoidance of failure due to hydraulic heave by seepage water in the ground is based on the 1997 eurocode (EN 1997-1 §2.4.7.5 (1)P Bond et al. (2013)). The verification of resistance heave is based on Terzaghi and Peck (1964) soil column. Terzaghi and Peck (1964) introduced analytical solutions and flow nets while investigating groundwater flow and stability in excavations (section: 4.1.4). Although this method is more than half a century old, the safety factor is still based on one of the oldest heave methods calculations.

The vertical equilibrium method looks at the design value of the destabilising total pore pressure at the bottom of the column and the stabilising total vertical stress. Terzaghi and Peck (1948) suggested calculating the factor of safety against heave as

$$ SF = \frac{\sigma - u_{stat}}{u - u_{stat}} = \frac{s * \gamma' + p'}{\Delta u} \tag{4.9} $$

u_{stat} $[kN/m^2]$ Groundwater pressure in the absence of flow
p' $[kN/m^2]$ vertical overburden or surcharge pressure at the ground surface

However, it should be noted that Terzaghi clearly expressed that his derivation intended to model the heave mechanism specifically Terzaghi and Peck (1948). Despite his statement the theory, is commonly used to predict factors of safety against piping in engineering practice. The stability criterion used by contemporary engineering practice does not restrict the stability investigation to a certain pre-defined volume as it was suggested by Terzaghi but rather uses the criterion in a broad term and requires satisfying the criterion in any volume or on any surface (Garai (2016)).

Eurocode 7 (Bond et al. (2013)) requires the satisfying of two criteria for both hydraulic heave and piping. Criteria 1 investigates the equilibrium conditions of a given volume; $S < G$ (figure 4.1b). where S is the seepage force on a column, and G is the submerged weight of the same column. Criteria two investigates a horizontal surface, suggesting that the quicksand conditions must be met, section 2.3.1.

A third criterion is not mentioned in Eurocode 7 (Bond et al. (2013)), but is still widely used is that where the unit volume is investigated through the hydraulic gradient in the vertical direction with respect to the critical hydraulic gradient, equation 3.3.
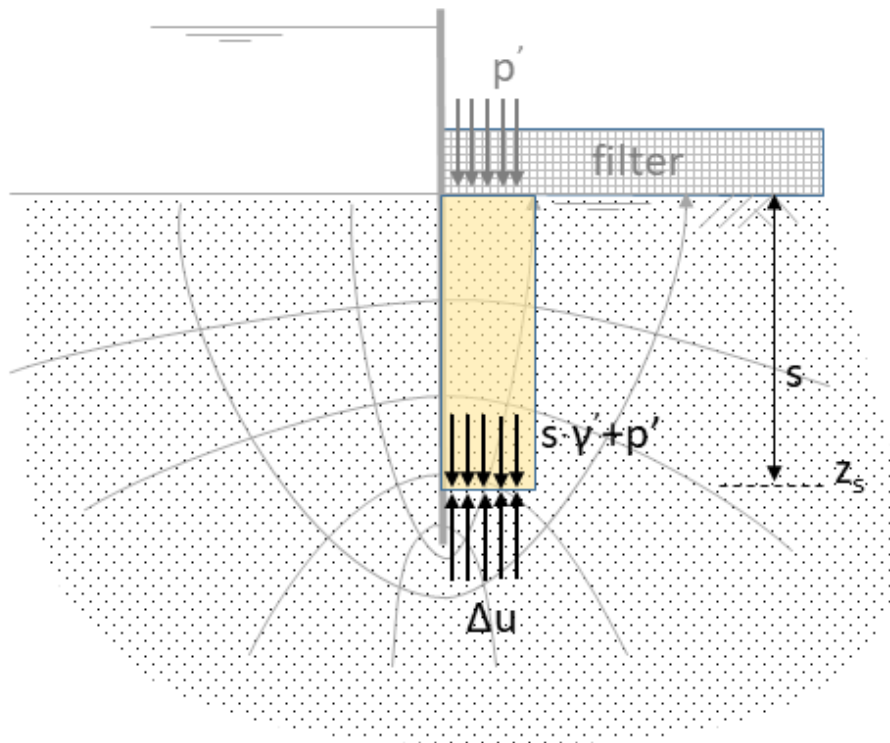
Figure 4.5: Vertical equilibrium, hydraulic heave, based off European Committee for Standardization (2022)

4.2.2. Internal grain erosion

Three stability criteria in an upward flow have been deduced from equilibrium investigations of a given volume, a horizontal surface and unit volume. These equilibrium conditions investigate the stability of a restricted part of space or plane, containing many soil particles. However, piping or sand boiling starts on the surface of the soil when an individual grain is removed. Therefore those conditions mentioned in section 4.2.1 used for hydraulic heave and piping can be considered as 'global' conditions.

Garai (2016) suggests that a 'local' equilibrium should be applied when the stability of an individual grain situated on the top of the matrix in non-cohesive soils is investigated. Garai (2016) conducted several experiments to determine the 'local' stability criterion between upward flow and grain movement on a micro level. The equilibrium of a soil grain particle, developed by Terzaghi and Peck (1948), in an upward flow can be defined by the velocity difference between the terminal velocity (v_t) of the grain and the velocity of the upward flow (v_w). The criterion for the stability of grain can be defined as:

$$v_t > v_w \tag{4.10}$$

v_t $[m/s]$ terminal velocity of the grain
v_w $[m/s]$ upward flow velocity of the water

(a) Spherical grain in an upward vertical flow

(b) Developing position instability of grain on the surface of a soil matrix in non-cohesive soil
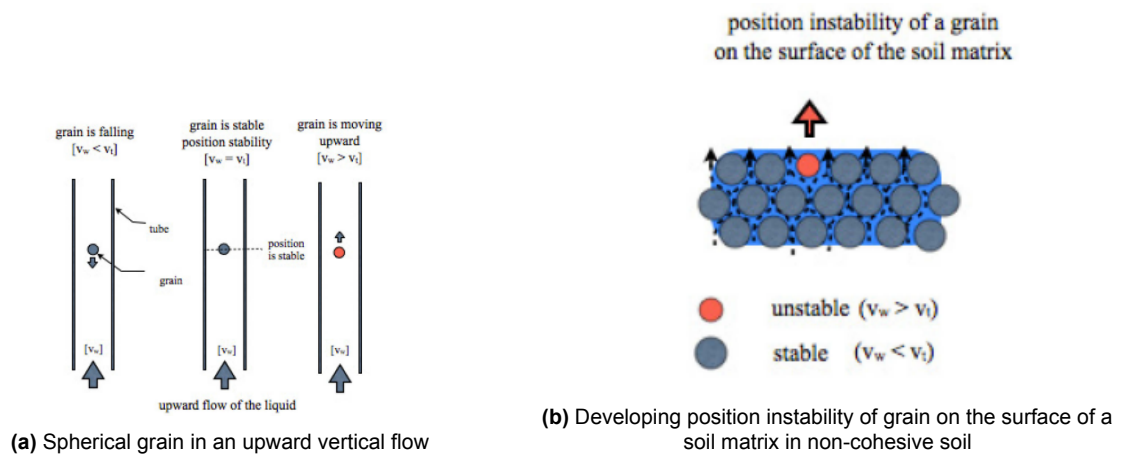
Figure 4.6: Stability investigation of a single grain Garai (2016)

Figure 4.6a presents the three types of movement a grain can experience in the vertical direction. When the terminal velocity of flow v_t is greater than upward flow v_w the grain falls in the column or remains part of a solid grain matrix. If both velocities are equal the grain is in a stable position, suspended in a thick solid-liquid state. When the upward flow has a velocity greater than the terminal velocity the suspended grains will begin to move upwards out of the soil column.

## 4.3. Factors Influencing Critical Hydraulic Gradient (i_c)

In addition to recognising each component of the physics of backward erosion piping (section: 3.3), it must be acknowledged that the individual physical parameters interact as an overall system. Knowing the physics behind backward erosion piping is the basis of understanding how one such parameter influences critical hydraulic gradients and alternatively quicksand. Water flow drives the backward erosion piping process and the soil resists it. Based on this concept the influencing factors can be easily distinguished as those that hinder pipe development and those that promote pipe development. The following influential factors discussed in this section are exit configuration, soil characteristics, cover layer thickness and seepage velocity.

4.3.1. Exit configuration

The shape of the exit is an important factor in assessing piping potential, as it dictates the flow pattern in the subsurface and the resistance near the exit (Robbins and Van Beek (2015)). Exits can be small or large, where a small exit will constrain flow. If the size of the exit is such that the flow is not restricted, the exit configuration is still a relevant parameter. de Wit (1984) conducted experiments with different types of exits (figure 4.7) while observing other characteristics, such as sand type, seepage length and thickness to observe how the exit type influences the critical gradients. de Wit (1984) determined pipe initiation requires local fluidization of the sand bed, in which the flow lines converge towards the exit, thereby creating local high hydraulic gradients. In contrast, a large exit area will not lead to converging flow lines to the same extent as a smaller exit, such that pipe initiation requires a larger overall gradient.

Recent experiments with a circular exit by van Beek (2015) indicated that the 2D Sellmeijer model overestimates the critical hydraulic gradient by approximately a factor of

2.
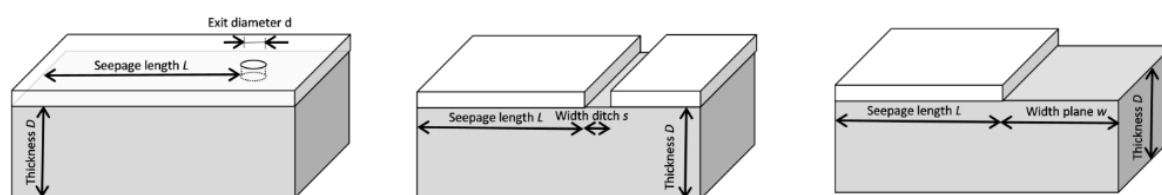
Figure 4.7: Influence of configuration on initiation gradient (experiments **J.M.deWit1984ResearchTests**)

4.3.2. Grain properties

Relative density

The relative density of the aquifer describes the state of the granular structure. Initiation of the pipe, near the exit, requires local fluidization of the grains, which occurs when the local gradient exceeds the critical heave gradient found by Terzaghi, Peck, and Gholamreza (1996) (introduced in section 3.3.3).

$$i_c = \frac{G_s - 1}{1 + e}$$

(4.11)

Where:

G_s	$[kg/m^3]$	specific gravity of solid soil particles
e	$[-]$	void ratio of soil

Being dependent on porosity, the critical heave gradient is lower for loose samples than for dense samples. Dense samples can provide additional strength due to the interlocking of grains and dilatancy, pneumonia where soils under pressure become viscous (van Beek, Bezuijen, and Sellmeijer (2013)).

The influence of relative density on pipe progression is more complex. A loosely packed bed, ensues easier fluidization of the pipe, due to the lower critical hydraulic gradient. Next to this, loosely packed beds are more permeable and more flow can enter the pipe, creating more drag on the particles in the pipe bed. In turn, easily eroded to their loose state while in a loosely packed bed. The resistance of the pipe is therefore expected to be lower, favouring pipe development near the pipe head.

Grain Size

The grain size of the moving particles in the pipe affects many of the other parameters in the process. The grain size in the aquifer affects the permeability of the sandy layer and in turn also the hydraulic conductivity. Aquifers consisting of finer grains often have a lower hydraulic conductivity, resulting in higher hydraulic gradients. Fluidisation highly depends on the grain properties, where the weight of the particles determines the moment of expansion in the pipe, the moment the mixture becomes a fluid sand-water combination. Baldock et al. (2004) determined the relation between examination porosity and flow velocity. The higher the porosity of the solution the higher the velocity.

4.3.3. Role of cohesion

Cohesion is a measure in soil mechanics that, together with the coefficient of friction determines the strength of the soil against shear failure. Shear failure and uplift are mechanisms that usually go hand in hand. Uplift occurs when the normal stress (in tension) exceeds the

tensile strength. In soils, tensile strength is usually zero, which means that uplift can occur at zero effective normal stress. But in the absence of cohesion, the shear strength is also zero at zero effective normal stress.

Greater cohesion means strength. Van Leeuwen (2008) says *"it is very likely that the cohesive sealing soil layer offers some resistance to distortion. This is because the cohesive ground material has some tensile strength, which means that the base layer can behave like a beam. This can cause local instabilities worked against"*.

Cohesion in sand is nil or absent, with clay and peat known to have generally little cohesion. Literature on the influence of cohesion on the cracking process is unknown, however, based on theoretical considerations, several expectations have been established (hypotheses or postulates) by Erkens et al. (2019):

- Cohesion makes it probable that the layer in question, at the limit potential is first lifted (floats up), detaching (delaminating) from the underlying non-cohesive well-permeable material (often sand).
- The intervening space fills with water; a water cushion is formed.
- As the water cushion grows, the length of the bottom of the lifted increases low; this creates a stretch in the bottom of this layer.
- Bursting will occur if the strain is sufficiently large. Greater cohesion is possible to delay the moment of eruption and be accompanied by the formation of a larger water cushion and greater uplift at ground level. With great cohesion, it is conceivable that equilibrium is reached without any eruption taking place. During the growth of the bubble, the water pressure at the base of the lifted layer decreases.

4.4. Summary

Experiments and field observations have made a general description of the piping process possible, however, certain failure nodes of the failure path have been investigated more than others. The piping process after uplift and heave has been extensively researched by many, with and without a confining cover layer. The hydraulic heave process has only been investigated without a confining cover layer.

Terzaghi and Peck (1948) performed experiments, carrying on from work completed by Bligh (1910), Lane (1934) and Harza (1935), on construction pits with varying water levels, where no confining cover layer was present. A fluidization zone with half its depth was observed. From these experiments, the fundamental theory and formulas for hydraulic heave have been established, including the vertical equilibrium method for grain movement.

Since Bligh (1910) produced one of the first and foremost design rules concerning piping, many variations and additions have been made. Many of such alterations and variations do not take into consideration the effect of a confining cover layer being present. An adaption of Bligh was created for Dutch levee design, where a gradient reduction rule was implemented. However, this reduction factor is highly contested among engineers, depending greatly on grain parameters and flow velocity.

Through the formulation of the backward erosion failure path (van Beek, Noordman, et al. (2019), van Beek, Robbins, et al. (2022) and van Beek, Bezuijen, and Sellmeijer (2013)), mitigation methods, such as a seepage wall were constructed. A seepage wall reduces the

concentration of flow under the levee system, instead forcing flow to navigate down and around the wall. At the lowest point of the barrier, flow disperses out, reducing the possibility of piping to occur.

To determine the depth of a mitigation measure, Eurocode 7 states that the hydraulic heave zone needs to be determined, using a more than half-a-century-old Terzaghi and Peck (1948) method. No model is available for determining hydraulic heave where a confining layer is present, therefore Terzaghi and Peck (1948) is suggested in combination with a safety factor and an addition model. This results in a highly over-conservative mitigation measure. Eurocode 7 also suggests another model that can be used to determine the hydraulic heave zone, the internal grain erosion method, but this is not applicable in the Netherlands due to the grain properties not meeting the requirements.

Part II

Research

5

Groundwater flow calculations

5.1. Introduction

The review of the literature and the analysis of the backward erosion piping failure path in the context of a system with a confining cover layer have led to several unanswered questions about the effect of such a layer on hydraulic heave.

This chapter aims to conduct numerical groundwater models in the PLAXIS software, and how, ultimately a seepage wall as a mitigation measure may prevent backward erosion piping. Terzaghi and Peck (1964)'s research was used as the baseline for the model geometry and soil parameters. Two models are considered; without a confining cover layer and with a confining cover layer. Within the two models, several input parameters were altered to understand how such parameters affect the groundwater flow through the system.

A sensitivity analysis is conducted to get insight into the case-dependent sensitivity of the varied input parameters

5.2. General Model Set-up

Careful consideration was taken into account during the creation of the PLAXIS model, ensuring that all the right boundary conditions were applied.

(a) Without a confining cover layer **(b)** With confining cover layer
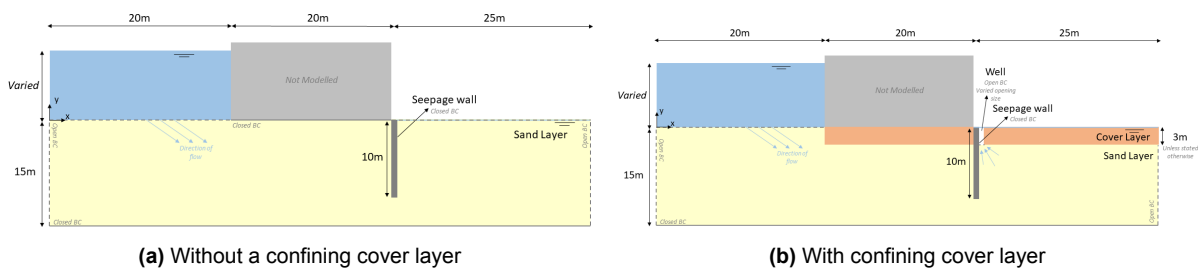
Figure 5.1: Schematic of the PLAXIS models

5.2.1. Geometry and Boundary Conditions

Two types of model set-ups were used for the numerical modelling in PLAXIS, varying slightly in geometry and boundary conditions, figure 5.1. Levee geometry is greatly determined by its surroundings and soil properties, therefore for this study, a generic levee geometry was

designed, based on Sellmeijer (1988) experiments. A 20m wide, 10m high rectangular levee, was situated on a 15m foundation of non-cohesive sand. Left and right of the levee are open boundaries allowing water to flow from the high water side (left) to the hinterland (right). At the x-axis minimum and maximum points, the boundary is open, allowing water to flow out of the system along this boundary. The bottom boundary, y-min is closed, and no flow is allowed to flow through.

During the flow calculations, the 'levee' block is not modelled (figure 5.2), rather a no-flow boundary or closed boundary was inserted along the $y = 0$ boundary. Flow calculations in PLAXIS do not calculate stresses and deformations, only looking at flow through a structure, therefore, the weight and deformation caused by the levee on the subsoil are neglected. A seepage wall of 10 meters is placed at the toe of the levee, with also a no-flow boundary, forcing the water to travel down and around the wall.

Slight alterations were conducted for the model where a confining cover layer is present (figure 6.3b). A nearly impermeable cover layer is introduced. This layer is considered closed and will be referred to from here on out as an impermeable boundary. Unless stated otherwise a 2m cover layer is used in the calculations.

The confining cover layer must undergo uplift or a defect must be present through the layer to allow flow to the hinterland. Following the backward erosion piping failure path (figure 3.4) and for the model's purpose, horizontal piping (failure node 5) is not considered. Only vertical hydraulic heave along a supposed seepage wall is considered (failure node 6). All failure nodes up until failure node 5 are considered to have occurred. An opening of $0.5m$ is used unless otherwise specified. Within the well only flushed clean water is present, the phreatic water line is located at the top of the well.

5.2.2. General Input Parameters

Table 5.1 presents the soil properties of the sand and cover layer. Within this section soil properties and parameters were altered to understand the importance and impact of the hydraulic gradient at the top of the model. There are various types of soils, classified into three types; Sand, Loam and Clay, based on their composition. The soil parameters used for the confining cover layer, porous sand layer and identified fluidization zone were verified from multiple sources Verruijt (2001), van Beek, Bezuijen, and Sellmeijer (2013), Bentley (2022) and Terzaghi and Peck (1964) to establish a likely soil parameter profile for a case in the Netherlands.

Parameter	Name	Cover layer	Subsoil	Unit
General				
Soil model	Model	Mohr-Coulomb	Mohr-Coulomb	-
Drainage type	Type	Drained	Drained	-
Unsaturated unit weight	γ_{unsat}	16	20	kN/m^3
Saturated unit weight	γ_{sat}	17	21	kN/m^3
Mechanical				
Young's modulus	E'_{ref}	$20 * 10^3$	$50 * 10^3$	kN/m^2
Poisson's ratio	υ	0.33	0.3	-
Cohesion	c'_{ref}	5	1	kN/m^2
Friction angle	φ'	31	35	$\circ$
Dilatancy angle	ψ	1	5	$\circ$
Groundwater				
Horizontal permeability	k_x	$0.1 * 10^{-3}$	*Varied*	m/day
Vertical permeability	k_y	$0.1 * 10^{-3}$	*Varied*	m/day

Table 5.1: Material properties of the dam and subsoil, case Terzaghi with cover layer

Sand is considered cohesionless, but PLAXIS is unable to work with small values of cohesion and tensile strength due to numerical issues alternately leading to stability problems, therefore has been set to a value of $c = 1kN/m^2$.

To access the effect of certain parameters on the hydraulic gradient behind the screen the parameters were altered for both calculations as follows:

- Water levels; $2m$, $4m$, $6m$ and $8m$ to simulate how the rise in water will affect the system
- Horizontal and vertical permeability;

    - isotropic $k_h = 10m/day$ and $k_v = 10m/day$
    - anisotropic $k_h = 30m/day$ and $k_v = 10m/day$

Introducing the confining cover layer into the calculation inserts more boundary conditions and parameters. The confining layer acts as a closed, no-flow boundary to the hinterland, forcing the water through the well created. Therefore the additional parameters were altered to investigate their importance.

- Well opening; $0.25m$, $0.5m$, $0.75m$ and $1m$
- Impermeable cover layer thickness; $1m$, $2m$ and $4m$

5.3. Situation without cover layer

Terzaghi and Sellmeijer conducted many experiments and research considering excavation pits and levees with free exit flow. To provide a baseline and a better understanding of the flow under a levee, the situation of a free exit flow was reproduced in PLAXIS.
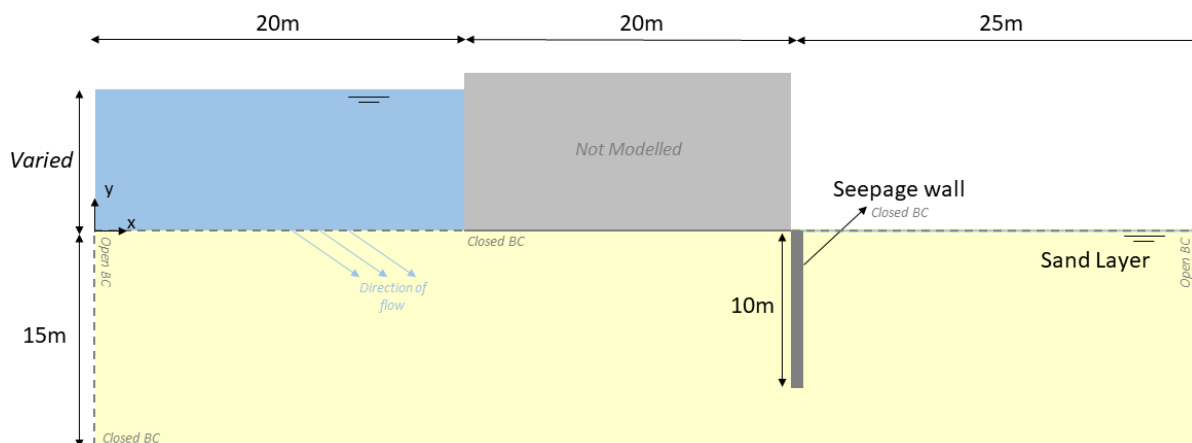
Figure 5.2: Schematic of the PLAXIS model without a cover layer

5.3.1. Groundwater head (ϕ) and Flow (q)

Groundwater head and flow share a perpendicular relationship, Darcy's law 2.1, often presented in the form of flow nets (figure 5.4). A flow net is a graphical representation of the flow of water through a soil mass, the combination of the flow path (flow lines, figure 5.3b) and an equal total head (equipotential lines, figure 5.3a). Key points to note concerning flow nets are the angle of intersection between each flow line the equipotential line must be $90°$ and two flow lines or equipotential lines must never cross one another. Flow nets provide valuable information about how the flow behaves in the system.

A flow net is not a standard representation created by PLAXIS Output therefore Figure 5.4 is a manual representation, combining the PLAXIS groundwater flow and head (figure 5.3) output using the rules mentioned above. A representation of the levee has been inserted into the figure to show the location within the model.
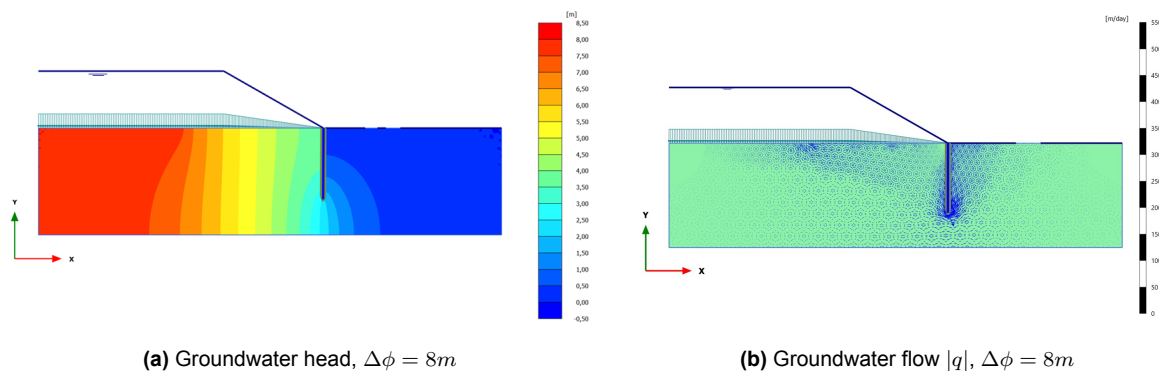

(a) Groundwater head, $\Delta\phi = 8m$ **(b)** Groundwater flow $|q|$, $\Delta\phi = 8m$

Figure 5.3: Flow Calculations, $\Delta\phi = 8m$

Flow

Always seeking the quickest path of least resistance, a high concentration of flow is expected at the left corner of the levee boundary as water tries to avoid the boundary. Water continues to travel close to the underside of the closed 'levee' boundary, indicated by the perpendicular head contours and parallel flow lines close to the boundary. Water entering further from the levee boundary travels further vertically down before traversing parallel to the levee but at a lesser concentration.
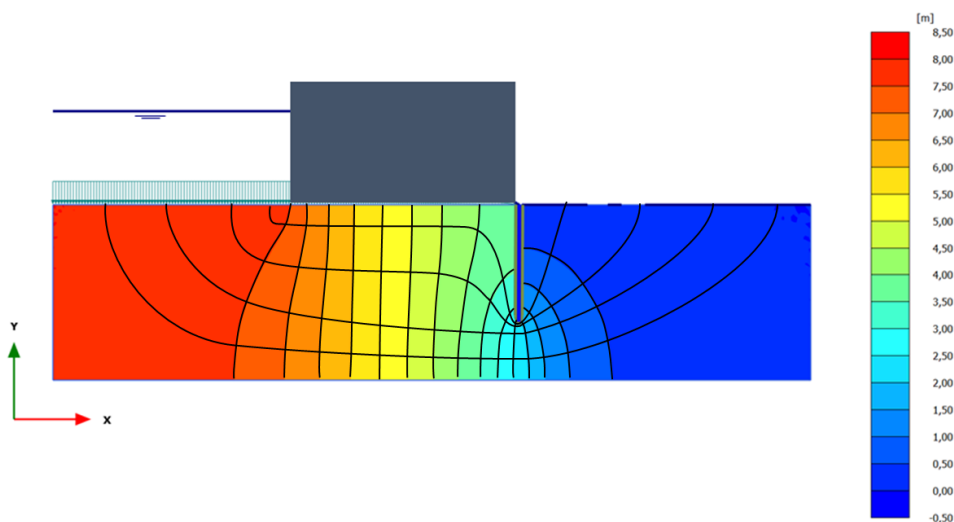
Figure 5.4: Flow net, no confining cover (manually drawn)

The placement of a seepage wall is an obstacle for the water trying to reach the region of the lowest hydraulic head. Flow is forced down and around the wall, creating two interesting points within the flow:

- A stagnation point is observed in the flow figure (figure 5.3b) to the left of the seepage wall. When the flow is blocked by the seepage wall and begins to travel in the vertical direction, an area is bypassed. Flow does not travel at right angles when not forced, bypassing this area, and creating an area with near-zero flow velocity.
- Figure 5.3b indicates extreme groundwater flow rates at the tip of the seepage wall. Although the flow rates were expected to be high at this point, the flow velocity arrow in figure 5.3b is considered out of proportion, resulting from numerical inconsistencies within the model. Results considered out of bounds were removed from the data and not displayed in the plots.

Hydraulic Head

While the figures discussed above considered the case where $\Delta\phi = 8m$, multiple cases were modelled with different hydraulic heads across the system, in isotropic soil conditions.
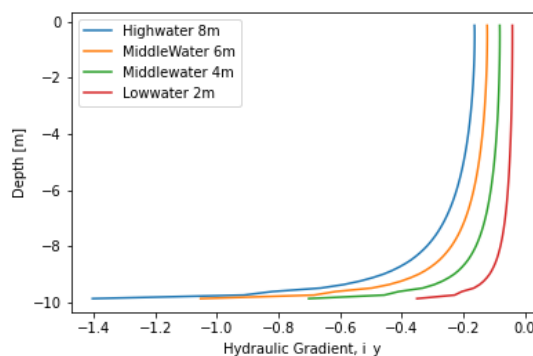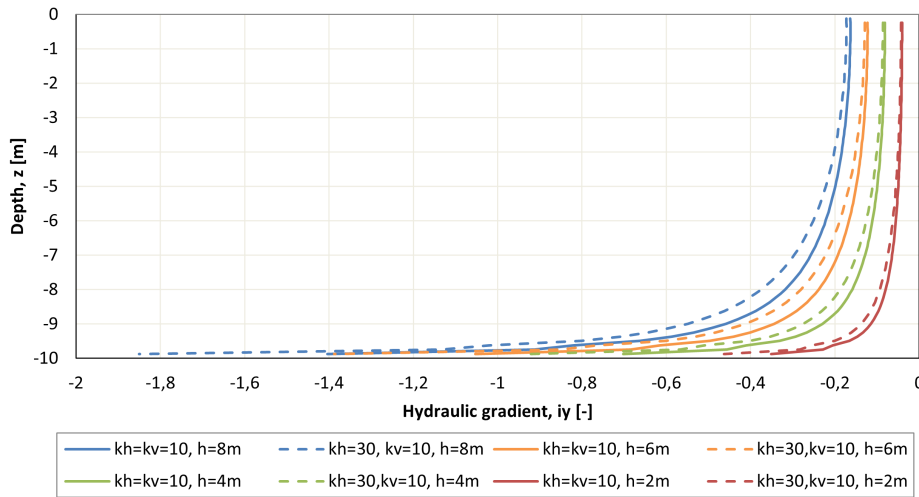

Figure 5.5: Hydraulic Gradient, Isotropic hydraulic conductivity over multiple head differences

The hydraulic gradient along the length of the seepage wall is portrayed in figure 5.5, for an isotropic situation, with altering head differences over the entire system. All the water levels produce a hydraulic gradient peak at the seepage wall tip, with varying degrees of magnitude. Following Darcy's law $q = ki$, a high water level ensures a greater flow concentration at the seepage wall tip, resulting in a greater hydraulic gradient compared to that where a lower water level is in play. Immediately after rounding the tip the gradient sharply falls, as the water spreads out travelling upwards to the open surface.

5.3.2. Hydraulic Conductivity

Darcy's law states that the hydraulic gradient i is a function of the groundwater flow (figure 5.3b) and the hydraulic permeability k of the soil. Two conditions were modelled to determine whether for this case Darcy's law holds. Isotropic hydraulic conductivity ($k_h = k_v = 10m/day$) and anisotropic hydraulic conductivity ($k_h = 10m/day, k_v = 30m/day$) conditions were investigated throughout the entire soil package. Figure 5.6 provides the relation between isotropic and anisotropic hydraulic permeability situations concerning different $\Delta\phi$.

Figure 5.6: Hydraulic gradient over different water levels and permeability's, $2m$ cover layer thickness. Solid and dashed lines represent an isotropic and anisotropic situation respectively.

Darcy's law concerning two-dimensional; anisotropic behaviours can be formulated from all the directions in the system, x- and y-directions. Expanding equation 2.1 into the following

$$v_x = -k_x \frac{\partial \phi}{\partial x} = k_h i_x$$
$$v_y = -k_y \frac{\partial \phi}{\partial y} = k_v i_y$$

$$(5.1)$$

Following the definition of permeability, the higher the k value the more porous the material will be, and more flow will flow through an area with time. At the tip of the seepage wall, figure 5.6 indicates a sharp increase in the hydraulic gradient, especially in the anisotropic conditions (dashed lines). At the tip of the seepage wall, the flow is flowing around the tip of the wall, travelling primarily in the horizontal direction before transversing upwards. This point of high flow concentration experiences a greater flow velocity when the soil is under anisotropic conditions because of having greater permeability in the horizontal direction, and less flow resistance. From equation 2.1 the greater the hydraulic gradient will be when the

hydraulic conductivity and flow velocity increase.

As the flow travels further to the region of the least head, the effect of the horizontal permeability will decrease as the flow increasingly flows in a near-vertical direction. This explains why at the top of the wall the hydraulic gradient of the isotropic and anisotropic cases a nearly equal, and values of the vertical permeability k_v are the same.

5.3.3. Model Validation

Eurocode 7 (European Committee for Standardization (2022)) hydraulic heave design rule was used to verify the model. Along the vertical axis located close to the seepage wall ($x = 4.25$) the hydraulic head values were extracted from PLAXIS to calculate the safety factor of heave occurring along this axis. Equation 4.9 states that the safety factor is the relationship between the downward pressure and upward water pressure. The porewater pressure difference, figure 5.7a, involves the hydrostatic situation and the situation where flow is present ($\phi = 8m$).
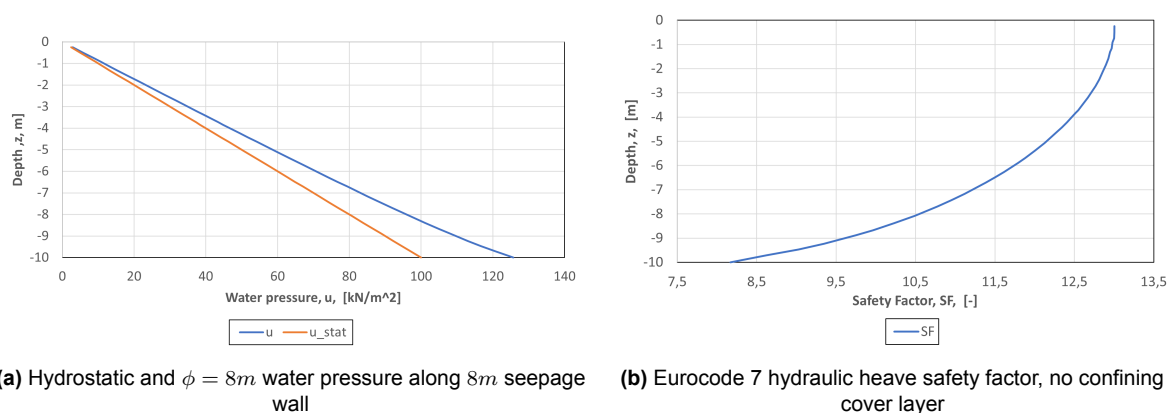

(a) Hydrostatic and $\phi = 8m$ water pressure along $8m$ seepage wall

(b) Eurocode 7 hydraulic heave safety factor, no confining cover layer

Figure 5.7: Groundwater flow model verification

When the calculated safety factor is greater than 1 is the area considered to be safe from hydraulic heave. Flow velocity is greatest at the tip of the seepage wall resulting in the lowest safety factor, as seen in figure 5.7b. However, the seepage wall tip of the grains is still located in a tightly packed soil layer unable to fluidize, even when the safety factor is less than 0. Fluidization must occur at the surface first and travel to the seepage wall tip.

Porewater pressure at the surface level is $0kN/m^2$, due to the water escaping out of the system in combination with the flow having no exit restrictions. Not allowing the conditions to build up pressure for uplift or increase flow velocity to initiate fluidization.

5.3.4. Summary: Groundwater flow model without confining cover layer

With the placement of a seepage wall as a mitigation measure against backward erosion piping, the flow must find a new path of least resistance from the highest hydraulic head region to the lowest. In this case, the river to the polder side, forcing the flow to find an alternative path, down and around the seepage wall. The flow path detour reduces the hydraulic head due to the sudden vertical path. Flow nets are an effective method to analyse the flow of a system. Where the flow lines merge closer together the flow has increased velocity than in areas where those lines are further apart. Deducted from the flow net once the high concentration of flow rounds the tip of the seepage wall, the flow travels back upwards to the surface but loses concentration along the way. Flow exits the surface over a greater area.

The high hydraulic gradient located at the tip of the seepage wall, due to the high con-
centration of velocity, is of no concern about hydraulic heave as the surrounding soil is still
fixed in a matrix, preventing the soil particles from fluidizing.

5.4. Situation with cover layer

Continuing from the model presented in the previous section, 5.3, this chapter will discuss
the model with a confining cover layer, this situation will consist of a confining cover layer,
stretching under the polder and dike, as shown in figure 5.8. A crack through the cover layer
has been implemented, to act as a well, uplift is assumed to have already occurred, and will
not be modelled.

The freedom of groundwater flow is reduced through the low permeable layer above
the sand, with the well being the only exit point to the phreatic water level situated on top of
the cover layer. The two-meter confining cover layer was used in all the calculations unless
stated otherwise.
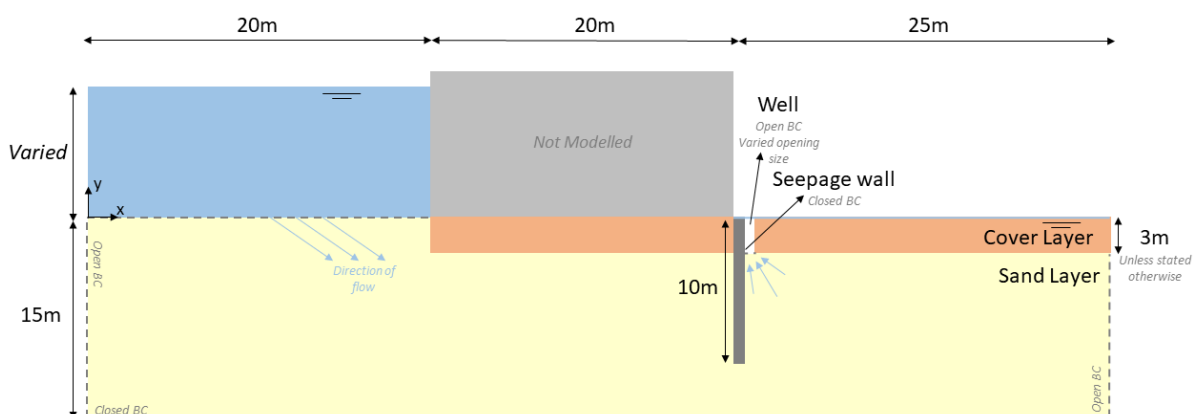
Figure 5.8: Schematic of the Plaxis model without a confining cover layer

5.4.1. Boundary conditions

The addition of the cover layer adds extra complexity to the model requiring additional bound-
ary conditions to ensure that the parameters under investigation are solely investigated.

Flow conditions
Implementing the impermeable cover layer under the levee and polder alters the path of flow.
Water is unable to reach the region of the low head, increasing the water pressure until uplift
and heave occur, creating a crack or well. A clean flushed well (no sediments, only water) is
modelled through the confining layer.

Limit potential and head reduction rule
Water pressures under the cover layer are expected to build, potentially causing the layer to
bulge upwards until a crack occurs. To ensure that the cover layer remains in hydrostatic
equilibrium throughout the process (uplift and cover layer bulging are outside the scope of this
thesis), the cover layer limit potential must be determined through equation 3.2.

5.4.2. Groundwater head (ϕ) and flow $|q|$

Figures 5.9a and 5.9b respectively show the groundwater head and flow for the situation of a cover layer beneath the dike and polder. A hydraulic head difference is enforced over the entire system. Compared to the situation in section 5.3.1, the water does not have free flow to the region of the lowest hydraulic head, located above the cover layer. The cover layer resists this, forcing the flow through the well at the toe of the dike, represented by the high flow concentrations in figure 5.9b.

(a) Groundwater head, $\Delta\phi = 8m$ **(b)** Groundwater flow $|q|$, $\Delta\phi = 8m$
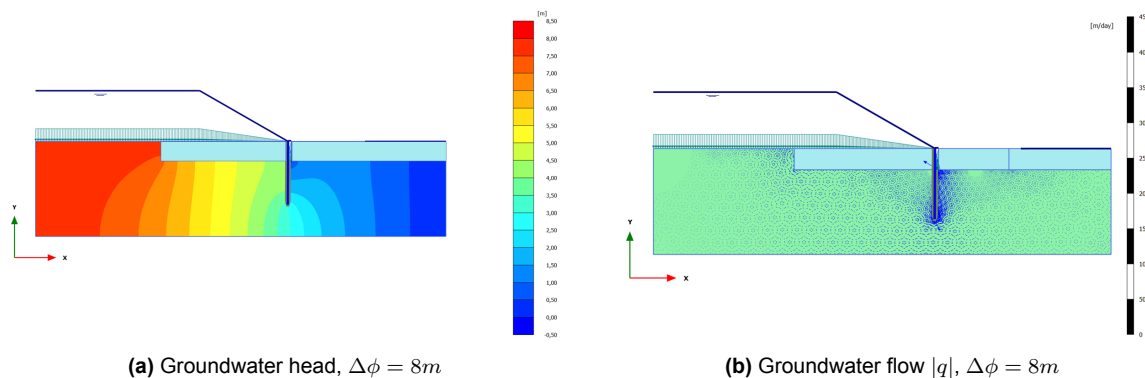
Figure 5.9: Flow Calculations, $\Delta\phi = 8m$

A flow net (figure 5.10) was produced combining the figures 5.9a and 5.9.
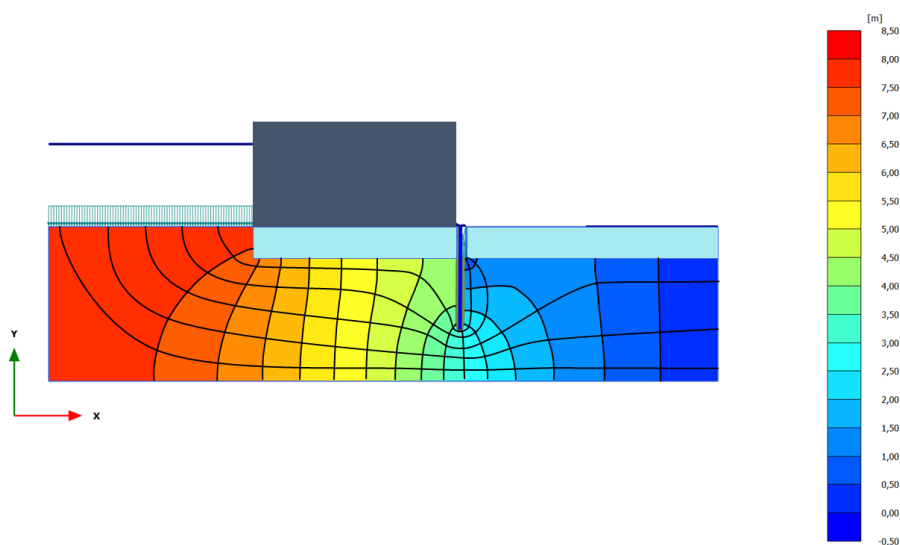
Figure 5.10: Flow net, confining cover layer (manually drawn)

Flow

Figure 5.9b shows that the flow bears many similarities with the flow diagram where no cover layer is present (figure 5.3b). Water travels from the higher region to the lower region with high-velocity concentrations located at the bottom left corner of the dike and tip of the seepage wall. After rounding the seepage wall tip the dynamics of the flow changes. Flow does not have free outflow along the entire length of the polder, but rather on a single exit point, the well. The restricted exit flow leads to a peak in the hydraulic gradient seen in figure 5.11.
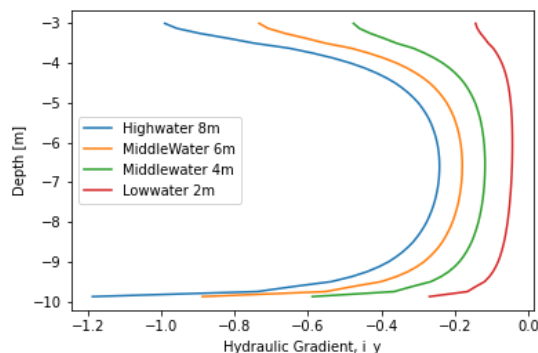
Figure 5.11: Hydraulic Gradient, Isotropic hydraulic conductivity over multiple head differences

Four water level situations are portrayed in figure 5.11 to assess the effect of high water on the system, while the other parameters remain constant throughout. Darcy's law (equation 2.1), $i = \Delta\phi/\Delta y$, states that as the hydraulic head increases over a certain y-length, the hydraulic gradient proportionally increases. Flow is restricted by the cover layer, creating a large hydraulic head change over a small vertical length. As the hydraulic conductivity is constant, this, in turn, concludes with an increase in flow velocity ($q = -ki$, equation 2.1).

Three points of high flow velocity are produced from the created flow net, figure 5.10. Flow velocity is greatest at the points where the flow lines are the closest to each other; cover layer corner with the free exit boundary, bottom of seepage wall and entrance to well. Although the cover layer corner is now 2 meters under the surface compared to the free flow case, the flow behaviour will be the same. The same goes for the point at the tip seepage wall. At the entrance to the well, the flow follows Darcy's equations as explained above.

Through the confined cover layer, a well is present, allowing the water to escape to the lowest region of the hydraulic head. Figure 5.12 displays a close-up of of the flow figure, figure 5.9. A condition within the well is that the well is full of clean flushed water where the hydraulic head is consistent with the imposed water level. It is considered that the well is hydrostatic, hydraulic head constant throughout, which explains why the hydraulic gradient is zero along the depths of 0 to 3m.
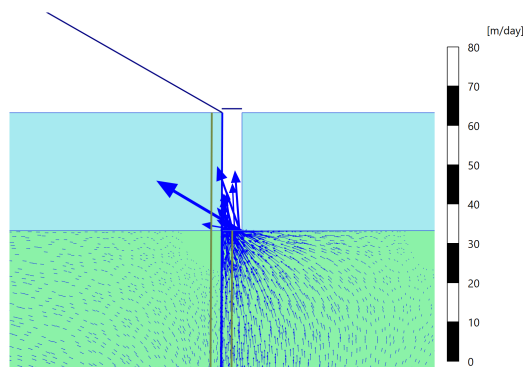

Figure 5.12: Close up well: Groundwater flow $|q|$, $\Delta\phi = 8m$

At the sand-well interface, a high concentration of velocity arrows can be seen in figure **??**. This is the point of the lowest hydraulic head within the entire system. The flow is funnelled to this point as a result of all the restrictions having been placed on the system. The arrows are proportionally large compared to those in the sand layer, which is due to the drastic drop in pore water pressure at the interface. The flow arrives at this point from all angles, vertically and horizontally, in a varied degree of concentration.

5.4.3. Hydraulic Conductivity

Hydraulic permeability is another key parameter within Darcy's equations (2.1). Two different conditions of hydraulic conductivity will be investigated, isotropic ($k_h = k_v = 10m/day$) and anisotropic ($k_h = 3m/day$, $k_v = 10m/day$). Results are displayed in figure 5.13 and display a unique behaviour.
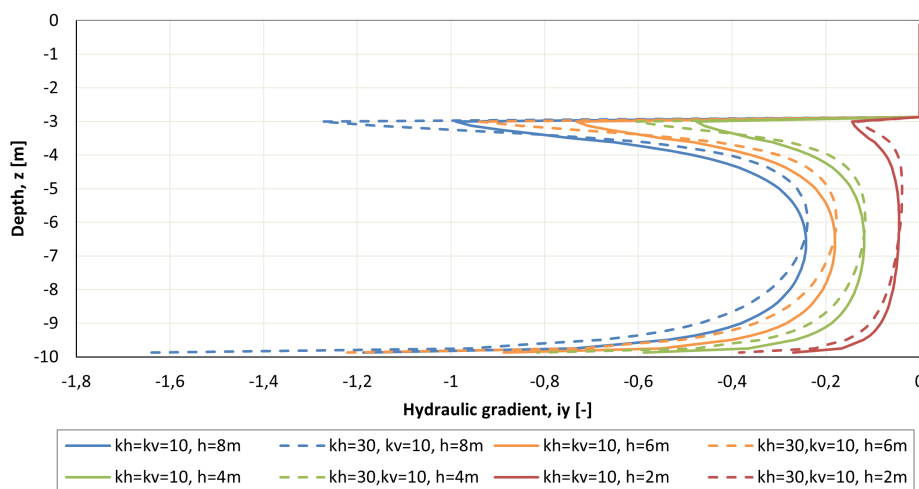
Figure 5.13: Isotropic and anisotropic hydraulic permeability's, at different head levels

All anisotropic cases (dashed) showed a higher hydraulic gradient peak at good entrance ($-3m$) and seepage wall tip ($-10m$) than the corresponding isotropic (solid) cases. This behaviour can be related to the direction (s) and velocity (q) of flow at these locations, flow travels predominately fast and horizontally. Permeability during the anisotropic case is greater in the horizontal direction, allowing flow to travel easier and faster in this direction. Following Darcys, equation 2.1, a greater permeability in the x-direction results in a greater flow velocity q_x. Immediately after rounding the seepage wall tip, the pressure and horizontal velocity of the water and the notion to reach the lowest head region the quickest, the flow shoots upwards in a vertical direction. The peak is instant and subsides almost just as soon as the pressure reduces when flow spreads out. At the entrance of the wells, large amounts of flow trapped under the cover layer also travel horizontally towards the exit where it shoots upwards, again ensuring a greater gradient in the vertical direction at this point compared to the isotropic situation.

The anisotropic cases display a lower hydraulic gradient than the isotropic case between the depths of $-3.75m$ and $-6.5m$ ($\Delta\phi = 8m$) seepage wall length. Flow within this region is highly spread out under the cover layer with greater horizontal flow velocity towards the well entrance. Low vertical velocity ensures a lesser hydraulic gradient in this region.

5.4.4. Well opening

Terzaghi and Peck (1948) never fully considered a constricted flow exit when formulating the hydraulic heave equations used today in the design process. Establishing to what extent the cover layer properties have on these processes is critical to the design process. This section aims to determine whether or not the following statement can be considered; it is expected that when the well opening size were to increase significantly, Terzaghi's free exit calculations would become dominant converging to the results presented in section 5.3.

Four different well openings, $0.2m$, $0.5m$, 0.75 and $1m$, were implemented into the isotropic 2m cover layer calculation. The well length is kept constant ($8m$) and the initial water level is kept at $\phi = 8m$.

When the well is small the pressure build-up is greater, with the well acting as a valve, where water at the point of the well entrance will have the greatest velocity, shooting upwards. Increasing the well size, the situation represents more and more the Terzaghi situation with no cover layer, where water flow is allowed to flow freely, not restricted by the cover layer. The peak at $3m$ reduces with each increasing step in well opening size, presenting more like Terzaghi's free exit calculations.
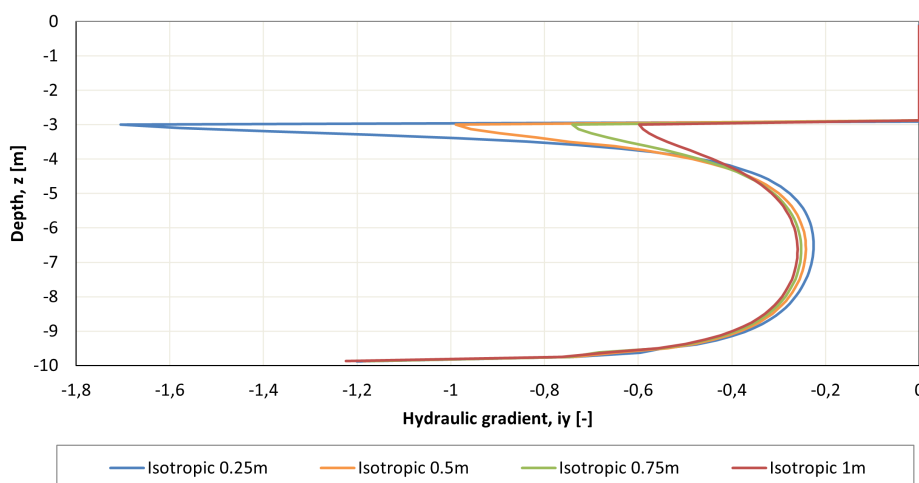
Figure 5.14: Well size, $\Delta\phi = 8$

5.4.5. Confining Cover Layer Thickness

A confining cover layer is never of equal thickness varying between project locations, even locations within projects. With a thicker cover layer, more weight is placed on the sand subsoil underneath, compacting and altering the stress distribution of the sand layer. The curves in figure 5.15 display the results of two water level situations, $\phi = 8m$ (solid line) and $\phi = 2m$ (dashed line) with various cover layer thicknesses; $4m$, $3m$, $2m$ and $4m$.
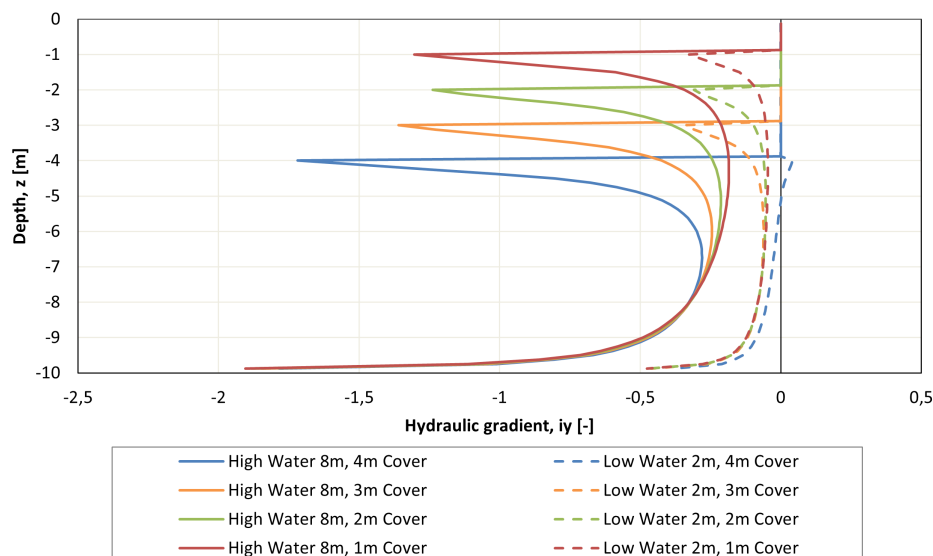
Figure 5.15: Confining cover layer thickness

Two hydraulic gradient peaks are visible at the tip of the seepage wall and the entrance of the well. The entrance of the well moves vertically due to the cover layer varying in thickness. The peaks corresponding to a cover layer thickness of $1m$, $2m$, and $3m$ at the well entrance have a hydraulic gradient at around $-1.3m$ for both high and low water levels.

The flow of water is not affected by the confining cover layer at the depth of the seepage wall tip ($-10m$), resulting in all the curves beginning at the same hydraulic gradient corresponding to the respective water levels. Once at the depth of approximately $-7.5m$, the curves begin to show variations in gradient.

5.4.6. Model Validation

This model was also verified using the Eurocode 7 safety factor (equation 4.9). The confining cover layer is considered non-porous or impermeable, preventing flow from travelling through. When the flow is present in the system, the cover remains always hydrostatic, displayed in the water pressure figure 5.16a. Water pressure on the sand directly under the cover layer is determined by the thickness of the layer and the density of water. The absence of flow through the sand layer ensures that in this situation the sand layer is also portraying hydrostatic conditions, with pressure only dependent on water density and depth.

Using the Terzaghi and Peck (1964) vertical equilibrium equation the safety factor was determined along the vertical axis under the well ($x = 4.25m$) and the confining cover layer immediately next to the well ($x = 4.75m$). Safety factors less than one are deemed unsafe, risk of hydraulic heave is high.

Figure 5.16b shows the impact of a cover layer and the risk of hydraulic heave. The cover layer ensures that the flow is restricted with concerns to the exit position, forcing most of the flow to exit via the well, creating a high concentration of flow and loss of water pressure just below the entrance to the well. At this location, ($x = 4.5$, $y = -3m$), the safety factor is noted to have a value of $SF > 15$ (figure 5.16b, point located off the plot), with no risk of hydraulic heave.

At the location just next to the well, directly under the cover layer ($x = 4.75m$, $y = -3m$), pore pressure does not experience a sudden drop in pore water pressure as water is unable to escape from under the confining cover layer, resulting in a lower safety factor $SF = 11$.

It has been determined in PLAXIS that a seepage wall increases flow concentration at the seepage wall tip (section 5.4.2), causing high pressures to occur, as seen in figure 5.16a. Correspondingly the safety factor is closest to one at this point, indicating the location most at risk of hydraulic heave. However, the grains are tightly packed together resulting in grains having no place to move to, resulting in no fluidization. At the location situated under the confining cover layer $0.5m$ horizontally away from the seepage wall tip, the safety factor is greater than that next to the tip as a result of the reduced water pressure.
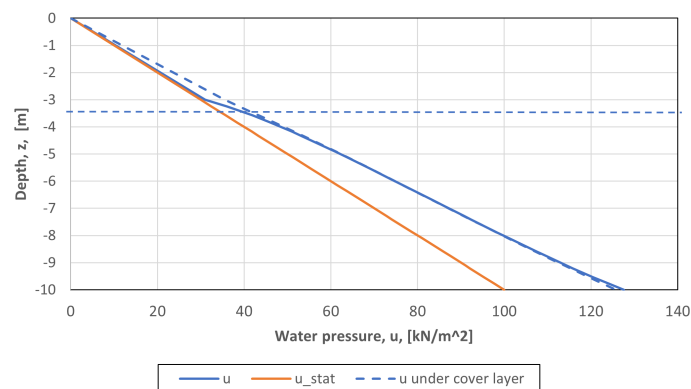
(a) Hydrostatic and $\phi = 8m$ water pressure along seepage wall
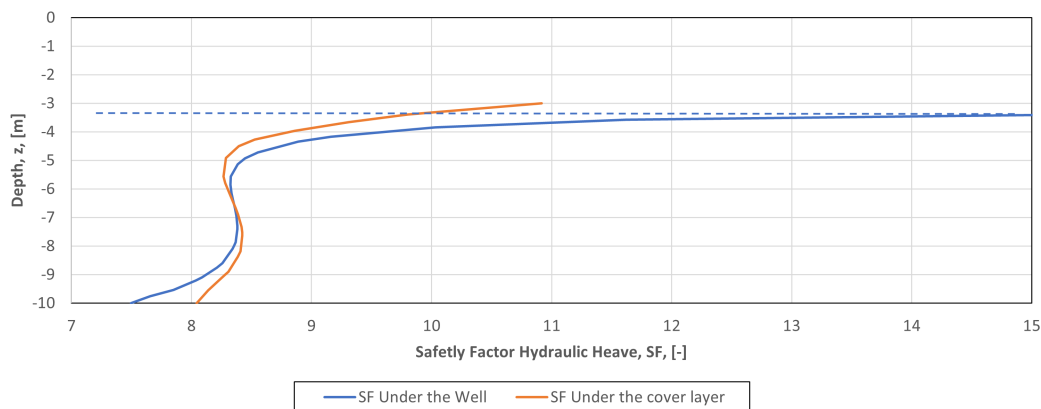
(b) Eurocode 7 hydraulic heave safety factor, confining cover layer

Figure 5.16: Groundwater flow confining cover layer model verification

5.5. Conclusions

Conducting simple groundwater models without (section: 5.3) and with a confining cover layer present (section: 5.4) has been able to reinforce and establish important relationships between hydraulic heave, hydraulic gradient and model parameters, such as hydraulic conductivity, well opening size, and confining cover layer thickness.

An unrestricted flow exit model, based on Terzaghi and Peck (1948), where a seepage wall as a mitigation measure is present, was modelled. Terzaghi and Peck (1948) formulated

fluidization design rules based on excavation pits rather than levee systems. This model had the purpose of determining whether Terzaghi and Peck (1948) theory could be correctly calculated in the PLAXIS software. Terzaghi's heave criterion, equation 2.6, relies heavily on the hydraulic gradient equation formulated by Darcy (equation 2.1), with the relationship between the hydraulic conductivity, flow velocity, and hydraulic gradient. The groundwater calculations for a system without a cover layer determined that flow through the system follows the formulas presented by Terzaghi and Peck (1948) and Darcy.

From PLAXIS results Darcy's flow laws (equation 2.1) were verified. The model confirms that flow is an important factor when considering the hydraulic head and gradient values. The lower the flow, the less velocity through the system resulting in a lesser hydraulic gradient and a lower chance of hydraulic heave occurring. This confirms that Darcy's law (equation 2.1) is critical in the groundwater flow calculations.

The calculation conducted with a $3m$ cover layer indicated that the size of the well opening has a substantial effect on the hydraulic gradient at the entrance of the well. A high hydraulic gradient is noted at this location due to the increase in pressure, created by the flow restriction. As the well opening increases the effect from the confining cover layer will reduce, increasingly reflecting behaviour observed in the free exit situation.

The confining cover layer introduces an external force on the sand, increasing the pore-water and soil stresses in the system. This has a huge effect on the vertical equilibrium introduced by Terzaghi and Peck (1948), a design rule to establish when hydraulic heave could occur. A well acts as a valve for flow, forcing water through a small opening to the region of the lowest hydraulic head, further increasing pressure and respectively the hydraulic gradient.

Through model verification, where the hydraulic heave safety factor from European Committee for Standardization (2022) was calculated, indicated what the impacts are of a confining cover layer with well, on the systems hydraulic gradient. A system without a restricting cover layer, where a seepage wall is present, has the highest hydraulic gradient at the tip of such a seepage wall. These high flow concentrations result in a greater pore water pressure, leading to a low hydraulic gradient safety factor. A low safety factor is also observed at this location when a confining layer is present. However, at a depth of approximately half the seepage wall length, the effects of the confining cover layer weight can be noted. Instead of pressure reducing closer to the surface, the pressure increases, not only from the weight of the cover layer but also from the pressure build-up from the flow unable to escape to the ground surface.

It is not yet possible to determine the full extent of the effect the cover layer thickness has on the heave process at the well entrance since the groundwater calculations do not consider the weight of the layers. For the time being, the boundary of the cover and sand layer is taken to be closed. To determine the stresses within the system and the importance or disadvantage of such stresses within the heaving process, further analysis is done in Plaxis, elaborated in the next chapter.

Effective stress analysis

6.1. Introduction

The review of the literature study, presented in chapter 3, led to a classification of current design rules dominated by open exit hydraulic heave. Furthermore, groundwater flow calculations determined the parameters having the greatest impact on flow through the system. Nevertheless, several questions remain concerning the process leading to hydraulic heave when the exit is restricted by a confined cover layer. Questions, such as the relevance of the volumetric weight of such a confined cover layer on the effective stress within the system will be quantitatively analysed. An additional failure node has been introduced to the backward erosion failure path for the purpose of this study, failure node 4a in figure 6.1.
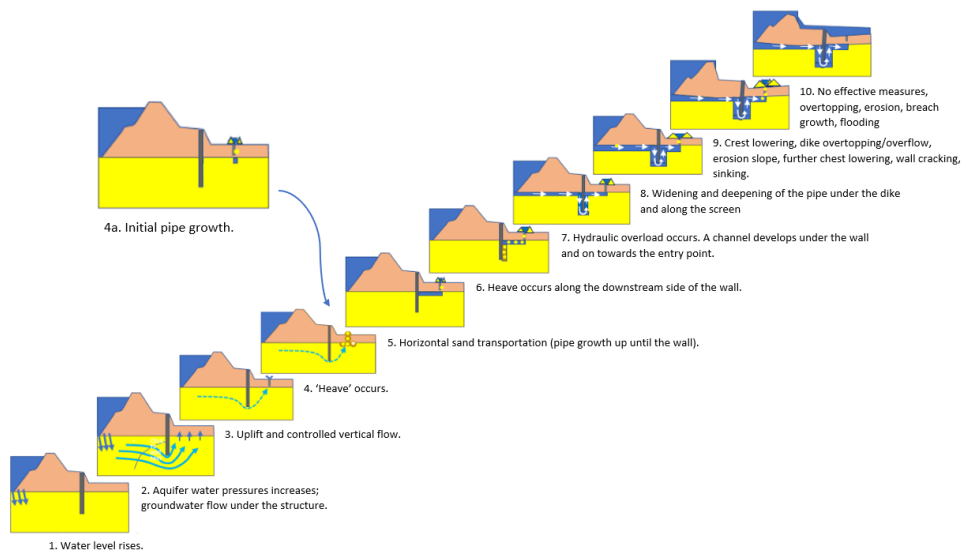
Figure 6.1: Introduction of initial heave failure node with the backward erosion piping failure path

This chapter is divided into seven sections to describe the method and results necessary to answer some of the research questions. Section 6.2 clarifies the purpose of this chapter, highlighting the important geotechnical aspects to be considered. Section 6.3 explains the general calculation process within PLAXIS with section 6.4 explaining the general model geometry and important parameters. Sections 6.5, 6.6 and 6.7 examine the calculations carried out on three scenario studies, free exit (plane strain condition) and constricted exit (carried out in both plane strain and axis-symmetric conditions):

6.2. Background Information

The focus of this chapter is to investigate the rate of progressive heave commonly known as fluidization. An important aspect of the hydraulic heave process is particle suspension or the suspension of particles from a fixed soil matrix into a fluidized state. To achieve the transition from a solid to a liquidized state a vertical equilibrium must be undone. As described in section 3.3.3, the seepage pressures and the submerged weight of grains must become unbalanced. At the point where the equilibrium is broken the vertical effective stress (σ') has a value of zero, when the cohesion is zero, beginning the process of hydraulic heave.

The finite element software PLAXIS can produce vertical effective stress (σ') outputs in the form of compression(-) and tension(+) results. Sand is considered to be cohesionless, however, cohesion will be set to a value of $c = 1kN/m^2$ to ensure greater stability within the sand layer. Effective stress values close to the $0kN/m^2$ benchmark will be considered to fluidize due to factors outside the scope of this study. Therefore, the fluidization region in the sand layer is to be represented when the effective stress is greater than $-2kN/m^2$ ($\sigma' > -2kN/m^2$), including the entire tension zone in the suspension zone. All areas with an effective stress value less than $-2kN/m^2$ are considered to be in compression and fixed in a sand matrix.

6.3. Calculation Methodology

The flow diagram in figure 6.2 presents the modelling process used throughout this chapter. A sand column, (geometry introduced in section 6.4), will undergo hydrostatic and flow conditions to investigate the point of fluidization initiation and eventual progression. The fluidization process is initiated by increasing the hydraulic head over the sand layer. To represent the progression of fluidization a new material set is needed to be introduced, representing the newly fluidization material, $\sigma' > -2kN/m^2$ zone. At each newly introduced phase, the model is again calculated and the question posed is whether or not fluidization zone growth can be observed.

1. K_0-procedure for the generation of the initial stresses under horizontal groundwater level
2. Hydrostatic flow
3. Initiation of flow (*)
4. Alteration of soil properties to represent areas under fluidization (*)

As figure 6.2 indicates, phases 3 and 4 will repeat until no further growth in the fluidization zone can be observed. The calculation phases are described in detail below.
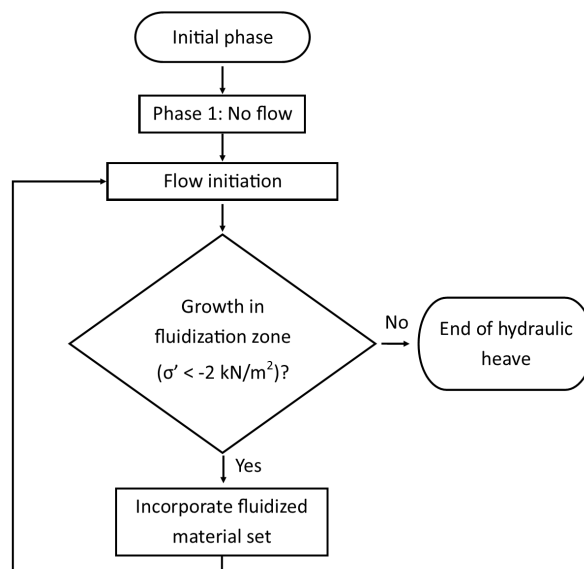
Figure 6.2: Flow diagram of model method

6.3.1. Description calculation phases

Initial Phase
- Hydrostatic
- Generation of initial conditions
- Calculation type: K_0 procedure

    - Does not include external forces in calculations
    - Initial geometry conditions
    - Initial stress state; effective stresses, pore pressure, state parameters
    - Does not check on stress equilibrium
    - $\sigma'_h = K_0 * \sigma'_v$, $\sigma'_v = \sigma_v - u$

- Pore pressure calculation type: steady-state groundwater flow

The initial stresses in a soil body are influenced by the weight of the material and the history of its formations. Geotechnical engineering problem analysis requires the specification of a set of initial stresses, usually characterised by an initial vertical effective stress ($\sigma'_{v,0}$). The non-porous cover layer present over the entire length of the geometry, the well has yet to be introduced.

Phase 1: Hydrostatic flow
- Hydrostatic
- Balanced initial stress state determined; the influence of water-filled well included
- Calculation type: Plastic
- Pore pressure calculation type: steady-state groundwater flow

The system is modelled in a hydrostatic condition ($\Delta\phi/ds = 0$) to re-establish an equilibrium where the water-filled well is taken into consideration. Through establishing a hydrostatic phase and a properly balanced initial stress state, the results from this phase will be used as a benchmark for the calculation where flow is present.

Phase 2: Initiation of Flow
The following phases are dependent on each other, if this phase occurs the next will also.

- Presence of flow
- Calculation type: Plastic
- Pore pressure calculation type: steady-state groundwater flow

From a hydrostatic condition, the model will undergo an increase in the hydraulic head, representative of rising water levels during floods. The increase in the hydraulic head is brought on at the bottom boundary, $y = -8m$. Porewater pressure will be determined by the steady-state groundwater flow calculation type. Flow calculations are to determine the steady-state pore pressure based on hydraulic conditions applied to the model.

Phase 3: determination and alteration of fluidization zone
- Presence of flow
- Calculation type: Plastic
- Pore pressure calculation type: steady-state groundwater flow

Through the analysis of the effective results, the effective stress region greater than $-2kN/m^2$ can be determined as a zone of fluidization and the material properties altered to represent water. The effective stress will also be analysed to determine how close the model is to failure about uplift or instability at the entrance of the well. The well is not reinforced and therefore is a possibility that the well entrance may collapse.

Subsequent phases
Once the maximum hydraulic head and fluidization zone have been identified and material properties altered, a new phase is added where the hydraulic head is increased and the potential of progressive hydraulic heave is again analysed, until no further erosion lens growth is observed.

6.3.2. Scenario calculations

Three scenarios are to be modelled, presented below

- Free exit, plane strain condition (figure 6.3a):
  The column is considered a long infinite sand embankment with no flow restrictions

- Constricted exit

  - Rigid cover layer, plane strain condition (figure 6.3b):
    The confining cover layer is considered to be ridged and stiff. Plane strain condition is implemented.

  - Rigid cover layer, axis-symmetric condition (figure 6.3c):
    Axis-symmetric conditions allow the analysis of the problem in three dimensions. The input of the project is two-dimensional, but because of the rotational symmetry, the project is analysed in a symmetric three-dimensional problem. Representing a cylinder rather than along an infinite length. Due to the axis-symmetric nature of the model, only half of the geometry is required, revolving around the centre axis.

6.4. General Geometry

Two types of geometry were used for the PLAXIS calculations introduced in section 6.3.2. All the geometries subjected a $8m$ porous sand sample to a head drop, simulating the flow of water down and around an implemented seepage wall. A general description is given here and details concerning the individual calculations can be found in later sections.

Based on the groundwater model presented in chapter 5, the stability models have been simplified to reduce potential stability issues and narrow the results to focus on answering the research questions. Inspiration for the simplified models was taken from suspension cylinder tests completed by Baldock et al. (2004), introduced in section 4.1.7. Although a seepage wall is not present in the model, it is considered that the depth of the model represents the length of such a wall.

Figure 6.3 displays the geometry of the three calculations to be performed. All the geometries consist of a sand column reaching a depth of $8m$ with a diameter of $8.5m$ as shown in figure 6.3. In the scenario where a confined cover layer is taken into consideration a linear elastic non-porous cover layer is laid, with a thickness of 4m. In all the calculations an upward flow of water is generated through an inflow at the base, with a constant head maintained in the column.

(a) Without Confining Cover layer **(b)** With Confining Cover layer **(c)** External Force on plate
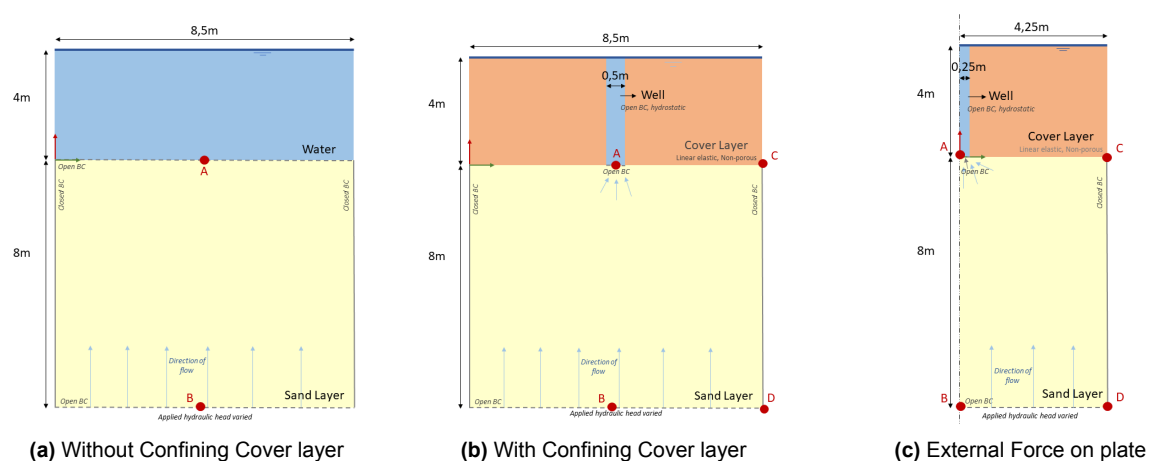
Figure 6.3: Geometry of PLAXIS models

6.4.1. Soil Parameters

Adjustments to the soil parameters have occurred in comparison to the groundwater flow calculations, to ensure greater stability. The soil parameters of the sand subsoil were taken from the groundwater calculations, with no variation. Table 6.1 provides the relevant soil parameter values for all the materials.

Cohesion
When defining the sand soil dataset careful consideration of the cohesion factor was needed. Sand has little interparticle-locking properties, but PLAXIS encounters stability issues when a load-bearing plate or structure is placed on a low cohesive soil layer where flow occurs, resulting in near zero effective stress. Sand begins to erode leaving no stable footing causing the load-bearing structure to collapse. To overcome this issue, a cohesion of $1kN/m^2$ was

applied which is a rule of thumb within the PLAXIS Geo-engineering committee.

| Parameter	Name	Cover layer	Subsoil	Fluidized material	Unit
General					
Soil model	Model	Linear Elastic	Mohr-Coulomb	Mohr-Coulomb	-
Drainage type	Type	Non Porous	Drained	Drained	-
Unsaturated unit weight	γ_{unsat}	17	17.54	0	kN/m^3
Saturated unit weight	γ_{sat}	-	21	10	kN/m^3
Mechanical					
Young's modulus	E'_{ref}	$200*10^3$	$50*10^3$	10	kN/m^2
Poisson's ratio	υ	0.33	0.3	0.499	-
Cohesion	c'_{ref}	-	1	1	kN/m^2
Friction angle	φ'	-	35	35	°
Dilatancy angle	ψ	-	5	0	°
Groundwater					
Horizontal permeability	k_x	-	10	1000	m/day
Vertical permeability	k_y	-	10	1000	m/day

Table 6.1: Material properties of confining cover layer, sand subsoil and slurry mixture

6.5. Free exit, without cover layer

In this section, a simple plane strain model was set up to define the benchmark for PLAXIS, Terzaghi calculations and calculations where a confining cover layer will be present. In this calculation, a $8m$ sand layer experiences a vertical upward flow, created by a head boundary located at the bottom (y-min) boundary. An external water level is located at $y = 4m$.
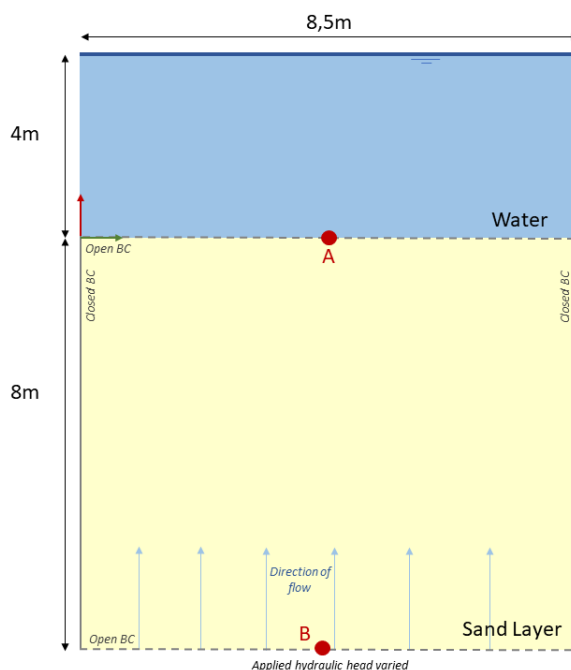
Figure 6.4: Geometry, no cover layer

The head at the bottom of the model ($y = -8m$) was increased to show the sand behaviour within the column. Figure 6.5 displays the total, effective stresses, and pore water pressure

for two hydraulic head differences over the sand layer, $\Delta\phi = 2m$ and near sand suspension $\Delta\phi = 8m$. As the hydraulic head increases, the more dominant the porewater pressure becomes in the total stress equation. The effective stress decreases respectively until the entire sand column reaches $0kN/m^2$.

It is noted that fluidization occurs over the entire soil body instantaneously, not occurring in phases throughout. Once the hydraulic gradient is reached the entire soil layer will fluidize.
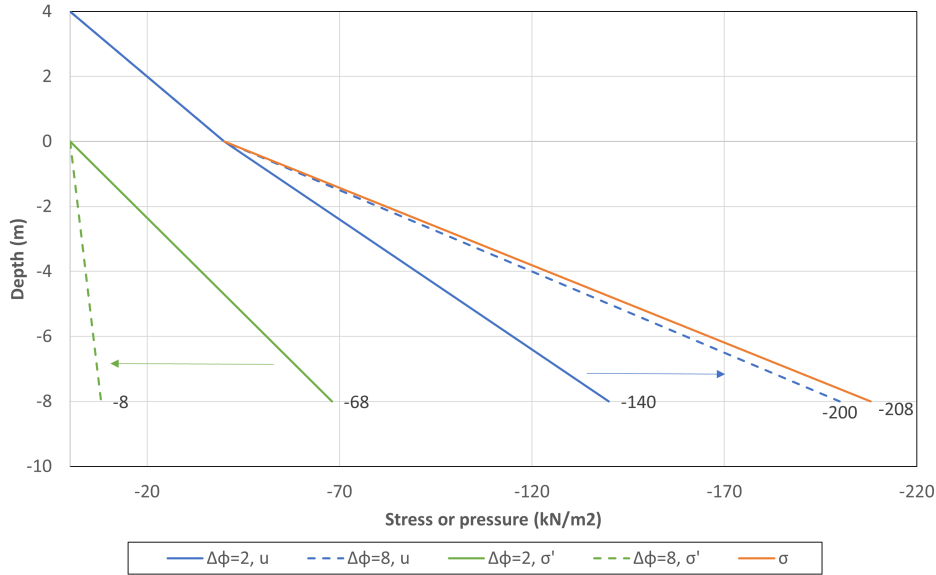
Figure 6.5: PLAXIS Stress distribution, column of sand without cover layer

6.5.1. Model verification

Simple calculations can be carried out to determine whether and when the sand should fully begin to move in this scenario. This is a process to verify the results achieved during the PLAXIS model.

Terzaghi
A critical hydraulic gradient of $i_c = 1.1$ was determined using the formulas for Terzaghis's critical heave ($i_c = \frac{\gamma_{sat} - \gamma_w}{\gamma_w}$), equation 3.3. At this hydraulic gradient, all the sand will be in suspension. Darcy's flow equations ($i = \frac{\Delta\phi}{\Delta s}$), equation 2.2, determined the required head difference over the system to ensure that the critical hydraulic head is reached, $\Delta\phi = 8.8m$. Due to the reference system located at the sand and water interface a head of $\phi = 12.8m$ is required to be applied at the bottom of the sand layer.

Stress Calculations
Stress equations for total stress and porewater pressure anywhere in the model when an applied hydraulic head of $\phi = 12.8m$ concluded that the entire soil is suspended.

$$\sigma = (\gamma_{sat} * H) + z * \gamma_w = (21 * 8) + (4 * 10) = 208 kN/m^2 \tag{6.1}$$
$$u = (H + h) * \gamma_w = (8 + 12.8) * 10 = 208 kN/m^2 \tag{6.2}$$
$$\sigma_v = \sigma - u = 0 \tag{6.3}$$

6.5.2. Summary

Applying Terzaghi, it can be concluded that stress hand calculations can verify the results PLAXIS produced. At the calculated hydraulic head of $\phi = 12.8m$, the system reached the critical head gradient of $i_c = 1.1$, fluidising the system completely.

6.6. Confining cover layer: plane strain conditions

The following two chapters introduce calculations where a cover layer has been applied to the models; a rigid cover layer undergoing plane-strain conditions and rigid a cover layer under axis-symmetrical conditions. This chapter explains and verifies the calculation of the results during the plane-strain model, presented again in figure 6.6.
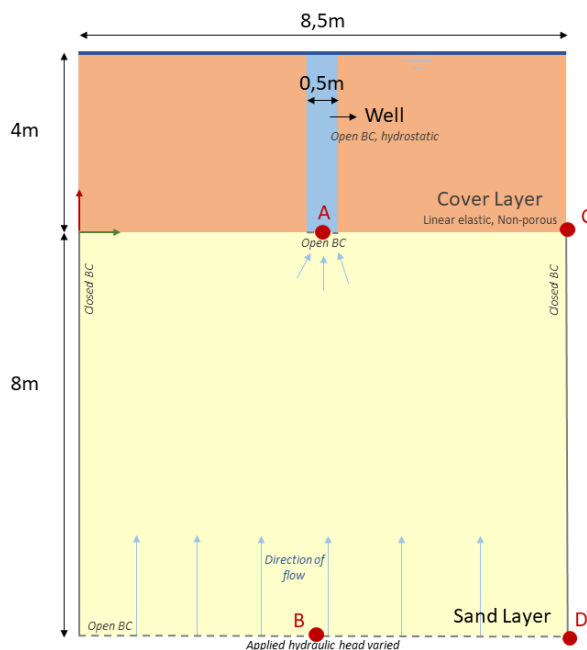
Figure 6.6: Geometry with confining cover layer

Two vertical cross-sections; the middle of the well (A-B) and the edge of the model (C-D) have been analysed in terms of the total, effective and porewater pressures at different flow conditions. Certain points along these cross-sections of theoretical calculations have been conducted; entrance to the well (point A), bottom sand layer under the well (point B), cover-sand layer interface (point C) and bottom sand layer at the edge of the model (point C).

6.6.1. Additional Boundary conditions

Apart from the general geometry described in section 6.4, additional boundary conditions and influencing geometry are required.

Well

In the scenarios where a cover layer is present an opening through the layer is required. Considering that the uplift process has already occurred it is assumed that the well through the confining cover layer is already present and filled with flushed clean water. The water pressures are generated based on the phreatic level located at the top of the confined cover layer.

During the fluidization iteration process, when the new soil material is introduced, the well will not contain this material property, rather will continue to be flushed with clean water. The well in itself has no material properties, relying on the adjacent confining cover layer properties to provide stability. Due to the confining cover layer being portrayed as an elastic material, the well has infinite strength.

Confining cover layer

A linear elastic model type is used to characterize the cover layer to avoid disruptive deformations in this layer. Results in this layer are not relevant to answering the research questions therefore the analysis of deformations and stresses is not required. By setting the drainage type to non-porous, the boundary conditions are set to close around this layer, preventing flow from travelling through this layer. A larger Young's modulus is applied to ensure a greater stiffness to limit the deformation of the cover layer.

Fluidized material properties

As fluidization begins, soil particles begin to move in suspension within the water located in the well. Studying the fluidization iteration requires a change in soil properties when the soil becomes suspended, portraying a liquefied substance, and enabling possible growth to continue. As this research does not look at the inner workings of particle suspension, the new soil material presenting the fluidized material is considered to not have any particles, only water.

The new material properties are based on water, however, due to instability around the entrance to the well, a greater stiffness was needed to avoid well collapse. A Young's modulus of $10kN/m^2$ was applied.

6.6.2. Calculation stages

The general model methodology was followed during the building and analysis of the results produced in PLAXIS, (described in section 6.3). Figure 6.7 displays all the stages during the cover layer, plain strain condition model. Phase 5 has combined the stages of determining and expanding the fluidization while increasing the hydraulic head. After two fluidization zone determinations and an increased hydraulic head, the model failures stopped the calculation process.
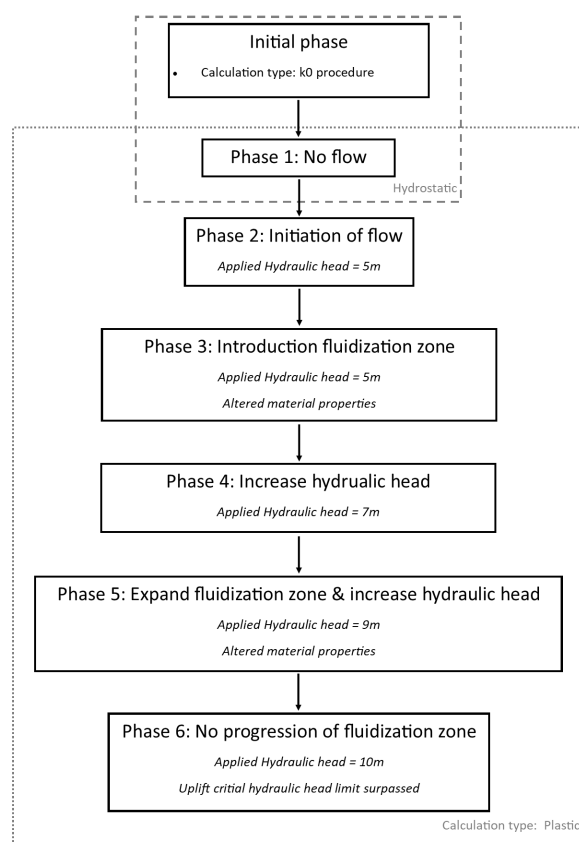
Figure 6.7: Calculation stages, model with cover layer plane-strain condition

The progression of fluidization was considered to be at its greatest just before the point of model failure. For the stage where the flow is initiated the maximum hydraulic head that can be applied to the system must be determined, leading to the analysis of the hydraulic head versus the initial erosion lens growth.

6.6.3. Initial erosion lens growth

Following the initial and first, no flow or hydrostatic, phase a hydraulic head is applied to the system at the bottom boundary, and increases in subsequent stages at an interval of $h = 1m$. The results received do not characterize the fluidization progression but rather the hydraulic head producing the maximum fluidization zone right before failure. The water slurry mixture has yet to be introduced into the model.

Four different well opening sizes were taken through the $4m$ cover layer, with the results plotted in figure 6.8. No growth in the fluidization zone is observed when flow conditions are hydrostatic. Instant erosion lens growth is observed once flow begins in the system continuing almost linear until instability in the model occurs and the erosion lens begins to collapse. PLAXIS stops the calculation when collapse occurs. These failure points occur at different hydraulic heads depending on the well opening size. Due to the low cohesive sand being deformed under the well, but also the levee structure, the sand is no longer able to bear the structure.
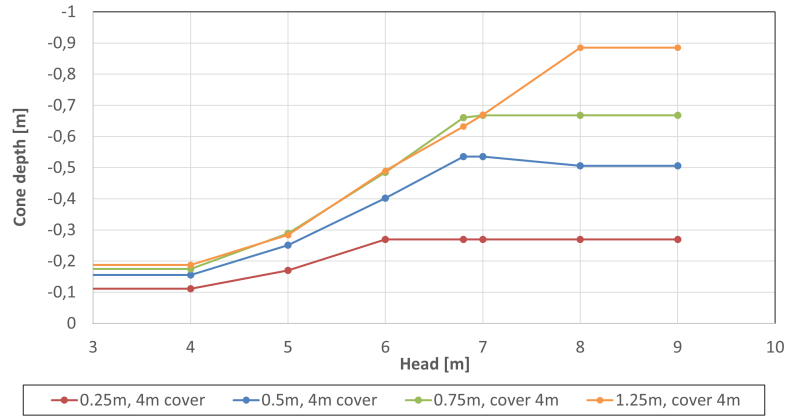
Figure 6.8: Initial zero effective stress ($\sigma' = -2$)

6.6.4. Fluidization growth iteration

A well opening size of $0.5m$ through a cover layer of $4m$ is further used in the stability calculations. Figure 6.8 suggests that the sand layer is stable up until an applied hydraulic head of $\phi = 6.5m$. During the iteration in the following section, a hydraulic head of $h = 5m$ will be used during the initiation of the flow stage to ensure stability in the model.

Since the initial hydraulic head right before failure was determined (previous section), providing the greatest fluidization zone before model failure, the effective stress zone ($\sigma' > -2kN/m^2$) can undergo the soil property alteration. New phases were added to the calculation process representing the hydraulic head increase and the progressive fluidization, presented in section 6.3. Effective principal and vertical effective stresses for all the phases are displayed in figures 6.9, 6.10 and 6.11.
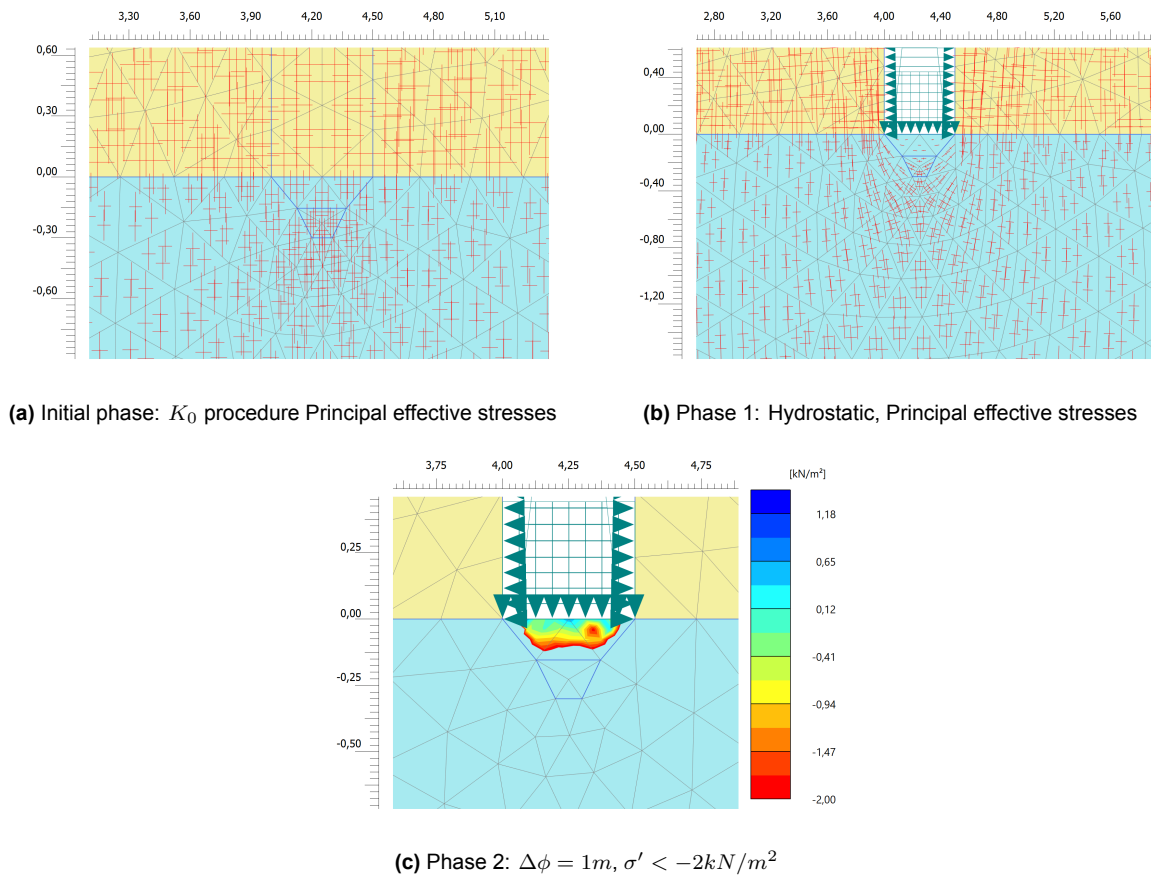
Initial Phase: K_0 procedure
During this phase the initial conditions are generated, the self-weight of the soil is not included and the soil is in the state of rest where no displacements are developed. The principal effective stresses are observed in figure 6.9a. Vertical in-situ effective stresses are considerably larger than their horizontal counterpart, relating to the ratio of the horizontal stress to the vertical stress, also known as the coefficient of earth's pressure (K_0), $\sigma_H = K_0 * \sigma_v$.

Element meshing of the model resulted in a smaller mesh region around the well, therefore high concentrations of stress crosses are noted, especially at the cover-sand layer interface. Water is present in the well, producing less effective stress in the direct subsoil. At a significant depth, it is expected that the effect of the well will disappear. Although in figure 6.9a the stresses increase under the well with increasing depth, they do not reach the magnitude of the stresses just outside the zone affected by the well.

Phase 1: Hydrostatic through system
Zero head difference is experienced over the system, hydraulic head applied to the base of the sand column is $\phi = 4m$. The weight of the confining cover layer is greater than the weight in the well, where the applied load is affecting the underlying sand layer. Stresses or pressures are developed in the vertical direction due to the application of the weight of the cover layer, causing rotation of the effective stress orientation, creating a so-called pressure bulb. This pressure bulb can be seen in the principal effective stress figure 6.9b. The cone shape bulb reached a depth of approximately $y = -0.15m$

(a) Initial phase: K_0 procedure Principal effective stresses

(b) Phase 1: Hydrostatic, Principal effective stresses

(c) Phase 2: $\Delta\phi = 1m$, $\sigma' < -2kN/m^2$

Figure 6.9: Effective and Principal stresses of begin phases

Phase 2: $\Delta\phi = 1m$

Flow into the system was increased by 1m, initiating the heaving process, where grains will be lifted out of the sand layer into the well and if enough force is available, out the top of the well to create sand boils. Figure 6.9c shows the zone where the effective stress is near fluidization $\sigma > -2kN/m^2$. The pressure enforced on the sand area by the cover layer introduced a pressure bulb, created by shear stresses rotating principal effective stresses.

Phase 3: $\Delta\phi = 1m$

Once the predicted fluidization zone had been identified this zone underwent a material property change. Continuing on from phase 2 an additional phase was created, with the displacement set to zero. The flow throughout the column remained equal to the previous phase, $\Delta\phi = 1m$. Figure 6.10a displays that the entirety of the altered fluidized zone is in suspension with an extra point-shaped area sustaining effective stress values of less than $-2kN/m^2$ located at the bottom, negative y-direction.

(a) Phase 3: new material property, $\Delta\phi = 1m$, Effective stress $> \sigma' = -2kN/m^2$

(b) Phase 3: new material property, $\Delta\phi = 1m$, Principal effective stresses

(c) Phase 4: $\Delta\phi = 3m$, Effective stress $> \sigma' = -2kN/m^2$

(d) Phase 4: $\Delta\phi = 3m$, Principal effective stresses
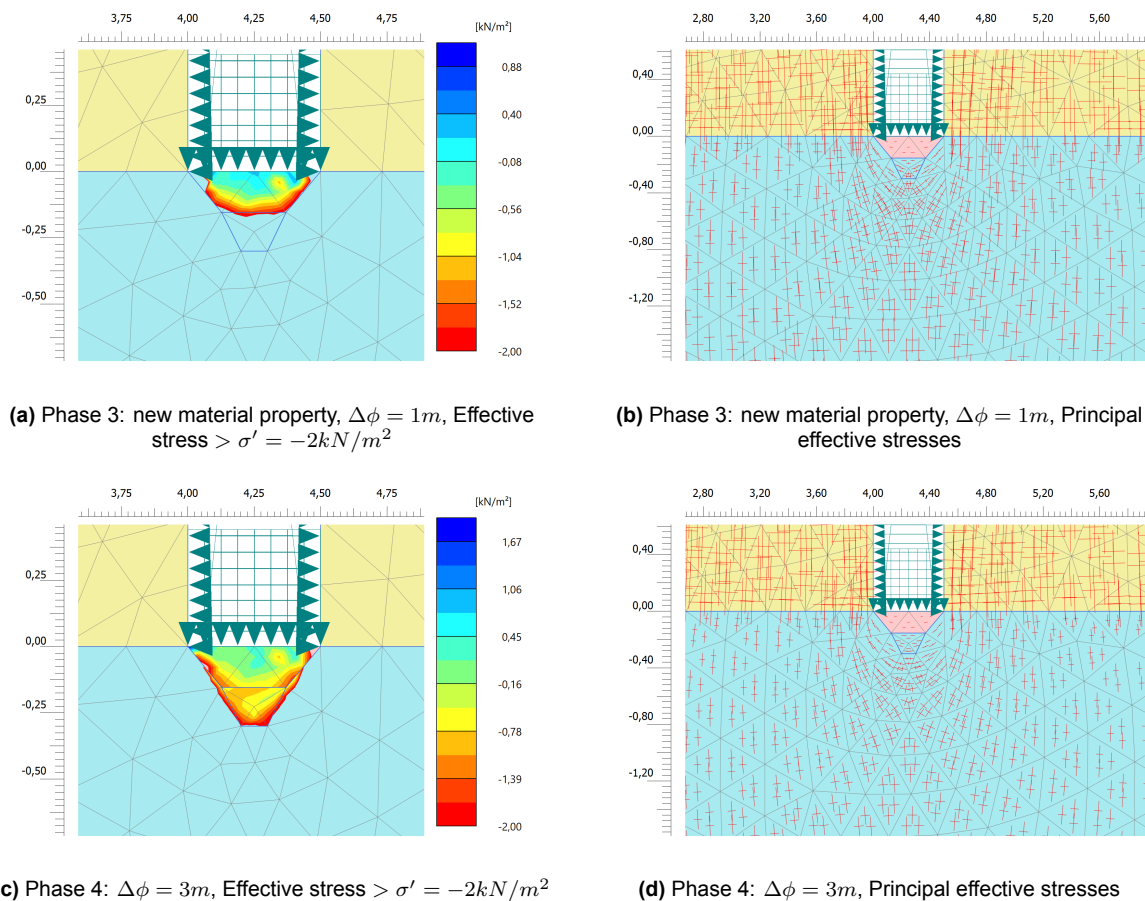
Figure 6.10: Effective and Principal stresses of heave growth through soil properties alteration

Phase 4

The applied hydraulic head was increased to assess the effect of rising water levels on the erosion lens growth. $\phi = 7m$ was applied to the bottom of the column, ensuring a hydraulic head difference of $\Delta\phi = 2m$ across the column. Particle suspension equilibrium states (equation 3.3.3) that fluidization of a sand bed will occur when the seepage pressures counterbalance the submerged weight of the grains. More flow ensures that a larger area of sand particles becomes suspended due to the increased upward pressure overcoming the downward load of the cover layer. Concerning the fluidization zone seen in figure 6.10c compared to the situation with less concentration of flow, presented above, phase 3 (section 6.6.4), the area is larger and more pronounced. Progression seems to be restricted to the bottom area, forming a more cone-like shape.

Phase 5

Within phase 5, the hydraulic head difference is increased to at $\Delta\phi = 5m$ and the suspended zone is increased, as seen in figure 6.11a. This zone again represents the entire fluidized altered zone with an effective stress of less than $-2kN/m^2$, however, no progression could be observed. Furthermore, the figure indicates that less area is suspended than in the previous phase, ending the iteration.
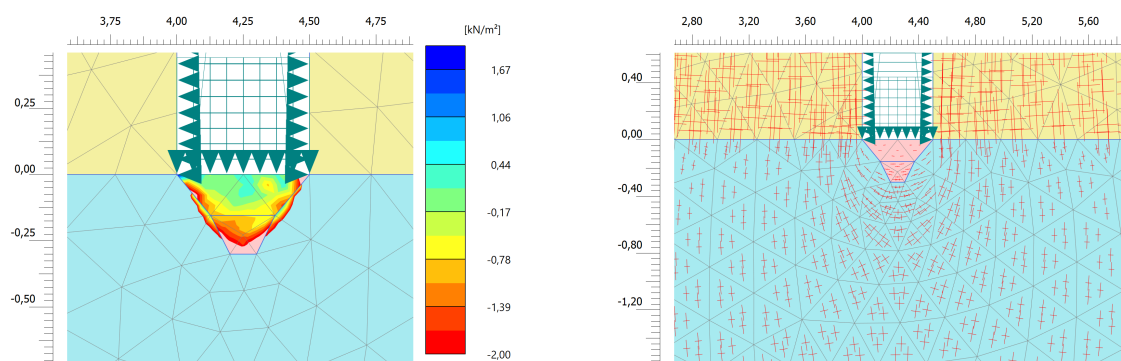
(a) Phase 5: $\Delta \phi = 5m$, Effective stress $> \sigma' = -2kN/m^2$

(b) Phase 5: $\Delta \phi = 5m$, Principal effective stresses

Figure 6.11: Effective and Principal stresses of failure phases

Phase 6

When the hydraulic head difference increases substantially the well can not sustain the amount of water trying to flow through. Pressure begins to build up under the cover layer, enabling uplift to occur again. Once the limit head potential is reached the model is considered to have failed due to the backward step in the backward erosion piping failure path. Uplift of the cover layer will be observed at the sand-cover layer interface furthest away from the well opening.

6.6.5. Model verification

Verification of the model is required to ensure that the model has been created correctly, and the right boundary conditions applied, producing reliable results. Three verification methods were applied:

- assessment of the soil stresses along a vertical cross-section at the centre of the well and outer vertical boundary
- establishing the vertical and horizontal stresses during the K_0 procedure and first plastic phase
- application of the Newmark diagram to determine what extent the confining layer has on the sand layer

Stresses in soil under hydrostatic conditions

Volumetric weight is added to the sand layer by the confining cover layer located on top, altering the stresses in the soil compared to the scenario without a cover layer. The total, effective stresses and porewater pressures produced by PLAXIS of the two vertical cross-sections made through the model (A-B and C-D) are presented below in figure 6.12. The pore pressure distribution in the soil layer is hydrostatic, based on a hydraulic head of $4m$. The cover layer is non-porous ($u = 0kN/m^2$), while the water level in the well is at $y = 4m$.
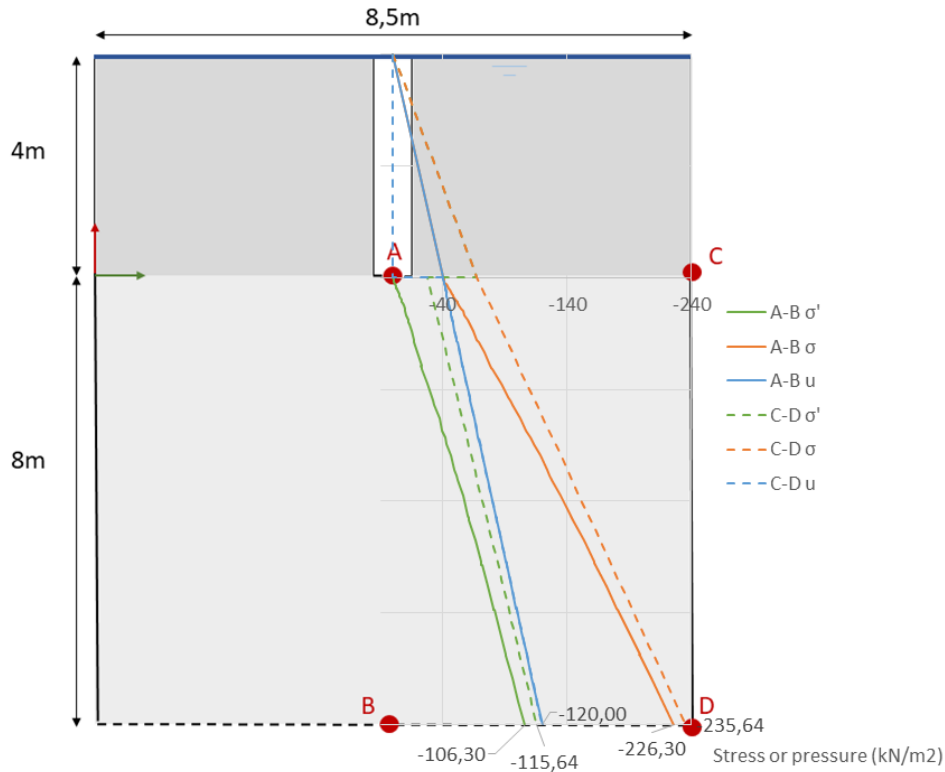
Figure 6.12: Stresses in soil, hydrostatic

Note: all hand calculations give positive compressive stresses, with the figures still retaining the PLAXIS notation of compressive being negative.

To determine whether or not the weight of the confining cover layer still influences the cross-section C-D stress hand calculations have been carried out.

- Point C: Edge, cover-sand interface
  Only the cover layer's saturated unit weight and layer thickness are needed to determine the total, effective and water stresses. The confining cover layer is non-porous therefore no porewater pressure can proceed here. This lack of porewater pressure in the cover layer results in a jump in the effective stress at the interface, from $u = 0kN/m^2$ to $u = -40kN/m^2$. From the top of the layer to the interface the effective stress is equal to the total stress and at the interface where pore pressure is introduced the effective stress is reduced to a value of $\sigma' = 28kN/m^2$.

$$\sigma = (\gamma_{sat-cover} * H_{cover}) = 17 * 4 = 68kN/m^2 \tag{6.4}$$

$$u = H_{cover} * \gamma_w = 40kN/m^2 \tag{6.5}$$

$$\sigma' = \sigma - u = 28kN/m^2 \tag{6.6}$$

Uplift nor fluidization is expected to occur at this location as effective stress does not reach the tension phase $\sigma'_v > 0kN/m^2$, nor exceed the calculated total stress $\sigma = 68kN/m^2$.

- Point D: Edge, bottom sand layer
  At the bottom of the model, the weight of the entire system is taken within the total stress

calculation. Water is present throughout the model.

$$\sigma = (\gamma_{sat-sand} * H_{sand}) + (\gamma_{sat-cover} * H_{cover}) = (21 * 8) + (17 * 4) = 236 kN/m^2 \quad (6.7)$$

$$u = (H_{sand} + H_{cover}) * \gamma_w = (8 + 4) * 10 = 120 kN/m^2 \quad (6.8)$$

$$\sigma' = \sigma - u = 116 kN/m^2 \quad (6.9)$$

- Point B: Center of well, bottom boundary
  Analysing the vertical effective stress at point B, the lower boundary of cross-section A-B can determine whether or not the confining cover layer still affects the sand layer at this depth. The depth of the point, the width of the well and the thickness of the cover layer all have an impact on whether or not the total stress will be affected by the shear stresses caused by the well opening.

$$\sigma = (\gamma_{sat-sand} * H_{sand}) + z * \gamma_w = (21 * 8) + (4 * 10) = 208 kN/m^2 \quad (6.10)$$

$$u = (H_{sand} + z) * \gamma_w = (8 + 4) * 10 = 120 kN/m^2 \quad (6.11)$$

$$\sigma' = \sigma - u = 88 kN/m^2 \quad (6.12)$$

Equation 6.10 presents the stress calculation where the well's opening has no effect at the given location. This is considered the upper boundary. The lower boundary was calculated in the total stress calculated above, at the edge of the model where no effect of the well is felt. PLAXIS provides a total stress equalling $\sigma = 226 kN m^2$, falling between the two boundaries indicating that shear stresses are present at this depth.

Horizontal and vertical stresses during initial phases.
K_0 is the at-rest earth coefficient, the ratio σ'_h/σ'_v, between the horizontal and vertical effective stresses at a point in a soil mass. The procedure used within PLAXIS includes the initial geometry conditions when establishing a systematically stratified equilibrium. However, no external forces, including the effect of water present in the well, are considered and for this reason, the pore pressure is zero $u = 0 kN/m^2$.

$$\sigma_v = \gamma_{sat} * z = 17 * 1 = 17 kN/m^2 \quad (6.13)$$

$$\sigma'_v = \sigma_v - u = 17 kN/m^2 \quad (6.14)$$

$$\sigma'_h = K_0 * \sigma'_v = 0.5 * 17 = 8.5 kN/m^2 \quad (6.15)$$

During the first *plastic* calculation carried out under hydrostatic conditions, phase 1, the water present in the well is taken into consideration. The equilibrium is re-established including the horizontal water pressures created in the well. The component of the horizontal stress equals the water pressure at a depth of $1m$ in the well from the top. The confining cover layer is considered a linear elastic non-porous, having therefore no pore pressure throughout the layer $u_v = 0 kN/m^2$

$$\sigma_v = \gamma_{sat} * z = 17 * 1 = 17 kN/m^2 \quad (6.16)$$

$$\sigma'_v = \sigma_v - u = 17 kN/m^2 \quad (6.17)$$

$$\sigma_h = u = \gamma_{water} * z = 10 * 1 = 10 kN/m^2 \quad (6.18)$$

The confining cover layer is essentially two separate vertical forces loaded onto rigid plates. During the initial phase, the weight of water in the well is not taken into consideration during the
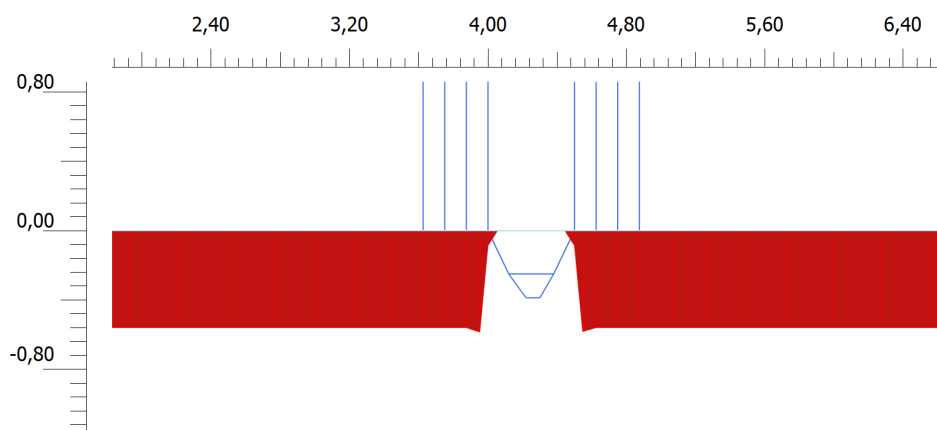
**Figure 6.13:** Effective stress at $y = -0.0001m$, initial phase

K_0 procedure, producing the stress distribution immediately under the confining layer shown in figure 6.13. At the edges of the confining layer, the stresses are larger, as a consequence of the constant displacement of the layer. According to Boussinesq, constant pressure distribution under a stiff foundation strip will cause the emergence of plastic zones at the edges. The stresses in the centre of the layer can be calculated as follows, corresponding with the PLAXIS calculation

$$\sigma = \sigma' - u = 17 * 4 - (4 * 10) = 28 kN/m^2 \qquad (6.19)$$

Newmark

Newmark developed a method for the determination of the vertical normal stresses at a certain depth, $z = y$, caused by some arbitrary load distribution on the surface (Verruijt (2001)). The Newmark influence chart is an illustration used to determine the vertical pressure at any point below a uniformly loaded area of soil. This diagram is used to verify the results obtained from PLAXIS, when the flow conditions are hydrostatic, at a depth of 2m under the confining cover layer.

Each ring within the Newmark diagram consists of 100 segments or rectangles. There are 10 rings. A load of magnitude, q on each of the 1000 rectangles in the diagram gives rise to a stress of $\sigma'_y = 0.0001q$, in the point at a depth y below the origin. This means that a load of magnitude q on a surface that covers n rectangles leads to a stress σ' at a depth y below the origin of magnitude $\sigma' = n * 0.001q$. Figure 6.14 presents the Newmark diagram of the situation where a well is present through the confining layer in plane strain conditions, looking at a point $y = 2m$ below the well centre.
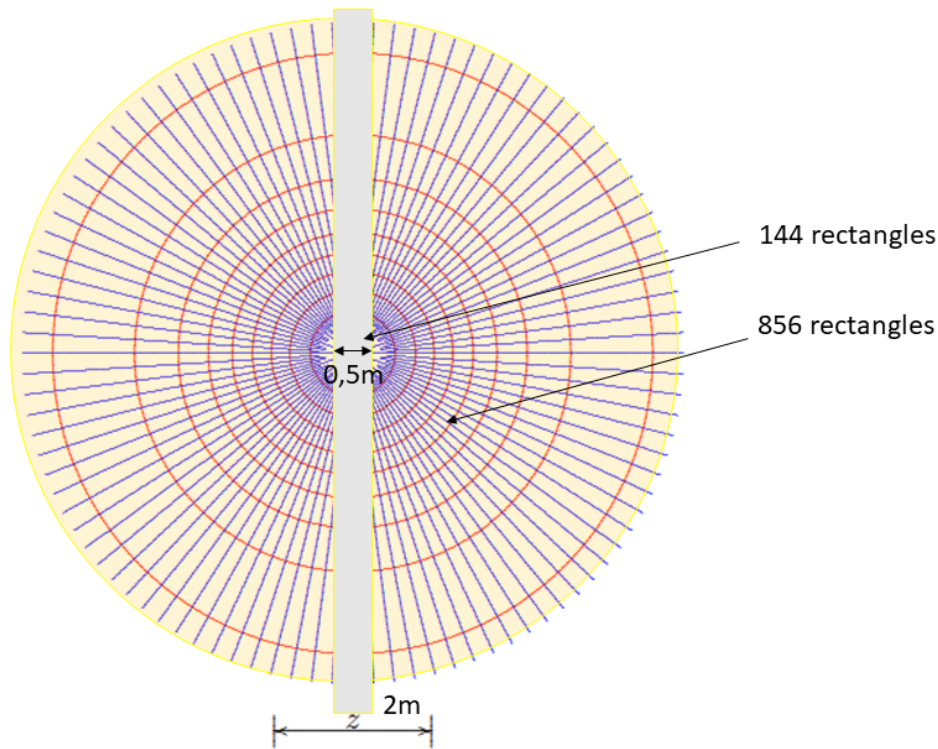
Figuur 29.3: Zon van Newmark.

Figure 6.14: Newmark diagram, plane strain conditions, $z = y = 2m$

The load area has been drawn in figure 6.14, with the well shaded in grey. The well covers an area of 144 rectangles and because the load area extends the diagram it is taken that the load area covers the remaining rectangles $n = 1000 - 50 = 856$. This means that that stress is $\sigma' = 0.856q$. The load of magnitude is the effective stress value of the confining cover layer minus the pore water pressure, determined in equation 6.6, $\sigma'_y = 28kN/m^2$. Newmark determines that when the well is created through the cover layer, the stress at a depth of $y = 2m$ will be $\sigma'_y = 0.856 * 28 = 24.1kN/m^2$.

Plaxis produces at this depth an effective stress value of $\sigma' = 47.44kN/m^2$. To verify this against PLAXIS the entire effective stress value is required, including the effective in the sand at this depth.

$$\sigma'_y = 0.856 * q + ((z * \gamma_{sand}) - (z * \gamma_w)) = 24.1 + ((2 * 21) - 20) = 46.1kN/m^2 \qquad (6.20)$$

6.6.6. Summary

The placement of a cover layer in a plane-strain model drastically changed the characteristics of the flow in the system. The calculations indicate that the size of the well-opening majorly influences the stability of the model. When the opening of the well is tiny the entrance to the well collapses or experiences failure at a considerably less head than that of a larger well opening. Larger well openings allow a greater entrance for flow to travel through, reducing the pressures on the sand-cover layer interface. These calculations determined the maximum head value before failure at four well openings

Fluidization growth was presented through an iteration following the determination of the initial head before failure. Repeating the investigation of increased head and observing

low effective stress compression and tension ($\sigma' > -2kN/m^2$) regions provided an iteration representing progressive heave.

A confined cover layer applies a weight to the sand subsoil soil, creating a pressure bulb under the opening of the well. This pressure bulb greatly affects the strength of the sand matrix requiring increased water pressure to suspend the sand particles.

The calculation was verified by multiple methods such as, stresses in soil, determining whether the K_0 procedure was computed currently and using the Newmark diagram to calculate the vertical effective stress. All verification methods concluded that the correct boundary conditions and input were used, within respectable boundaries.

6.7. Confining cover layer; axis-symmetric conditions

Previously the models were modeled under plane-strain conditions, with the out-of-plane direction extending for an infinite length. This scenario will be performed under axis-symmetric conditions, representing a slice of one radian extending circularly. The axis-symmetric analysis allows you to analyze a 3D problem that is rotationally symmetric about an axis. The input is 2-dimensional, but because of the rotational symmetry, an analysis of a symmetric 3-dimensional problem can be carried out.

Figure 6.15 displays the geometry for this scenario. The geometry is identical to the previous scenario, however, only half is required, due to the symmetry. Once again the modelling flow diagram, (figure 6.2) has been applied during the construction of the phase stages.
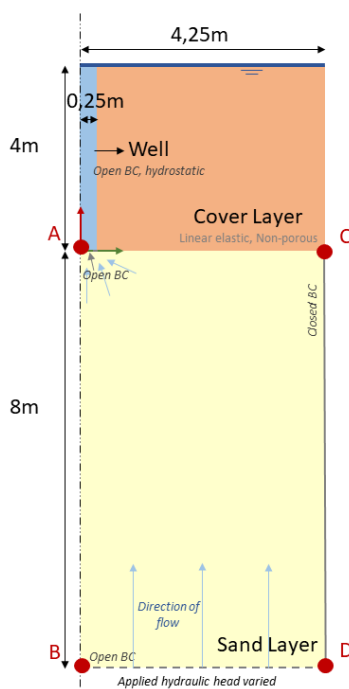
Figure 6.15: Geometry, axis-symmetric

6.7.1. Fluidization growth iteration

Just as in section 6.6.4 a PLAXIS calculation was performed to determine whether or not the erosion lens under the well entrance would grow. The following phases were applied

- Initial phase
- Phase 1: Hydrostatic
- Phase 2: Flow initiation

Figures 6.16a and 6.16b present the results of the effective stress when $\sigma' > -2kN/m^2$ respectively, for phase 1 and 2 respectively. The unmistakable pressure bulb effect created by the pressure difference between the confined cover layer and the water in the well is evident.

(a) Phase 1: hydrostatic

(b) Phase 2: $\phi = 5m$
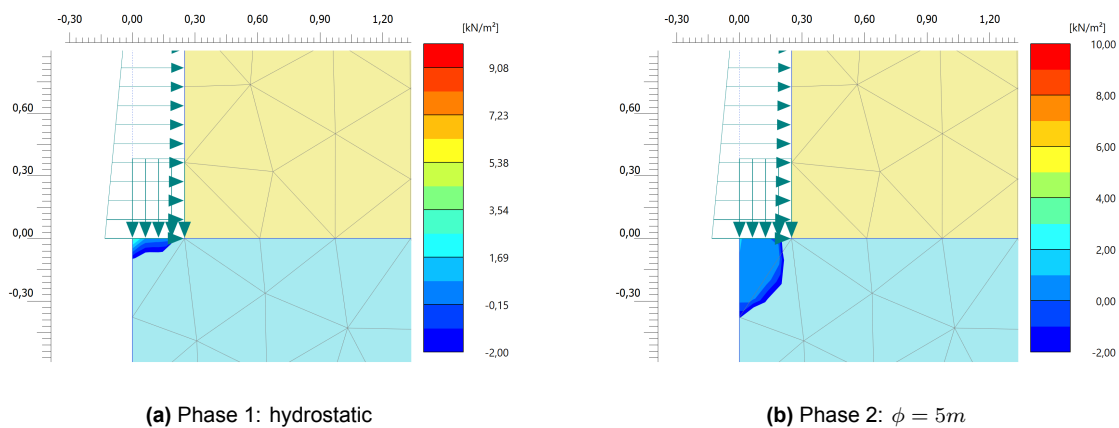
Figure 6.16: Effective stress $< -2kN/m^2$

No iterative erosion lens growth could be established due to PLAXIS not being able to calculate a stable model. The incremental displacement plots presented below, figure 6.17a and 6.17b indicate the issue.

(a) Hydrostatic

(b) $\phi = 5m$
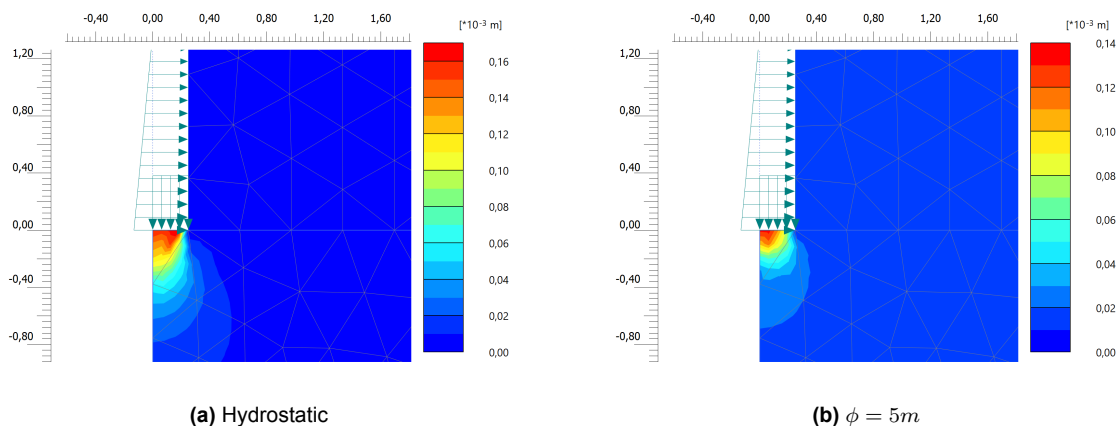
Figure 6.17: Incremental displacements $|\Delta u|$

PLAXIS requires a stable footing for any force applied to a surface, being a force on a plate or straight onto a soil layer. The pressure bulb indicates that the lens growth is round rather than vertically down. With this bulb-like growth not only will sand become suspended in the vertical direction, perpendicular to the cover layer structure but also horizontally at the sand

cover layer interface. With the introduction and increasing flow, sand particles begin to become suspended under the well entrance and sand cover layer interface. As seen in figure 6.17b the sand supporting the cover layer becomes unstable, causing PLAXIS to deem the structure unstable and ending the calculation.

6.7.2. Model Verification

Several checks were carried out to verify the reliability of the corresponding PLAXIS model.

Stresses in Soil under hydrostatic conditions
To check the validity of the model, the stresses were examined and compared to hand calculations. Figure 6.18 presents the stresses along two cross-sections; through the middle of the well (A-B) and the outer edge of the model (C-D). The model was considered hydrostatic for the following hand calculations.


(a) Hydrostatic

(b) $\phi = 5m$
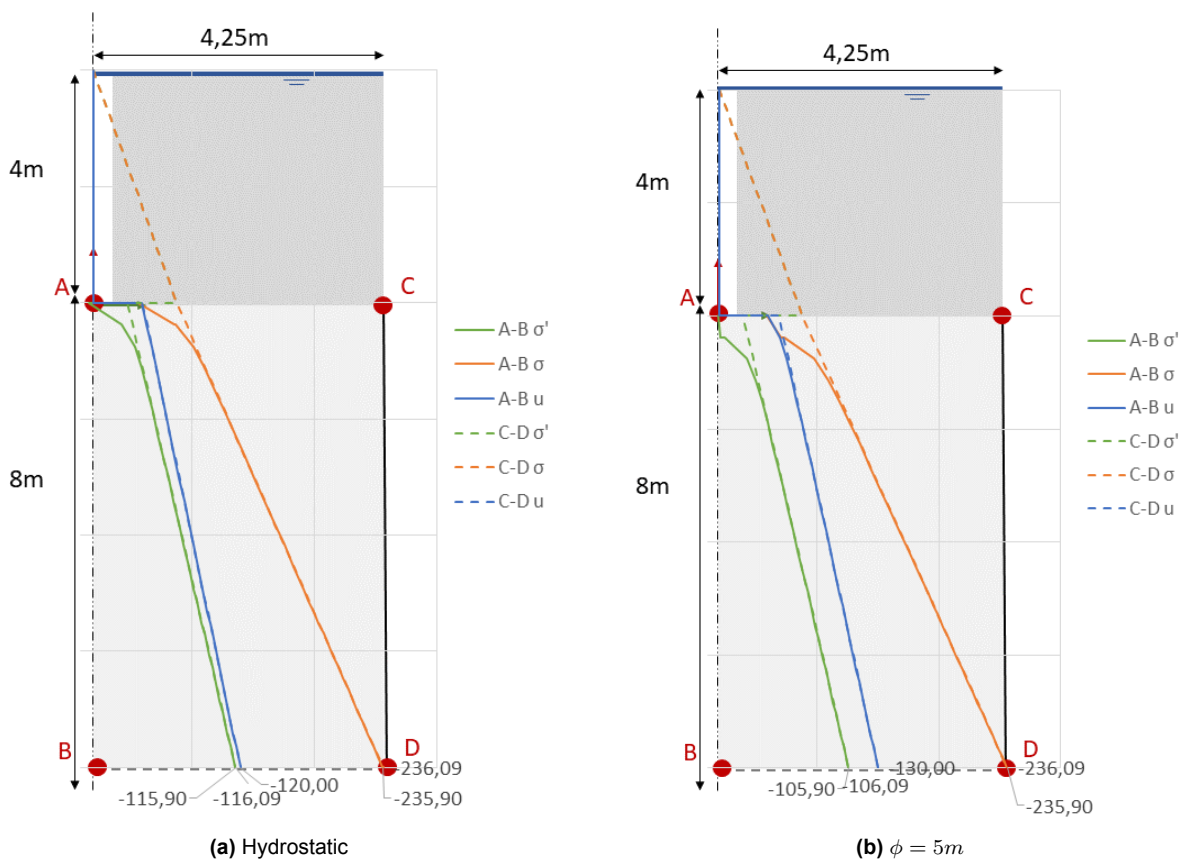
Figure 6.18: Stresses in soil, axis-symmetric condition

- Point D: Edge, bottom boundary
  Point D is significantly far away from the well to feel the pressure difference caused by the opening of the well. The hand calculation corresponds with the results obtained from PLAXIS.

$$\sigma = (\gamma_{sat-sand} * H_{sand}) + (\gamma_{sat_{cover}} * H_{cover}) = (21 * 8) + (17 * 4) = 236 kN/m^2 \quad (6.21)$$

$$u = (H_{sand} + H_{cover}) * \gamma_w = (8 + 4) * 10 = 120 kN/m^2 \quad (6.22)$$

$$\sigma' = \sigma - u = 116 kN/m^2 \quad (6.23)$$

- Point B: Center of well, bottom boundary
  At a depth of $-8m$ the pressure bulb is hardly felt. Hand calculations 6.24 - 6.26 provide the upper and lower boundaries when no shear stress, caused by the rotation of principal stresses, is present along the axis. Any values falling within these boundaries indicate that shear stress is present within the system.

$$\sigma = (\gamma_{sat-sand} * H_{sand}) + (\gamma_{water} * z) = (21 * 8) + (10 * 4) = 208 kN/m^2 \qquad (6.24)$$

$$u = (H_{sand} + H_{cover}) * \gamma_w = (8 + 4) * 10 = 120 kN/m^2 \qquad (6.25)$$

$$\sigma' = \sigma - u = 88 kN/m^2 \qquad (6.26)$$

Comparison of figure 6.18 and equation 6.21 indicate that directly under the well on the bottom horizontal boundary the sand layer produces results nearly equal to those of the hand calculations. Rotation of the vertical stress is expected, however, is contained closer to the well's entrance, due to the 3-dimensional aspect of the model.

Horizontal and vertical stresses during initial phases
At a depth of one meter below the groundwater level ($y = 3m$), the vertical stresses should only be affected by the weight of the material above. The horizontal stresses are influenced by the calculation type the phase experiences. During the initial phase, the K_0 procedure, horizontal equilibrium between the water pressure in the well and the adjacent confining cover layer was not taken into consideration when determining the horizontal effective stress

$$\sigma'_h = (\sigma_v - u) * K_0 = ((z * \gamma_{cover}) - u) * K_0 = ((1 * 17) - 0) * 0.5 = 8.5 kN/m^2 \qquad (6.27)$$

Phase 2 was calculated using the plastic calculation type where the horizontal equilibrium, not considered in the K_0 produce, is now considered. As a result, the equilibrium is to be re-established in the well and an adjacent confining cover layer, $\sigma'_v = \sigma'_h = 10 kN/m^2$.

Newmark
Under axis-symmetric modelling conditions, Newmark's vertical normal stress determination was again used to verify the PLAXIS results. Figure 6.19 shows Newmark's circle with the well presented in grey. The well covers an area of 50 rectangles and the applied load, or cover layer covering the remaining rectangles $n = 1000 - 50 = 950$. Newmark establishes the stress value to be $\sigma'_y = 0.95q$, 2m under the well entrance. The load of magnitude equal to that found during the plane strain conditions, determined in equation 6.6, $\sigma' = 28 kN/m^2$, resulting in an expected vertical stress value of $\sigma' = 0.95 * 28 = 26.2 kN/m^2$.

Plaxis produces at this depth an effective stress value of $\sigma' = 49.78 N/m^2$. To verify this against PLAXIS the entire effective stress value is required, including the effective in the sand at this depth.

$$\sigma'_y = 0.95 * q + ((z * \gamma_{sand}) - (z * \gamma_w)) = 26.2 + ((2 * 21) - 20) = 48.2 kN/m^2 \qquad (6.28)$$
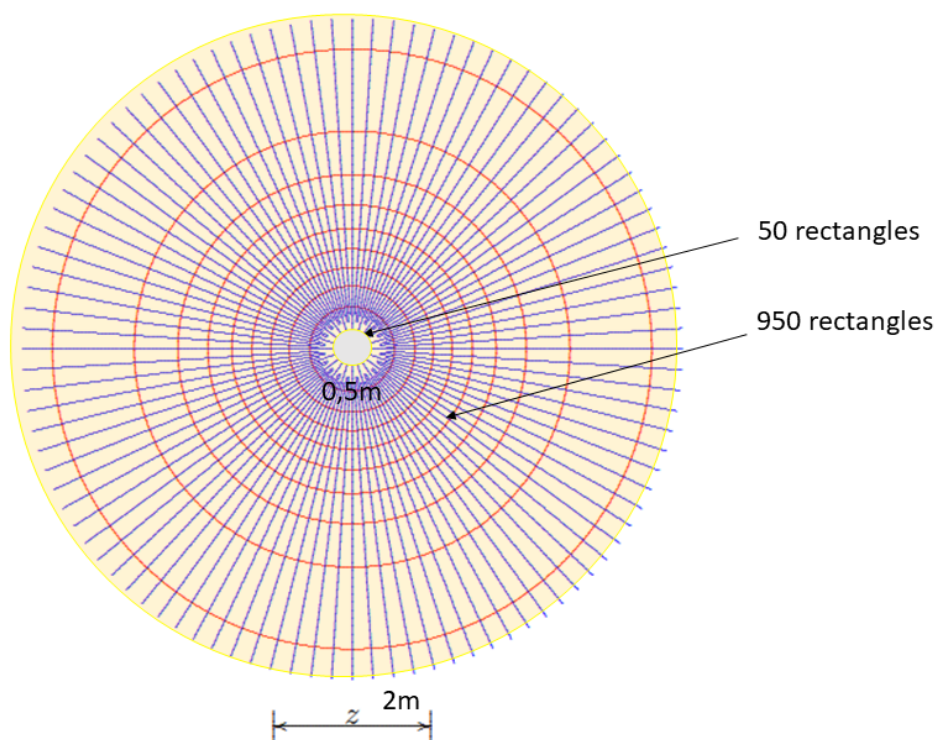
Figure 6.19: Newmark diagram, axis-symmetrical conditions, $z = 2m$

6.7.3. Summary

An axis-symmetric condition model was carried out on the confining cover layer geometry to assess the possible differences compared to a plane-strain condition model. The comparison to the model in plane strain condition will be performed in the following section.

6.8. Comparison stability results

Three different types of calculations have been conducted in PLAXIS, free exit and constricted exit where the confined cover layer was applied as a rigid layer in plane strain and axis-symmetric conditions. All calculations underwent hydrostatic and flow conditions to determine how the stresses within the soil would react.

Soil stress calculations at four locations were performed to provide insight into the effect of a cover layer and corresponding well on a sandy subsoil. Tables 6.2 and 6.3 give an overview of PLAXIS stress results in the sand layer through two cross-sections, A-B (location under well) and C-D (right outermost boundary). Both underwent calculations with the absence and presence of flow ($\phi = 5m$, calculations are found in appendix B).

	Point B		Point D	
Hydrostatic	Plane-strain	Axis-symmetric	Plane-strain	Axis-symmetric
σ	226	235.9	236	236
u	120	120	120	120
σ'	106	115.9	116	116

Table 6.2: Overview of total, effective and porewater stresses, *hydrostatic* condition, $[kN/m^2]$

$\phi = 5m$	Point B		Point D	
	Plane-strain	Axis-symmetric	Plane-strain	Axis-symmetric
σ	226	235.9	236	236
u	130	130	130	130
σ'	96	105.9	106	106

Table 6.3: Overview of total, effective and porewater stresses, $\phi = 5m$ condition, $[kN/m^2]$

Two modelling conditions were applied to the confined cover layer scenario, plane strain and axis-symmetrical. Plane strain conditions are infinitely long and normal to the plane section, and axis-symmetrical conditions present a rotationally symmetric model about an axis representing a more 3-dimensional problem. Tables 6.2 and 6.3 indicate that depending on the modelling conditions the stresses throughout the sand column are highly dependent on the modelling conditions.

Little to no influence of the well opening is experienced at the outer boundary, point D, where the PLAXIS results in both modelling conditions are equal. Hand calculations were also used to verify this, producing the total stress value of $\sigma = 236kN/m^2$. However, at point B, under plane strain conditions, a total stress value of $\sigma = 226kN/m^2$ was observed, indicating that a depth of $8m$ at the well opening still causes a small amount of shearing in the sand layer. This shearing causes vertical spreading of the effective stresses.

The soil stress hand calculations show that the weight of the cover layer and well opening is still felt at the bottom of the plane strain model. Principle effective stress figures indicate the rotational effects of the principal stresses are predominantly restricted to the upper part of the sand column, however, vertical shear stresses are still felt at the bottom of the model. It was expected that when there was to be no influence on the sand layer, the total stress would total $\sigma = 236kN/m$. PLAXIS calculates $\sigma = 226kN/m^2$, a difference of $10kN/m^2$. Suggesting that at this depth the pressure bulb is felt on the principal stresses.

Where plane strain conditions felt the presence of the well $8m$ into the sand layer, under axis-symmetric conditions the results experience less effect of the well. Tables 6.2 and 6.3 show the total stress differs by $0.1kN/m^2$ compared to the results achieved at point D and the manual hand calculations. Due to the 3-dimensional nature of the model, the shearing occurs closer to the well entrance, concentrating at a lesser depth.

Whether or not there was a presence of flow, the total stress along both vertical axis were not affected. It remained dependent only on the weight above the point. However effective stress decreases with increasing hydraulic head, as effective stress is dependent on the porewater pressure and total stress.

7

Discussion

This thesis aimed to qualitatively analyse the effect of groundwater flow, well geometry, and soil parameters on the hydraulic heave growth process commonly known as progressive fluidization. This chapter will discuss some of the important findings concerning current design rules and practices. All the parts of the report will be connected to provide the bigger picture.

7.1. Backward erosion piping process

The process of backward erosion piping requires a sequence of events to occur, and those events must occur in the correct order. This process of events had been formulated into a failure path, described in section 3.3. Hydraulic heave is an important failure node within the failure path, the process of grain suspension and movement. The literature study determined that hydraulic heave has been researched in depth about groundwater calculations where the weight of a confined cover layer is not taken into consideration, Terzaghi and Peck (1964) and Sellmeijer and Koenders (1991).

Levee systems within the Netherlands often comprise a confining cover layer, therefore it is important to assess the effect on the backward erosion piping process. The failure path was adapted to include an additional failure node, the initial hydraulic heave, for this study (figure 6.1). Within the current design practices, such as Terzaghi and Peck (1964). The guideline considers only when the sand layer becomes fully suspended, without consideration of an external force or overburden applied to the sand layer. With the addition of a new failure node, and initial hydraulic heave, the processes and parameters affected by the confining cover layer and well can be investigated.

7.2. Groundwater flow calculations

Current design rules only consider groundwater calculations when determining the critical head for hydraulic heave. Only the upper bound for hydraulic heave is taken into consideration, resulting in an over-conservative design. This would provide a representative situation where the levee systems would have no confining cover layer. However, this is not always the situation in the Netherlands. Section 5.1 and 5.4 describe the evidence for the relevance of including analysis involving the presence of a confining cover layer. In the groundwater calculations, it was observed that the hydraulic gradient followed Darcy's law, equation 2.1, very closely. Hydraulic gradient is a key parameter within the current design rule when determining hydraulic heave. At points of high flow velocity hydraulic gradient peaks were also seen:

- left corner of the levee closed boundary
- seepage wall tip
- well entrance

Terzaghi and Peck (1964) introduced that vertical equilibrium is when the weight of the particles and vertical flow are equally balanced. Once this is broken fluidization occurs. The applicability of this criterion for hydraulic heave has been investigated. Although the vertical equilibrium is seemingly broken at the locations mentioned above, hydraulic heave will not occur at the locations left of the closed levee boundary and the tip of the seepage wall. Literature has stated that the hydraulic gradient peaks can be considered fluidization areas only if the following conditions apply:

- soil around the location has already fluidized
- there is an outlet for the particles
- gradient is high enough to break the vertical equilibrium

The combination of these two criteria will lead to a comprehensive understanding of hydraulic heave when no confining cover layer is present.

Water levels were linearly altered, producing a linear relationship in hydraulic gradient difference behaviour along the entire seepage wall depth. At a low water level, the groundwater flow through the system is low, resulting in low hydraulic gradients. Increased water levels increase the hydraulic head difference over the system, with a greater chance of overruling the vertical equilibrium.

Peaks of hydraulic gradient located at the well entrance are the most important when considering hydraulic heave. From the analysis done with altering well opening sizes, it is considered to have the greatest influence on this peak. A smaller opening acts as a valve, forcing the flow at a higher concentration through this gap. A greater well opening allowed the water, the same volume, to enter the well entrance over a greater area, reducing the velocity. Decreased velocity results in a lower hydraulic gradient. When a well opening is significantly large the system acts as Terzaghi and Peck (1964) free exit situation, where no hydraulic gradient peak is observed at the well entrance.

The minimum and maximum vertical model boundaries were modelled open. Allowing water to travel out of the model through these boundaries, especially the vertical model boundary. Were those boundaries to be closed, an increased volume of flow would travel to the well entrance as the only place to reach the lowest region of the hydraulic head. The hydraulic gradient would significantly increase, allowing hydraulic heave to occur at lower water levels. At the tip of the seepage wall, the hydraulic gradient would increase a lot less than at the well entrance, as it is expected that the flow lines would not change dramatically. In relativity, a levee system does not have a domain boundary, arguing that the vertical boundary may have been insufficiently far away from the well entrance.

7.3. Effective stress, stability analysis

The effective stress analysis determined that current design rules should not rely entirely on groundwater calculations when assessing hydraulic heave. Given that the weight of the confined cover layer is not taken into consideration during groundwater calculations, the stresses within the soil layer can not be examined. Rotation of the principal stress due to

shear stress, illustrated in figures 6.10, results in a smaller area experiencing fluidization than expected from the current design rules.

The depth of the model is taken to be the average seepage wall length within a current levee strengthening project in the Netherlands, $8m$. The model length of $8.5m$ was assumed sufficient enough to ensure no influence of the well at the furthest boundary. However the depth/width ratio, of all three models, to be altered could lead to variation, where the reliability of the result depends greatly on project geometry. From project to project, location to location parameters and geometry will change. This report therefore only provides the important aspects of the process that require attention during design.

At the point, during the iteration, when the fluidization zone stops progressing, the perimeter of the zone is too large to enforce enough flow concentration to break the vertical equilibrium. However, when the hydraulic head was increased, progression failed to continue, instead the confined cover layer began to uplift. This finding suggests that the interlocking forces created during stress rotation are so large that pressure under the cover layer can not break the interlocking bonds before the potential limit is reached for uplift.

7.4. Research limitations

7.4.1. Model accuracy

Concessions are made on the model geometry due to the complexity of modelling backward erosion piping. Each failure node needs to consider a lot of parameters and requires perfect conditions to occur, making it difficult to model the entire process. Instead of modelling an entire levee system, for the effective stress calculations, only a sand column was modelled. The depth of the sand layer is considered to be the depth of a proposed seepage wall. However, field conditions can deviate from the calculations performed in this report, and hence result in a different groundwater and hydraulic gradient behaviour. For instance, soil heterogeneity can cause heave progression to progress in a different direction when searching for the weakest path. This has a different effect on the rate of heave progression. The larger the fluidization zone which results in hydraulic head drop, reducing the rate of progression.

Furthermore, aquifer properties such as depth/width/length ratio and seepage length were not extensively varied. Leakage was kept constant between the high water level and the polder, allowing flow to the polder. Although not incorporated in the models, these can be easily adapted to incorporate seepage length.

Model Instabilities
Model instabilities were experienced within the effective stress analysis calculations. Ideally, the sand layer under the confining cover should have a cohesion of zero, $c = 0kN/m^2$, and particles will not stick together. However, PLAXIS requires a stable foundation or surface when external loads or structures are applied. A slightly increased cohesion was given to the sand to ensure that the confined cover layer would not collapse into the sand layer in the first phase.

Once flow was introduced, high concentrations of flow were observed at the corner of the confining cover layer, sand layer and well entrance. Local instabilities were observed when the flow concentration reached the point where Terzaghi and Peck (1964) vertical equilibrium was disrupted. This ended the PLAXIS calculation.

With the application of the confined cover layer load, the principal effective stresses should experience less rotation concerning a case where less cohesion is enforced. The well through the confining cover layer is observed to produce less of a pressure bulb or pressure cone shape under the well, instead a more vertical rectangular fluidization zone is expected. Reducing the possibility of local instabilities under the confining cover layer, enabling PLAXIS to complete the calculation to a greater degree.

8
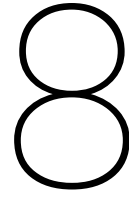
Conclusions and Recommendations

In this chapter, conclusions have been drawn to answer the research questions, based on the results presented in the previous chapters. Recommendations for future design and assessment of levees about hydraulic heave and well properties, as well as further research opportunities are also presented.

Failure due to backward erosion piping is known to occur in a sequence of processes. When the hydraulic head increases, water pressure builds up under the confined cover layer. Uplift and cracking of the nonporous layer are followed by pipe initiation, causing the formation of a pipe in the sand layer and a sand boil at the surface. The pipe progresses to the upstream side, after which the pipe widens and deepens, followed by the settlement and failure of the dike.

8.1. Conclusions

Main research question:

How does a restricted exit for groundwater flow affect hydraulic heave compared to Terzaghi's free exit situation?

This thesis has shown how a non-porous cover layer impacts the current design rules and the hydraulic head failure node within the backward erosion piping process. Current hydraulic heave design rules, related to backward erosion piping, are assessed against the groundwater flow calculations, with and without the presence of a confined cover layer. Pore pressure was calculated using a finite difference model, PLAXIS, through the proposed levee system. Hydraulic heave or fluidization ultimately relates to the relationship between applied tension and pore pressure, unable to be determined within groundwater calculations. Soil stability was assessed using stability calculations, to determine the extent of fluidization progression. The research was split into parts and four sub-questions were created to help answer the main question presented above. The key findings, which are further elaborated in the next paragraphs, are:

- Analysis of backward erosion piping failure path and current design rules indicate that hydraulic heave or progressive fluidization is determined through groundwater calculations rather than effective stress calculations.
- The rate of progressive fluidization can be explained by sediment transportation rate,

which is shown to depend on flow velocity, weight of confining cover layer and well opening size.

8.1.1. Analysis of backward erosion failure path and current design rules

Increasing the hydraulic gradient over a levee system initiates flow from regions of high hydraulic head to low, for example to a polder of the hinterland. The flow will begin to seep under the levee, finding the path of least resistance to the lower hydraulic head region. Higher concentrations of flow at the corners of the levee will cause an increase in hydraulic gradient, which is dependent on hydraulic conductivity and flow velocity.

The addition of a mitigation measure, in this instance a seepage wall, alters the generic failure path of backward erosion piping. Acting as a physical barrier, the seepage wall cuts off the flow's quickest path to the region of the least hydraulic head. One of the locations where a high hydraulic gradient is experienced is removed, the levee corner with the low region of the hydraulic head. Flow is instead forced to divert down and around the seepage wall. At the lowest point of the seepage wall, the flow concentration was high, resulting in a new location of high hydraulic gradient. Immediately after rounding the seepage wall tip, the flow disperses, drastically reducing the flow concentration converging to the surface.

When the hydraulic gradient is such that the confined cover layer has been uplifted and horizontal heave is occurring, one additional failure node is introduced to the ten-node backward erosion piping failure path. Horizontal piping (failure node 5 figure 4.4) will begin backtracking to the highest region of the hydraulic head, transporting sand back out. Upon reaching the seepage wall, a vertical hydraulic heave must occur again alongside the wall, previously not required to occur. At the bottom of the seepage wall the pipe travels, via the path of least resistance to the hydraulic head source, overloading the system, and carrying on the backward erosion piping failure path.

8.1.2. Modeling progressive fluidization

Groundwater calculations for the two situations with and without a confining cover layer determined the locations of high hydraulic gradients. A seepage wall was present in both situations. Hydraulic gradient peaks were experienced in both scenarios at the left corner of the levee boundary and seepage wall tip, as a result of high flow concentration. A third peak was introduced by the introduction of the well through the confining cover layer. Concerning initial fluidization only the hydraulic gradient at the entrance to the well is of great importance. The other locations are restricted by the surrounding solid sand matrix, eliminating the possibility of hydraulic heave and fluidization. The well provides an outlet for sand during heave and transportation.

Furthermore, it was noted that when the well opening increases in size the hydraulic gradient located at the confining cover layer and sand layer interface decreases dramatically. The well effectively acts as a valve, the smaller the opening the more the water is pressurised trying to get through, and the greater the hydraulic gradient. With an increased well opening the force behind the water decreases accordingly, reducing the hydraulic peak until the well diameter is too large to have any effect. In those cases, Terzaghi's free exit flow calculations will dominate.

Sand grains only become suspended when the vertical equilibrium between flow velocity and grain weight, introduced Terzaghi and Peck (1964), is broken. In previous research, it was noted that in some instances, where the water level between the polder and high water

remains constant, the pipe was exhibited to reduced and some saw total discontinuation. The iterations within the chapter 6 indicate how the hydraulic heave zone, $\sigma' = 0kN/m^2$, forms and grows (a zone of $\sigma' > -2kN/m^2$ was considered due to the cohesion having a greater value than $c = 0kN/m^2$).

The weight of the cover layer exerts a load on the sand layer. The installation of the well, and the removal of a small vertical section of the cover layer, created a pressure difference, as a result of unequal volumetric weights. Due to the pressure difference, vertical stress is spread unequally throughout the sand layer as a result of shearing. With the well having a lower volumetric weight, rotation of principal stresses, towards the centre, can be observed under the well following the isobar stress concept representing a bulb shape, hence the pressure bulb.

As the fluidization zone grows, the shape has key attributes similar to that of the pressure bulb. At first, the well acts as a valve, forcing the flow through a small opening, causing a greater flow velocity. As the fluidization zone grows the outer perimeter also grows, allowing flow to enter the region of the lowest hydraulic head at more points, reducing flow concentration. Flow is key to the suspension of particles and hydraulic heave, a higher concentration of flow causes fluidization. As the fluidization zone grows, less flow concentration is experienced along the boundary, alternately stopping the growth.

Hydraulic heave is one of the failure nodes in the bigger process of backward erosion piping. Each of the failure nodes is required to occur for levee failure to happen. The failure node piping is also considered a very important and determining event where extensive research has been carried out. The inclusion of this new method of determining hydraulic heave with a cover layer present in the overall design process could present valuable insight into the backward erosion process.

This research found that the inclusion of effective stress analysis into the current design rule is an essential step for hydraulic heave prediction. It also found that the groundwater flow approach is a poor approximation of hydraulic heave in reality, especially when considering small well openings. In groundwater flow calculations, the approach currently adopted is highly conservative but it does not closely resemble reality. However, not all situations would require such a step.

8.2. Practical Implications

In practice, the introduction of a mitigation measure such as a seepage wall, hydraulic heave and progressive fluidization, is just as relevant as pipe initiation and progression. Pipe completion can not be carried out without the hydraulic heave process. This research determined that heave initiation can not be predicted accurately for a situation where a confined cover layer is present because the initial gradient is highly dependent on the local exit conditions and effective stresses are not taken into consideration during the design process. Current design rules are heavily determined by Terzaghi and Peck (1964) and Sellmeijer (1988) formulas that dictate hydraulic heave under free exit conditions. The use of these calculations for prediction purposes leads to very conservative results about hydraulic heave problems. The prediction of effective stresses is essential to reducing results conservativeness and seepage wall length.

The understanding of the relevant processes does generate an insight into the rate of progressive fluidization and could help with the assessment reducing the current seepage

length design rules. The occurrence of a load-bearing structure, such as a confining cover layer is less likely to pose a risk than in one without because the weight introduces pressure into the sand layer, rotating principal stresses through shear stresses.

8.3. Recommendations

Full consideration of the problem at hand would be required to determine the extent of uncertainties within a project, especially regarding the design of a seepage wall and the degree of potential hydraulic heave. The inclusion of effective stress analysis during the design process could reduce seepage wall lengths and project costs.

However, this study focuses on one geometry with constant soil parameters (unless altered during a calculation). The interactions between cohesion, hydraulic head gradient and effective stress could be significantly altered were the geometry different. Therefore, these types of calculations would have to be carried out at each location under investigation .

Although this report has given insight into the mechanism of hydraulic heave and its fluidization process, many stability issues arose during modelling. The full extent of the process may not have been evaluated. PLAXIS offers many options for finite modelling but cannot calculate fully in the stress tension region. Hydraulic heave occurs at the compression tension interface, balancing the fine line that PLAXIS can calculate. Further investigation into how and what software is more suitable for the evaluation of hydraulic heave is required to provide better insight into the mechanism.

Further research should focus on the effects of cohesion. It is expected that with greater cohesion the intergranular forces between particles would be stronger, potentially preventing collapse. This said the subsoil layer would not be representative of a sand layer (cohesion of $0kN/m^2$), which defies the purpose of studying a sandy subsoil. Furthermore, an increase in cohesion ensures greater strength between particles (assuming that the remaining soil parameters are constant).

About the shape of the fluidization zone, it is recommended to complete a full sensitivity analysis where the confined cover thickness is altered. A clear zone shape was observed as a result of rotated vertical stresses, however, how would the system react were this effect to be significantly smaller or larger?

Bibliography

Baldock, T. E., Tomkins, M. R., Nielsen, P., and Hughes, M. G. (2004). "Settling velocity of sediments at high concentrations". In: *Coastal Engineering* 51(1), pp. 91–100. ISSN: 03783839. DOI: 10.1016/j.coastaleng.2003.12.004.

van Beek, V.M, Noordman, A, Robbins, B.A, and Griffiths, D.V (2019). "3D Numerical Simulation of Backward Erosion Piping Tube Experiments". In: *27th EWG-IE (European Working Group on International Erosion)*. Vancouver, pp. 33–35. DOI: 10.1680/jphmg.17.00016.

van Beek, Vera (2015). "Backward Erosion Piping; Initiation and Progression". PhD thesis. Delft: Delft University of Technology, p. 286. ISBN: 9789462599406.

van Beek, Vera, Bezuijen, Adam, and Sellmeijer, Hans (2013). "Backward erosion piping". In: *Erosion in Geomechanics Applied to Dams and levees*. Ed. by Stephane Bonelli and Francois Nicot. ISTE Ltd.: London. Chap. 3, pp. 193–269. DOI: 10.1002/9781118577165.ch3.

van Beek, Vera, Bezuijen, Adam, and Sellmeijer, Hans (2019). "Interaction between the failure mechanisms backward erosion piping and slope instabilty". PhD thesis. Delft: Delft University of Technology. ISBN: 9788578110796.

van Beek, Vera, Robbins, Bryant, Rosenbrand, Esther, and van Esch, John (2022). "3D modelling of backward erosion piping experiments". In: *Geomechanics for Energy and the Environment* 31. ISSN: 23523808. DOI: 10.1016/j.gete.2022.100375.

Bentley (2022). *PLAXIS 2D-Tutorial Manual*. Tech. rep.

Bligh, W.G (1910). " Dams, barrages and weirs on porous foundations". In: *Engineering Record* 64(26), pp. 708–710.

Bond, Andrew J., Schuppener, Bernd., Scarpelli, Giuseppe., and Orr, Trevor L. L. (2013). *Eurocode 7: Geotechnical design, worked examples*. Ed. by Silvia Dimova, Borislava Nikolova, and Artur V Pinto. Publications Office of the European Union: Italy. ISBN: 9789279337598. DOI: 10.2788/3398.

Boskalis (2015). *Pilot Verticaal Zanddicht Geotextiel*. URL: https://nederland.boskalis.com/projecten/detail/pilot-verticaal-zanddicht-geotextiel.html.

de Bruijn, Huub (2013). *Het pipingproces in stripvorm*. Tech. rep. Delft: Deltares.

Chen, Ye-Hong, Frank, T, Tsai, C, Asce, M, and Jafari, Navid H (2021). "Multiobjective Optimization of Relief Well Operations to Improve Levee Safety". In: *Journal of Geotechnical and Geoenvironmental Engineering* 147(7), p. 04021041. ISSN: 1090-0241. DOI: 10.1061/(ASCE)GT.1943-5606.0002532. URL: https://ascelibrary-org.tudelft.

```
idm.oclc.org/doi/abs/10.1061/%28ASCE%29GT.1943-5606.0002532%20https:
//ascelibrary-org.tudelft.idm.oclc.org/doi/10.1061/%28ASCE%29GT.1943-
5606.0002532.
```

Couwenberg, Floris (2021). "The effect of a Foreland on the Piping Assessment Results for River Dikes". PhD thesis. Enschede: University of Twente.

Deltares (2017). *D-Geo Flow Manual*. Vol. 1. Deltares: Delft.

Deltares (2020). *Factsheet D-Geo Flow*. Tech. rep. Delft. DOI: `Deltares:11205758-037-GEO-0001`.

Erkens, G, de Louw, P, Bootsma, H, and Kooi, Henk (2019). *Huidig en toekomstig opbarstrisico in de polder Middelburg en Tempelpolder*. Tech. rep. Delft: Deltares.

European Committee for Standardization (2022). *Eurocode 7: Geotechnisch ontwerp - Deel 1: Algemene regels*. Tech. rep.

Evans, J, Ruffing, D, and Elton, D (2015). *Fundamentals of Ground Improvement Engineering*. 1st ed. Vol. 1. CRC Press, TTaylor & Francis Group: London, New York. ISBN: 978-0-367-41960-8. DOI: `10.1201/9780367816995-8`.

Forster, Ulrich, van den Ham, Geeralt, Calle, Ed, and Kruse, Gerard (2012). *Onderzoekrapport: Zandmeevoerende Wellen*. Tech. rep. Delft: Deltares. URL: `www.rijkswaterstaat.nl`.

Förster, U, Bezuijen, A, and van den Berg, S.G (2015). "Vertically inserted geotextile used for strengthening levees against internal erosion". In: *XVI ECSMGE (Geotechnical Engineering for Infrastructure and Development)*. ICE Publishing. ISBN: 978-0-7277-6067-8. DOI: `10.1680/ecsmge.60678`.

Förster, U., Koelewijn, A. R., Rosenbrand, E., van Beek, V. M., Voogt, L., Bezuijen, A., and Akrami, S. (2019). "A coarse sand barrier as an alternative preventive measure against backward erosion piping". In: *17th ECSMGE (European Conference on Soil Mechanics and Geotechnical Engineering)*. Vol. 2019-September. International Society for Soil Mechanics and Geotechnical Engineering. ISBN: 9789935943613. DOI: `10.32075/17ECSMGE-2019-0545`.

Garai, J. (2016). "Hydraulic failure by heave and piping". In: *8th ICSE (International Conference on Scour and Erosion)*. CRC Press/Balkema, pp. 427–431. ISBN: 9781138029798. DOI: `10.1201/9781315375045-52`.

Harza, L.F (1935). "Uplift and Seepage under Dams on Sand". In: *Transactions of the ASCE (American Society of Civil Engineers)* 100(1).

Innovatieve Materialen (2015). "Verticaal Zanddicht Geotextiel". In: *Innovatieve Materialen*, pp. 18–20. URL: `https://pipingcontrol.nl/sites/default/files/Bestanden/Innovatieve%20Materialen%203%202015%20artikel%20VZG%20concept%20LR3.pdf`.

Kraaijenbrink, Peter (2022). *Soilmix als heavescherm dijkversterking GoWa*. Tech. rep. Delft: Deltares.

Kramer, Renier (2014). "Piping under Transient Conditions". PhD thesis. Enschede: University of Twente.

Lambe, T William and Whitman, Robert V (1969). *Soil Mechanics*. John Wiley & Sons. ISBN: 0471511927.

Lane, E.W (1934). "Security from Under-Seepage Masonry Dams on Earth Foundations". In: *Transactions of the ASCE (American Society of Civil Engineers)* 100(1).

Middendorp, Hans (2015). "Dijkdoorbraak in Wilnis in 2003". In: *Niet bang voor water?* Lecturium B.V. ISBN: 9789048436484. URL: `https : / / nietbangvoorwater . info / dijkdoorbraak-in-wilnis-in-2003/`.

Pol, Johannes (2022). "Time-dependent development of Backward Erosion Piping". PhD thesis. Delft: Delft University of Technology, p. 289. ISBN: 9789055841745. DOI: `10.4233/ uuid`.

Rijkswaterstaat (2023). *Rijkswaterstaat Water, Verkeer en Leefomgeving | Rijkswaterstaat*. URL: `https : / / www . rijkswaterstaat . nl / over – ons / onze – organisatie / organisatiestructuur/water-verkeer-en-leefomgeving`.

Robbins, B.A and Griffiths, D. V (2019). "Modelling of backward erosion piping in two- and three- dimensional domains". In: *Internal Erosion in Earthdams, Dikes and Levees*. Vol. 17. Springer, pp. 149–158. DOI: `10.1007/978-3-319-99423-9{\_}14`.

Robbins, Bryant A., Stephens, Isaac J., van Beek, Vera M., Koelewijn, Andre R., and Bezuijen, Adam (2020). "Field measurements of sand boil hydraulics". In: *Geotechnique* 70(2), pp. 153–160. ISSN: 17517656. DOI: `10.1680/jgeot.18.P.151`.

Robbins, Bryant A. and Van Beek, Vera M. (2015). "Backward erosion piping: A historical review and discussion of influential factors". In: *ASDO Dam Safety Conference*. September. New Orleans.

Rosenbrand, Esther and van Beek, Vera (2019). *Analysis Report Coarse Sand Barrier Analysis of medium-scale configuration (phase 2b)*. Tech. rep. Delft: Deltares.

Rosenbrand, Esther and Van Beek, Vera (2017). *Werken met D-Geo Flow*. Delft.

Rosenbrand, Esther, Wiersma, Ane, and Förster, Ulrich (2019). *Analysis report coarse sand barrier Delta Flume tests (phase 2c)*. Tech. rep. Delft: Deltares.

Sellmeijer, Hans, de la Cruz, Juliana López, van Beek, Vera M., and Knoeff, Han (2011). "Fine-tuning of the backward erosion piping model through small-scale, medium-scale and ijkdijk experiments". In: *European Journal of Environmental and Civil Engineering* 15(8), pp. 1139–1154. ISSN: 19648189. DOI: `10.1080/19648189.2011.9714845`.

Sellmeijer, J. B. and Koenders, M. A. (1991). "A mathematical model for piping". In: *Applied Mathematical Modelling* 15(11-12), pp. 646–651. ISSN: 0307-904X. DOI: `10.1016/S0307-904X(09)81011-1`.

Sellmeijer, J.B. (1988). "On the mechanism of piping under impervious structures". PhD thesis. Delft: Delft university of Technology. URL: `https://repository.tudelft.nl/islandora/object/uuid%3A7f3c5919-1b37-4de9-a552-1f6e900eeaad`.

Tanaka, Tsutomu and Verruijtii, Arnold (1999). "Seepage Failure of Sand Behind Sheet Piles". In: *Soils and Foundations - Japanese Geotechnical Society* 39(3), pp. 27–35.

Terzaghi, K, Peck, R.B, and Gholamreza, M (1996). *Soil Mechanism In Engineering Practice*. 3rd ed. John Wiley & Sons, INC. ISBN: 0-471-08658-4.

Terzaghi, Karl and Peck, Ralph (1948). *Soil Mechanics in Engineering Practice*. 1st ed. J. Wiley: New York. ISBN: 9780471852735.

Terzaghi, Karl and Peck, Ralph (1964). *Soil Mechanics in Engineering Practice*. 2nd ed. J. Wiley: New York. ISBN: 9780471852735.

Unie van Waterschappen (2019). *Dijken in Nederland*. URL: `https://unievanwaterschappen.nl/waterveiligheid/dijken-in-nederland/`.

US Army Corps of Engineers (1992). *Design, Construction, and Maintenance of Relief Wells*. USACE.

Vandenboer, K, van Beek, V. M, and Bezuijen, A (2018). "3D character of backward erosion piping". In: *Geotechnique* 68(1), pp. 86–90. ISSN: 17517656. DOI: `10.1680/jgeot.16.P.091`.

Verruijt, Arnold (2001). *Soil Mechanics*. Delft University of Technology: Delft. URL: `http://geo.citg.tudelft.nl/..`.

White, C.M (1940). "The equilibrium of grains on the bed of a stream". In: *Proceedings of the Royal Society of London. Series A. Mathematical and Physical Sciences* 174(958), pp. 322–338. ISSN: 0080-4630. DOI: `10.1098/RSPA.1940.0023`. URL: `https://royalsocietypublishing.org/`.

de Wit, J M (1984). *Research report on sand boil model tests*. Tech. rep. Delft.

A
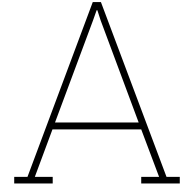
Additional Background

A.1. Limitations to Sellmeijer

Like most theoretical models the Sellmeijer rule has some limitations which need to be addressed. The main and most noticeable limitation is that the rule can only be applied to scenarios that match the two-dimension seepage conditions van Beek (2015). Although the design rule has been adapted three times, with each adaption resulting in a better design rule to describe the piping process in two dimensions, each adaption failed to account for the three-dimensional nature of the process.

1. 2-D Laplace (based on Darcy and continuity) to describe groundwater flow under a structure, with the use of the following boundary conditions:

   - the riverside ΔH equals the river water level.
   - the landside ΔH equals the polder water level.
   - hydraulic head around the pipe equals the hydraulic head in the pipe
   - the dike's blanket material is impervious

$$K_x \frac{\partial^2 \Delta H}{\partial x^2} + K_y \frac{\partial^2 \Delta H}{\partial y^2} = 0 \tag{A.1}$$

2. An equation (based on Poiseuille) to describe the laminar flow in the pipe as a result of the increasing permeability:

$$h^3 \frac{\partial \varphi}{\partial x} = 12\kappa \int \frac{\partial \varphi}{\partial y} dx \tag{A.2}$$

3. An erosion formula (based on White) to describe equilibrium between forces on grains at the bottom of the pipe, assuming that rolling resistance is decisive for onset of grain's movement:

$$\frac{\partial \varphi}{\partial x} = \frac{d_{70}}{h} \frac{\pi}{3} \frac{\gamma_p}{\gamma_w} \eta \frac{sin(\theta + \alpha)}{cos\theta} \tag{A.3}$$

The mechanism of piping is conceptually modelled. Three differential equations that describe the groundwater flow under the dike (Darcy and continuity), flow in the pipe (Poiseuile) and the physical equilibrium of the sand grains in the pipe (White (1940)) are numerically solved. Sellmeijer used Mseep to conduct many numerical calculations of the ΔH_{crit} for various combinations of parameters. An analytical formula was derived via an accurately fitted curve from the calculation results. Large-scale hydraulic model tests were used to validate the formula Sellmeijer and Koenders (1991).

A.2. Addtional Mitigation measures

A.2.1. Berms

Large buttresses or berms are the most common form of decreasing the possibility of backward erosion piping in levee systems. The seepage path through a barrier is extended by enlarging the dam body at the foundation on the plodder side. Seepage length increase, increasing the distance a pipe must travel under a levee. Berms have the huge disadvantage that significant inland land is required, in urban areas especially due to the higher factor of safety enforced. For this reason, especially in the Netherlands, other methods are being investigated to reduce the surrounding land required for a levee, tasked to protect while offering the same or higher degree of safety.

A.2.2. Relief Wells

First employed by the U.S. Army Corps of Engineers US Army Corps of Engineers (1992), relief wells are drainage systems in confined aquifers to counter pressure build-up under levees (figure A.1). This passive control measure (no active pumping) constructed along the polder side of a levee, consists of a drilled pipe in the soil through the impervious layer. When the total groundwater head in the lower layer is greater than the top elevation of the pipe water will flow, lowering the phreatic pressures Chen et al. (2021). Often a system of wells is placed to obtain the required reduced groundwater level and to ensure that this level remains.
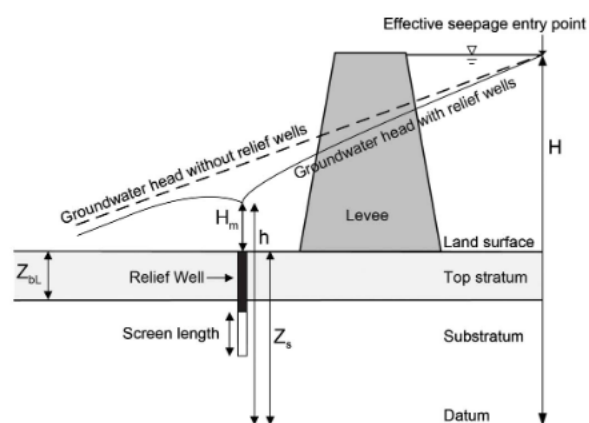
Figure A.1: Cross section of a levee with a plane of relief wells

A.2.3. Vertical Sand-retaining Geo-textile (Verticaal Zanddicht Geotextiel)

An example of such an innovative measure is the vertically inserted sand-retaining geotextile Förster, Bezuijen, and van den Berg (2015), a project developed and funded by Ruimte voor de Rivier and Rijkswaterstaat Innovatieve Materialen (2015). The main principle of operation of the vertical geotextile is preventing the continuous pipe development underneath the water-retaining structure from interfering with sand transport. The geotextile works as a filter, and the transportation of sand grains will be haltered while groundwater flow is not affected, because of its high permeability (figure A.2). The sand-tight screen consists of a three-meter high panel of double geotextile reinforce with a High-density polyethylene (HDPE) net structure and fitted with a geolock on both sides Boskalis (2015). Waterschap Rivierenland won with the technique the Waterinnovatieprijs 2013 van de Unie van waterschappen in the category 'droge Voeten' in collaboration with Deltares, Ten Cate and Stitching Ijdijk en Ruimte voor de Water.
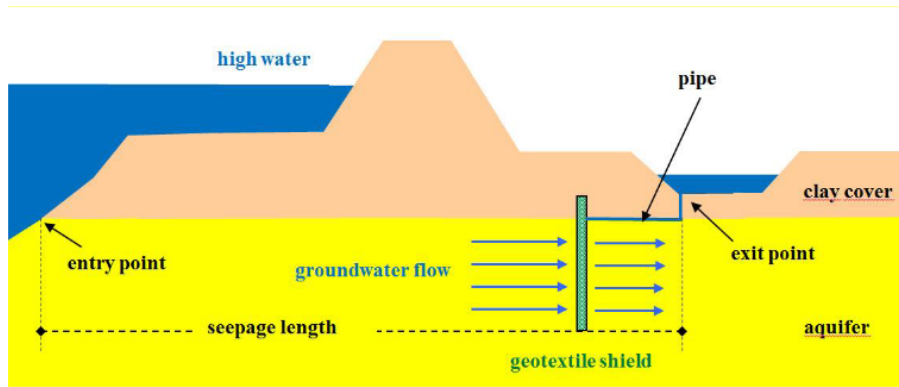
Figure A.2: Principle of operation vertically inserted geotextile Förster, Bezuijen, and van den Berg (2015)

A.2.4. Coarse Sand Barrier

Another alternative innovative mitigation measure against BEP is a coarse gained barrier (CSB). Similar to the vertical sand-retaining geo-textile, a slot is constructed at the toe of the levee and filled in with coarse sand Förster, Koelewijn, et al. (2019). The coarse sand provides more resistance to pipping than fine sand and is topped with clay to prevent discharge of groundwater by upward seepage,, displayed in figure A.3. The barrier was first applied in 2012 as a low-budget piping mitigation measure in an experiment at the Ijkdijk test facility Rosenbrand and van Beek (2019) due to limited financial resources
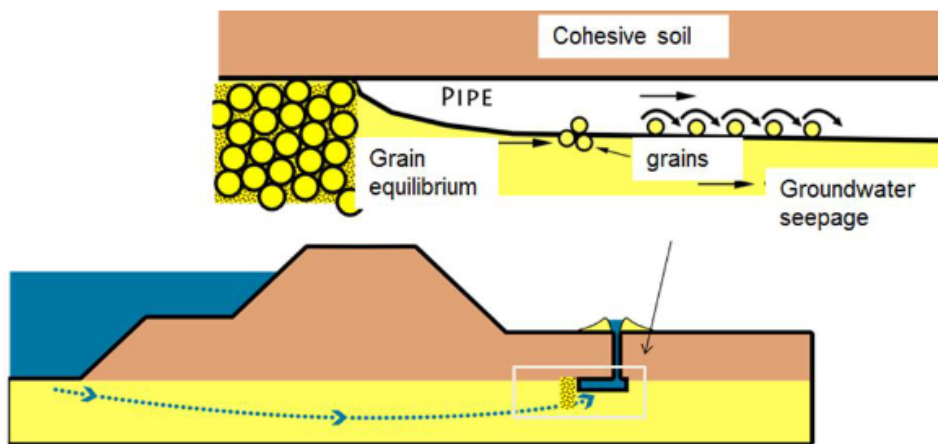

Figure A.3: Schematic illustration of a coarse sand barrier preventing progressive backward erosion piping. Arrows indicate the direction of seepage and sand transport Rosenbrand and van Beek (2019)

Calculations Stresses in Soil, presence of flow

A hydraulic head of $z = 5m$ has been applied to the boundary at the bottom of the model, ensuring a flow with a head difference dh of $1m$. Figure B.1 displays the stresses for the calculation.
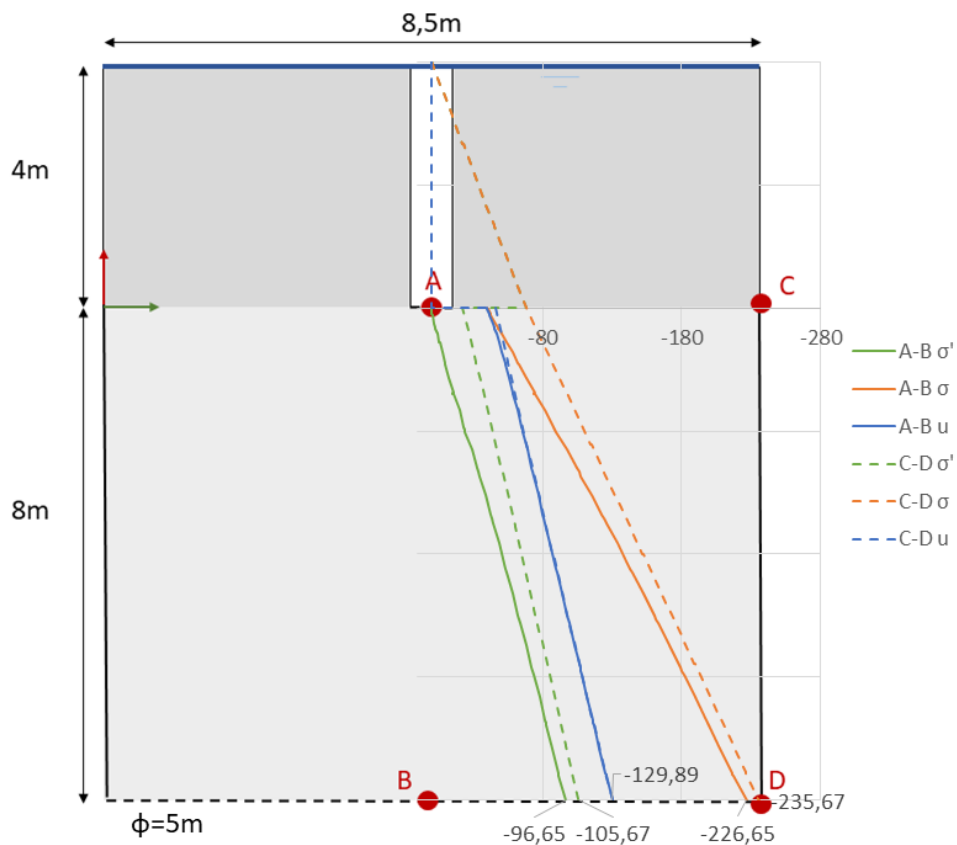
Figure B.1: Stresses in soil, presence of flow ($\phi = 5m$ as hydraulic boundary condition at bottom boundary)

Point D: Edge, bottom of sand layer

Total stress for the bottom of the edge calculation is identical for the hydrostatic case (equation 6.7). Due to the extra hydraulic head causing flow through the system, the porewater pressure

has increased, causing a decrease in effective stress. The total stress at this point becomes the lower boundary of the system under these conditions.

$$\sigma = (\gamma_{sat-sand} * H_{sand}) + (\gamma_{sat-cover} * H_{cover}) = (21 * 8) + (17 * 4) = 236 kN/m^2 \qquad \text{(B.1)}$$

$$u = (H_{sand} + z) * \gamma_w = (8 + 5) * 10130 kN/m^2 \qquad \text{(B.2)}$$

$$\sigma' = \sigma - u = 106 kN/m^2 \qquad \text{(B.3)}$$

Point B: Centre of well, bottom boundary
Equations B.4 and B.1 establish the total stress upper and lower bounds. The lower bound, equation B.4, does not consider the shear stress created by the well entrance and weight of the confining cover layer.

$$\sigma = (\gamma_{sat-sand} * H_{sand}) + z * \gamma_w = (21 * 8) + (5 * 10) = 218 kN/m^2 \qquad \text{(B.4)}$$

$$u = (H_{sand} + z) * \gamma_w = (8 + 5) * 10 = 130 kN/m^2 \qquad \text{(B.5)}$$

$$\sigma' = \sigma - u = 88 kN/m^2 \qquad \text{(B.6)}$$

However, at this location, PLAXIS determined that the total stress would be $\sigma = 10 kN/m^2$ greater than the lower bound, at a value of $\sigma = 226 Nk/m^2$. Suggesting that the well entrance still affects the sand layer at this depth.